INVESTIGATING CAUSES AND DETERMINE REPAIR NEEDS TO MITIGATE FALLING CONCRETE FROM BRIDGE DECKS

By

Dr. Nabil Grace, Principal Investigator

Dr. Elin Jensen, Co-Principal Investigator

Department of Civil Engineering
Lawrence Technological University
Southfield, MI 48075-0134

September 2012

Michigan Department
Of Transportation
1959 (10/08)

TECHNICAL REPORT

DOCUMENTATION PAGE

1. REPORT NO. RC-1567	2. GOVERNMENT ACCESSION NO.	3. MDOT PROJECT MANAGER Steve Kahl
4. TITLE AND SUBTITLE Investigating Causes and Determine Repair Needs to Mitigate Falling Concrete from Bridge Decks		5. REPORT DATE September 30, 2012
		6. PERFORMING ORGANIZATION CODE
7. AUTHOR(S) Nabil Grace and Elin Jensen		8. PERFORMING ORG REPORT NO.
9. PERFORMING ORGANIZATION NAME AND ADDRESS Lawrence Technological University 21000 West Ten Mile Road Southfield, MI 48075		10. WORK UNIT NO. (TRAIS)
		11. CONTRACT NUMBER 108621
		11a. AUTHORIZATION NO. 2009-0428/Z1
12. SPONSORING AGENCY NAME AND ADDRESS Michigan Department of Transportation Office of Research of Best Practices 425 W. Ottawa St. Lansing, MI 48909		13. TYPE OF REPORT & PERIOD COVERED Final Research Report; 10/01/09 – 06/30/12
		14. SPONSORING AGENCY CODE
15. SUPPLEMENTARY NOTES		

16. ABSTRACT

This study developed a procedure to identify concrete bridge decks that are exhibiting the characteristics associated with falling concrete. Field exploratory work on reinforced concrete bridge decks was supported by analytical and laboratory investigations. The field work included visual inspection, non-destructive tests, and sampling of full-depth cores and powder samples from the bottom of the bridge deck. Chief variables assessed were the chance of corrosion by the half-cell potential, chloride content at the location of the bottom reinforcement, and the concrete pH level. The chloride diffusivity was estimated from the chloride profile. The laboratory investigation was performed on bridge deck beams. The beams were constructed from concrete containing chloride levels known to cause corrosion as well as from a control concrete. Beams were subjected to freeze-thaw or saltwater followed by repeated loading to simulate field conditions. The following characteristics were quantified: chance of corrosion, corrosion rate, chloride content, flexural response as a function of environmental exposure and repeated loads, and ultimate strength. The size of the porous zone around the reinforcement was determined using an environmental scanning electron microscope. Finally, a strategy was developed to assess if a bridge deck exhibited the characteristics associated with falling concrete. The strategy included visual inspection of cracking and spalling, assessment of chance of corrosion, chloride content, and pH levels. If any of these measures exceed critical levels a service life calculation needs to be performed. Based on existing mathematical models, the time to corrosion initiation and time to corrosion cracking can be predicted. The resulting time is then compared to the age of the bridge. From this information proper planning for future repair needs can be made.

17. KEY WORDS Falling concrete, bridge decks, corrosion, spalling, non-destructive testing, field and laboratory investigation	18. DISTRIBUTION STATEMENT No restrictions.

19. SECURITY CLASSIFICATION – report Unclassified	20. SECURITY CLASSIFICATION – page Unclassified	21. NO OF PAGES 243	22. PRICE

ACKNOWLEDGEMENT

The project investigators are grateful to Mr. Steve Kahl and Mr. Michael Townley of the Michigan Department of Transportation (MDOT) for their support and collaboration throughout this project. The assistance of the Research Advisory Panel (RAP), the MDOT field support team, as well as the traffic control teams is greatly appreciated.

The research team at the Center for Innovative Materials Research (CIMR) at Lawrence Technological University consisted of several students and laboratory technicians. The project investigators wish, in particular, to thank Biniam Aregawi and Kibraeb Gebreselassie, for their dedicated efforts in the laboratory as well as the field investigations.

DISCLAIMER

The contents of this report reflect the views of the authors who are responsible for the facts and accuracy of the data presented herein. The contents do not necessarily reflect the official views or policies of the Michigan Department of Transportation, nor Lawrence Technological University. This report does not constitute a standard, specification, or regulation. Trade or manufacturer's names, which may appear in this report, are cited only because they are considered essential to the objectives of the report. The United States (U.S.) government and the State of Michigan do not endorse products or manufacturers.

TABLE OF CONTENTS

LIST OF FIGURES

LIST OF TABLES

EXECUTIVE SUMMARY

Nearly all of the bridges under MDOT jurisdiction are constructed with concrete bridge decks. These bridges may be supported either on concrete beams of different cross sections or on steel girders. Irrespective of such supporting systems, a few concrete deck slab problems are observed such as spalling at fascia overhangs and at the bottom of the deck. These problems add to the continuously increasing maintenance cost to rehabilitate deck slabs and to restore serviceability.

A comprehensive research study was conducted to develop performance thresholds and procedures to identify decks with spalling potential by conducting detailed field exploratory work supported by analytical and laboratory experimental work. The field investigation was conducted on three bridge decks located in Oakland County, Michigan, identified with ID numbers: 63174-S05-1 (carrying I-75 NB over 14 Mile Road), 3022-S02-4 (carrying I-96 WB over Milford Road) and 63022-S01 (carrying I-96 WB over Kent Lake Road). Their historical data, maintenance and inspection records, and major repair records were evaluated and synthesized. As a result of the Michigan climate, these bridge decks have been exposed to significant temperature variations, freeze and thaw cycles, and deicing salts.

The field investigation included visual inspection, non-destructive testing, and analysis on full depth cores obtained from the bridge decks. Half-cell potential measurements were used to evaluate the probability of corrosion of the bottom reinforcement layer on representative areas of the bridge decks. Powder samples of concrete were collected from both bridge decks and full-depth cores for chloride content evaluation, and pH level variation along the depth of the deck was determined from full-depth cores. Concrete core samples were evaluated under an ESEM (environmental scanning electron microscope) to evaluate the state of corrosion of the bottom reinforcement layer and determine the size of the interface layer between the reinforcement and the concrete; denoted the porous zone size. The corrosion products will fill up this space prior to causing pressure on the surrounding concrete. The onset of corrosion cracking will occur when the pressure causes tensile stresses that exceed the tensile strength of the concrete.

Various laboratory non-destructive tests were carried out on laboratory reinforced concrete beam specimens as they were subjected to different environmental and traffic loads representing field conditions. These tests included applying repeated load cycles and exposing

the specimens to aggressive environmental conditions such as saltwater exposure and freeze/thaw cycling. The tests were designed to quantify the adverse combined effects of traffic loads and freeze/thaw or saltwater exposures on the durability of reinforced concrete. Four specimens were used as control specimens, and the remaining sixteen specimens were subjected to either freeze/thaw exposure or saltwater exposure and then subjected to repeated load cycles. Non-destructive tests (NDT) and static load tests were conducted at various intervals to assess the development of the corrosion and its adverse effects.

The laboratory environmental exposures simulated the environment that could potentially support accelerated corrosion of the steel reinforcing bars in the concrete. After exposure, the results indicated existence of some corrosion products of the reinforcing bars. Due to the 24-month overall project duration, the formation of the corrosion products was not expected to reach the severity that could cause corrosion cracking and subsequent falling of concrete cover. Ultimate load capacity of the bridge deck specimens were not significantly affected by the presence of the corrosion products.

Service life in this study is defined as the time to which surface cracking due to corrosion of the bottom reinforcement is visible on the bottom surface of the bridge deck. The service life was determined for the field investigated bridges and a strategy was proposed to aid Michigan Department of Transportation (MDOT) in evaluating and determining the appropriate repair needs of bridge decks in Michigan. The proposed strategy includes: visual inspection, non-destructive testing, and service life prediction. The visual inspection will quantify: longitudinal and transverse cracks on top and bottom surfaces of bridge decks, spalling of concrete and rust stains on the bottom surface of the deck. For more in-depth assessment, inspectors should conduct measurements on the deck bottom of the half-cell potential, pH values and chloride content from locations of high risk of corrosion such as ramps and areas that have visible cracking. The half-cell potential measurements, the chloride content and pH values are examined against their respective critical values. These critical values are indicators that the environment around the steel reinforcement is in a state leading to high risk of corrosion. However, these measurements alone do not yield the *time to corrosion* or *time to cracking* due to corrosion. From the through-thickness chloride content the coefficient of diffusivity can be

determined, which is a chief parameter when estimating the *time to corrosion*. Furthermore, from the material and geometrical concrete, steel reinforcement, and bridge deck parameters including the porous zone thickness and the half-cell potential value the *time to cracking* due to corrosion can be estimated. The half-cell potential measurement is converted to a current density through an empirical relationship. The porous zone thickness, if not directly measured, can be estimated from data obtained in this study. Adding the *time to corrosion* to the *time to cracking* yields the service life (at which time the onset of spalling from the bottom deck is expected). Considering the service life against the age of the bridge, decisions can be made on the repair or replacement needs. In addition, this study presented a relationship between the number of freeze/thaw cycles and the age of bridge deck in service, which can be useful in the planning of rehabilitation work.

CHAPTER 1: INTRODUCTION

1.1 General

Falling concrete from bridge overpasses onto the roadway occurs approximately 10 to 12 times a year according to MDOT's spokesman Rob Morosi as quoted by Detroit News on May 7, 2004. Over the past years, a number of related incidents have been reported in the news, and a recent auto incident on February 23, 2006 caused major bodily injuries (http://www.redorbit.com/news/technology/404837/motorist_injured_by_concrete_from_bridge_falling_chunk_leads_to/).

Nearly all of the bridges under MDOT jurisdiction are constructed with concrete bridge decks. These bridges may be supported either on concrete beams of different cross sections or on steel girders. Irrespective of such supporting systems, a few concrete deck slab problems are observed such as spalling at fascia overhangs and at the bottom of the deck. These problems add to the continuously increasing maintenance cost to rehabilitate deck slabs and to restore serviceability.

1.2 Statement of Problem

The leading cause of deterioration in reinforced concrete bridge decks is a progressive breakdown that begins with chloride ions reaching the steel reinforcement from the application of deicing salts. Bridge deck spalling is highly related to the concrete durability and chloride-induced corrosion of the steel reinforcement. It is known that the alkaline conditions in concrete forms a passive oxide coating around the steel. However, carbonation of the concrete near the deck surfaces and presence of chloride ions can lower the pH levels and break down this coating (Ahmad 2002). The increased application of deicing salts during winter maintenance operations is the primary reason for corrosion in Michigan's wet-freeze environment.

The corrosion products (rust) have a greater volume than the original steel volume thereby exerting substantial stress on the surrounding concrete leading to localized damage such as concrete delamination and spalling. A repair is usually achieved by replacing the damaged concrete with a patch repair material. However, corrosion may occur either in: (1) the repair material, (2) the unrepaired concrete adjacent to the repair, and/or (3) in the interface between

these two areas. In particular, in overlay bridge deck projects further corrosion may develop in the bottom layer of steel reinforcement if there is a significant amount of chloride ions already in the old concrete or if the overlay material is permeable or cracked and allows additional chloride ingress. These embedded corrosion cells lead to delamination and spalling of concrete.

Many questions exist as to the bridge deck chloride content criteria. Bridge decks in snow-belt states generally contain significant amounts of chloride. Much uncertainty exists on how to interpret and apply the data. Krauss et al. (2009) reported that various State DOTs use critical chloride level from 0.04 to 0.07% by weight of concrete as the trigger for defining the concrete removal repair area. These critical chloride levels are still debated as a wide range of ±100% exits for both epoxy coated steel and for uncoated steel reinforcement (Materials and Technology Engineering and Science (MATES), Issue No. 46, 1990)

1.3 Objective of the Project

The project includes detailed field exploratory and laboratory tasks, aided with analytical and experimental work. The specific objectives of this research project are:

(i) To conduct field exploration and sampling to determine the concrete properties, condition, and steel condition that are highly associated with falling concrete.

(ii) To develop performance thresholds and procedures to identify decks with spalling potential.

(iii) To evaluate and select non-destructive field test methods to identify spalling potential.

(iv) To develop a procedure to identify decks with spalling potential.

(v) To determine the functional service life of the bridge decks and to propose implementation strategy for evaluating and determining future maintenance and repair activities.

1.4 Scope of Work

To meet the research objective, a comprehensive field investigation and laboratory investigation that included visual inspection, non-destructive tests (in-situ hardness, corrosion potential, chloride content, pH tests) and analysis of cores obtained from bridge decks were conducted. Furthermore, ESEM (Environmental scanning electron microscope) was used to determine porous zone thickness and evaluate corrosion state of the reinforcement. The

functional servce life was determined for laboratory specimens and field investigated bridges. The laboratory specimens were subjected to different environmental and loading conditions to simulate the prevailing condition in the State.

A literature review is presented in Chapter 2. An overview of the laboratory experimental test program is presented in Chapter 3. The field inspection and coring test program is presented in Chapter 4. Results and discussions from the laboratory investigation are presented in Chapter 5. Results and discussions from the field investigation are presented in Chapter 6. Service life calculation and implementation strategy are presented in Chapter 7. Conclusions from the entire research project are outlined in Chapter 8.

CHAPTER 2: LITERATURE REVIEW

2.1 History of Deck Slab Reinforcement

Premature deterioration of highway bridge decks as a result of corrosion of the reinforcing steel was first identified as a serious problem in North America in the late 1960 (Manning, D.G., 1996). The finding resulted in immediate improvements in concrete quality, an increase in specified concrete cover, and changes in construction and quality assurance practices (Cady, P.D., 1977).

It has been reported by the American Concrete Institute (ACI 222R-01) that a number of methods to control steel corrosion, have been adopted such as use of epoxy coated steel reinforcing, metallic coatings, corrosion inhibitors, and cathodic protection. With the exception of cathotic protection, these methods improved the performance of the deck slabs to some extent, they mainly delayed the onset of corrosion. It is observed that reinforcing steel coated with protective materials is effective in preventing corrosion. Epoxy coating in the reinforcement steel is widely used. Functional service life of 30 years has been reported for Wisconsin concrete bridge decks reinforced with epoxy coated reinforcement. (Lee et al. 2005). Fanous and Wu (2000) estimated that use of epoxy coated reinforcement in a typical Iowa bridge deck would yield a functional service life to 38 years. Use of uncoated steel reinforcement in the same bridge would yield a functional service life of 20 years.

2.1.1 Field Performance of Reinforced Steel in the Deck

Bridge decks reinforced with uncoated steel show signs of corrosion after 7 to 10 years (Lee et al. 2005). Therefore, states like Michigan, mandate bridge deck construction to include epoxy coated reinforcement with a minimum concrete cover thickness of 2.5 to 3.0 inches along with use of high quality concrete (Michigan Department of Transportation, MDOT, 2001). The function of the epoxy coating is to provide a barrier to oxygen, water and electrical current. Kirkpatric et al. (2001) observed that epoxy coating delayed the onset of cracking by 1 to 7 years. Similar findings by Weyers et al. (2006) showed that the epoxy coated reinforcement at best added about 5 years of corrosion resistance.

Michigan DOT, in the early 1980's, directed that all reinforced concrete superstructures had to be constructed with epoxy coated reinforcement (Novak et al., 2000). For reinforced concrete deck slabs, epoxy coated reinforcement was to be used in both the top and bottom mats. The use of epoxy coating in both the top and bottom mat reinforcement has proven to be very efficient in providing corrosion resistant reinforcing solutions. Lee and Krauss (2004) found that the resistance to corrosion was about 15 to 20 times higher in epoxy coated reinforcement mats compared to that of uncoated steel mats. This conclusion is relative to the electrical current passed over a macrocell. The lower the current the higher is the resistance to corrosion (Figure 2-1).

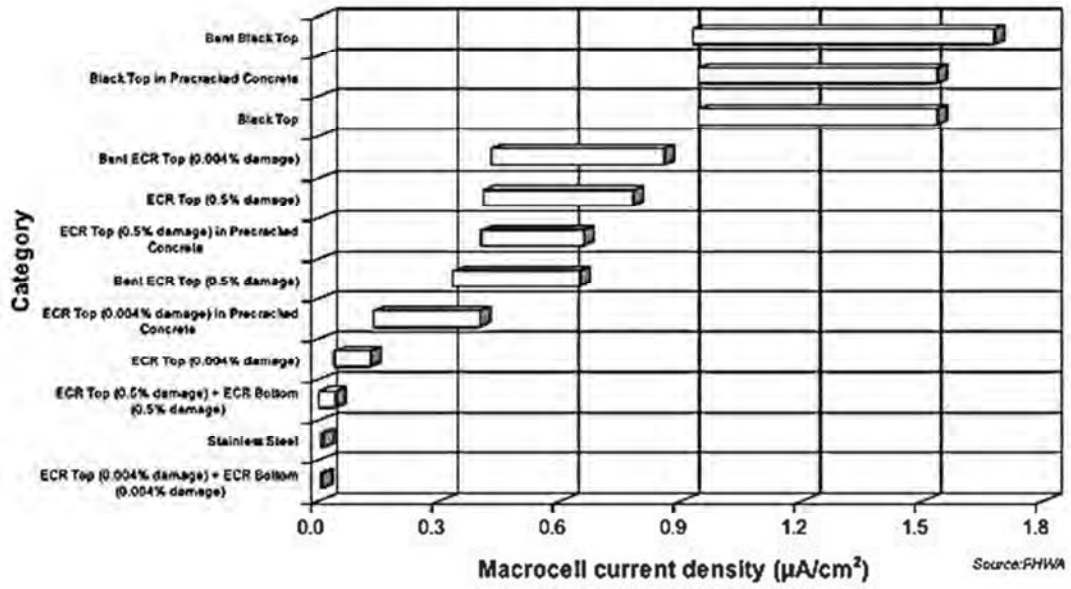

Figure 2-1 Resistance to corrosion of reinforced concrete with different reinforcement types and damage (FHWA)

Federal Highway Administration (FHWA) research carried out by Clear (1980), reported that a epoxy coating on top and bottom reinforcement mats will lower the rate of corrosion since both anode and cathode sites will be only limited to the damaged area. Use of corrosion inhibitor in concrete can prevent the corrosion of reinforcing steel. Calcium nitrate has been reported to be a viable corrosion inhibitor. It was first used in Japan to facilitate the use of salt breaching sands in reinforced concrete. Various tests have been conducted to test the corrosion inhibiting

characteristics of calcium nitrate. However, it has been reported that there is a critical chloride to nitrate ratio above which corrosion will occur (Clear, 1980; and Qian and Cusson, 2004).

2.1.2 Structural Performance of Epoxy Coated Reinforcements in Bridge Decks

Ramiraz and Hasan (1995) tested thirty-four slab specimens with splices and transverse steel in the laboratory to evaluate the structural performance of concrete bridge decks reinforced with epoxy-coated steel. Thirty specimens were tested under fatigue loading, and four were tested monotonically. Evaluations were made by comparing the performance of uncoated bar concrete specimens with that of epoxy-coated specimens under service and ultimate load conditions. In addition, a field evaluation was conducted to assess the in-service condition of concrete bridge decks reinforced with epoxy-coated steel in Indiana. The laboratory results indicated fewer but wider cracks in specimens with epoxy-coated reinforcement. No significant differences in the first cracking load were found between specimens with uncoated and epoxy-coated reinforcements. The splitting crack load and failure load were lower for specimens with epoxy-coated steel. Deflections of epoxy-coated specimens were larger. The differences in crack width and deflection were reduced with repeated loading. No signs of corrosion were found in the epoxy-coated steel samples extracted from cores taken in the six bridges evaluated.

Hamad and Jirsa (1993) reported the results of an experimental investigation on the effect of epoxy-coated transverse reinforcement on the strength of epoxy coated bar splices. Twelve beam specimens with multiple splices were subjected to a negative moment in a constant moment region at the center of the beam. The test variables were the amount of transverse reinforcement, bar sizes and the bar spacing. The nominal coating thickness was 0.31 inch (8 mm). All beams were tested monotonically until failure by splitting of the concrete cover in the splice region. The transverse reinforcement improved the deformation capacity of the beams and the bond strength of the splices. The improvement in bond strength was greater for epoxy coated bar splices than uncoated bar splices and was independent of the number of splices, bar size or bar spacing.

Hester et al. (1991) also conducted an experimental investigation on the effects of epoxy coating and transverse reinforcement on the bond strength splices. The test program included

static tests of 65 beam and slab splice specimens containing No. 6 and No. 8 size bars. The average coating thickness ranged from 0.24-0.43 inch. The specimens were failed in splitting mode. Test results indicated a significant bond strength reduction caused by epoxy coatings. It is reported that the reduction in splice strength is independent of the degree of transverse reinforcement. It was also noticed that the transverse reinforcement increased the splice strength for all bar surface conditions.

Choi et al. (1990) reported the test results of 284 beam specimens and 14 splice specimens. Parameters evaluated included the effect of coating thickness, deformation pattern, and bar size on the reduction in bond strength caused by epoxy coating. The average coating thickness ranges from 0.12-0.67 inch. The test results showed a significant reduction in bond strength for epoxy coatings in the range of 0.20-0.47 inch. It is reported that the coating thickness has little effect on the bond reduction for No.6 size bars and larger. For No.5 size bars and smaller, thicker coating caused greater bond reduction. Increasing the bar size generally increased the bond reduction caused by epoxy coating.

Cleary and Ramirez (1991) carried out an experimental investigation to evaluate the flexural bond characteristic of epoxy coated reinforcing bars in concrete bridge deck slabs under static loading. Test variables were splice length and the concrete compressive strength. Test results indicated that epoxy coating causes a significant reduction in bond strength. It has also been reported by the researchers that the reduction in bond strength increased with increasing anchorage length and increasing concrete strength.

In another experimental study by Cleary and Ramirez (1992), bond of epoxy coated reinforcement under repeated loading was investigated. The experimental program involved nine sets of specimens tested under repeated loading. In addition, five specimens containing epoxy coated steel were rested monotonically. It has been reported by the researchers that the failure bond ratio ranged from 0.82 to 0.96 with an average of 0.88. In terms of deflection and crack width, it was found that specimens with epoxy coating bars had fewer but wider cracks and larger deflections compared to specimens with uncoated bars. The difference in crack widths and deflections were reduced with increasing number of cycles of repeated loading. Deflections

increased with repeated loading for both types of reinforcement, especially in the first 200,000 cycles, and the changes were larger in the uncoated bar specimens. It is reported that concrete strength and stress range had no influence on the compared deflections.

2.2 Concrete Deck Deterioration

Bridge deck deterioration is the most frequent reason for categorizing a bridge as structurally deficient (Tsiatas and Robinson, 2002). Among all the modes of concrete bridge deck deterioration (scaling, spalling, cracking, abrasion damage, alkali aggregate reaction, delamination, sulfate attack, saltwater and freeze/thaw), spalling of concrete from the bottom of bridge deck is the most serious and troublesome, and normally it happens due to the corrosion of steel reinforcement (Russel, 2004).

Cracks provide an indicator for deterioration of bridge decks. Tsiatas and Robinson (2002) present three categories of cracks in bridge components: inadequate structural performance cracks, inadequate material performance cracks, and acceptable cracks. Details related to the formation of these cracks are depicted in Table 2-1. Cracking of structural concrete presents multiple problems. The first is the decrease in structural integrity of the bridge component. Secondly, the cracking creates a flow path for infiltration of chlorides. Tsiatas and Robinson (2002) indicated that cracks having widths as small as 0.004 to 0.008 inch allow penetration of water and chloride solutions.

The predominant form of bridge deck cracking is transverse cracking (Ramey and Wright 1997), which generally occurs over transverse reinforcing bars in regions of negative moment in continuous spans (in the top region of the deck). Overall, cracking is greater in continuous spans (than simple spans), longer spans (than shorter spans), and older decks (than newer decks). Alampalli et al. (2002) reported a direct correlation between severity of cracking and severity of vibrations. Strategies for reducing the amount of cracking include: using smaller than No. 5 size bars, experimenting with reinforcing bar arrangements, avoiding splicing transverse steel when possible, increasing deck thickness, standardizing deck thickness, increasing concrete cover to at least 2.5 in, when deicing salts are used, limiting water-to-cement (w/c) ratio to 0.4 to 0.45 and maintaining control on materials (Ramey et al., 1997).

Table 2-1 Categories of Cracks and Corresponding Mechanisms of Formation

Category of Crack*	Inducing Mechanism*
Inadequate structural performance	Excessive foundation settlement, excessive loading or construction overloads, excessive stresses due to thermal gradients, inadequate design or detailing, poor construction practices.
Inadequate material performance	Plastic shrinkage, drying shrinkage, reinforcement corrosion, freeze/thaw cycles, wet/dry cycles, chemical reaction
Acceptable	Cracks that must develop to properly distribute tensile stresses according to current design criteria.

*Source – Tsiatas and Robinson 2002

2.3 Physical and Chemical Deterioration of Concrete

Corrosion of steel reinforcement is a root cause for deterioration of steel reinforced bridge decks. Corrosion causes rust, iron hydroxide, to deposit on the surface of the reinforcement. The volume of the rust product is several times larger than the volume of the original steel. This additional volume exerts significant stresses on the surrounding concrete leading to localized damage and cracking. Corrosion induced cracking is manifested as surface cracks that run parallel to the reinforcement.

At high pH levels (12-13), as naturally occurring in concrete, a protective oxide layer forms on the surface of the steel reinforcements (ACI 222, 2001). This layer prevents corrosion by limiting access of oxygen and moisture and slows the corrosion rate of the steel reinforcement to about 0.0394 mils/year (0.1 μm/year). If this protective layer is breached, the corrosion rate may increase to as high as 3.94 mils/year (100 μm/year). Note that corrosion rate in most literature is reported in units of μm/year and therefore both metric and English units are used here. The breach is caused by high concentrations of chloride ions or decrease in the concrete alkalinity (e.g. due to carbonation). A single critical chloride content level cannot be defined;

rather a probable range should be considered. Additional detail on the threshold chloride concentration is presented in section 2.7.

The inter relationship between the crack initiation, onset of rust development and chloride content is illustrated in Figure 2-2 (a) and (b). Additional deterioration, in terms of spalling and delamination, are controlled by both environmental and traffic load factors. For the sake of simplicity, the rates are shown as linear in the figures.

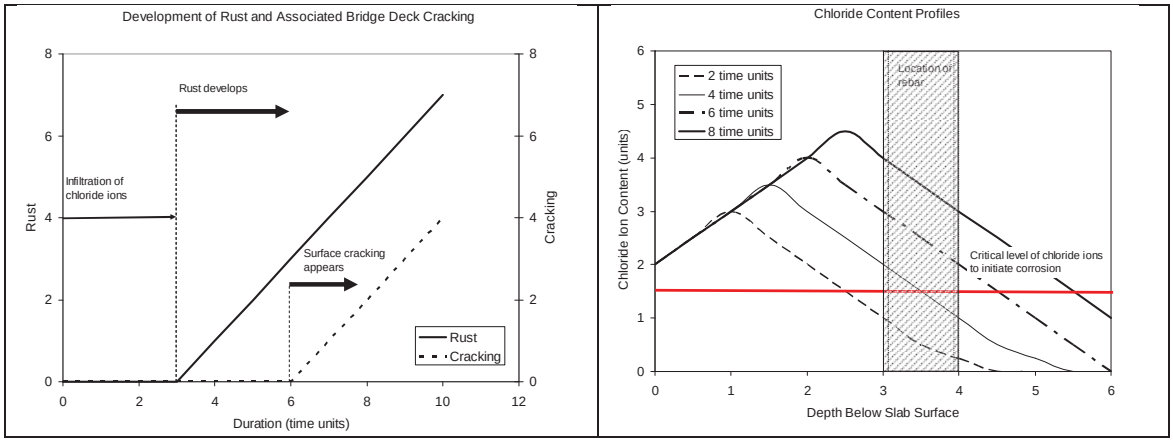

(a) Development of Rust and Cracking due to Corrosion

(b) Chloride Content versus Depth below Surface

Figure 2-2 Relationship between onset of crack, rust and chloride content

Deterioration of concrete also occurs due to chemical attack and by exposure to environmental loads such as freeze-thaw cycles. The success of bridge deck performance can be measured by the years of maintenance-free service that is provided (Young et al., 1998). Kirkpatrick et al. (2001) cited that the time to the first repair of a bridge deck commonly occurs when 2.5% of the deck surface area of the worst-condition span lane has deteriorated. Preliminary stages of concrete deterioration can occur without visible evidence. The initial deterioration can compromise the structure of the concrete and make the structure vulnerable to further attack (Young et al., 1998).

Four common types of chemical attack of concrete are acid attack, carbonation, alkali-aggregate reaction, and sulfate attack. Acid attack is a mode of chemical attack that is generally present only due to external sources such as in waste containment applications.

Carbonation is caused by atmospheric carbon dioxide dissolving in concrete pore water and creating an acidic solution (Mays, 1992). Although the shrinkage associated with carbonation can actually increase the chemical stability and strength of concrete (Kosmatka and Panarese, 1988), the lower pH present after this reaction can allow corrosion of the reinforcing steel (corrosion can begin when the pH reaches values less than approximately 11.5) (Mays, 1992). Other typical pH threshold values are in the range of 8.5-9.5.

Alkali-aggregate reaction is a result of the high pH in concrete paste (pH of approximately 13) or external alkaline source reacting with certain aggregates (Young et al., 1998). The reaction causes loss of integrity of the affected aggregates and ultimately swelling, pressure build-up, and subsequent cracking. A strategy for controlling alkali-aggregate reaction is to spread the reactive silica throughout the concrete avoiding localized concentrations.

Sulfate attack is another type of chemical attack in concrete that occurs in two stages. First, sulfate ions penetrate into the concrete and react to form gypsum. Second, the gypsum further reacts to form ettringite, which causes volume expansion and subsequent cracking. Control of sulfate attack is possible by lowering the permeability of the concrete and lowering the tricalcium aluminate (C_3A) content. These effects can be accomplished by using a lower w/c ratio, applying proper moist curing conditions, using mineral admixtures (all affecting permeability), and using low C_3A content cement (Type V or Type II).

The deterioration of concrete is strongly influenced by the microstructure of the concrete and void space distribution within the structure. Porosity is commonly related to the permeability of porous media. Although the porosity of concrete is generally greater than that of natural rock, the permeability of concrete can generally be lower due to the pore space distribution (Young et al., 1998). Concrete contains discontinuous pore space forcing water to flow by the mechanism of diffusion rather than by advection. Also, aggressive agents such as

chloride ions can penetrate the concrete surface by the mechanism of diffusion. In general, sulfate attack of concrete is generally slow.

2.4 Concrete Exposed to Freeze-Thaw

Several concrete material characteristics can affect the performance of concrete. This section focuses on the importance of air entrainment on freeze-thaw durability. Other factor such as construction practices and aggregate types may also affect the freeze/thaw performance.

Freezing causes a 9% expansion in volume of water. This freezing action is most detrimental when the pores within the concrete structure are fully or nearly saturated. In this case, pressure builds up causing localized fractures. If water can expand as little as 0.008 inch, stresses are reduced preventing this fracturing (Young et al., 1998). The accepted solution to this problem is the use of air entraining agents, which produce voids spaced at less than 0.008 inch. Four types of voids have been identified by Cordon (1979): gel pores, capillary cavities, entrained air, and entrapped air. Gel pores are interstitial cavities among hydration products and are approximately 0.00006 - 0.00008 inch diameter. Capillary cavities are formed by excess water not used by hydration and are approximately 0.02 inch diameter. Entrained air voids are tiny spherical bubbles of 0.00004 – 0.004 inch. Entrapped air voids are generally larger and formed if the concrete is not completely consolidated (Cordon, 1979).

Mohammed et al. (2000) reported results from a 55-year freeze/thaw investigation. It was observed that although air entrainment improves freeze-thaw resistance, it does not entirely prevent freeze-thaw damage. It was shown that air entrainment admixture effectively delays the onset of freeze-thaw deterioration. In addition, the type of Portland cement affects freeze-thaw resistance (Type III demonstrated the worst resistance) and that integrating air entrainment with the cement was more effective than adding it in solution.

2.5 Concrete Exposed to Deicing Salts

The single most destructive factor promoting corrosion of reinforcement is deicing salts (Cady and Renton 1975). The deicing agents cause detrimental effects on the concrete structures

leading to scaling. The use of air-entrained concrete can resist satisfactorily the scaling associated with deicing deterioration of concrete. Chloride distribution in bridge decks has been measured with depth in various investigations. Cady and Renton (1975) report that the chloride ion concentration was found to be negligible beyond 1.5 in of depth when measured on three bridges after seven years of service. Kirkpatrick et al. (2001) found high near surface chloride concentrations (acid soluble concentration of chlorides) extending to a depth up to ½ inch below the deck surface. The depth of further chloride ion penetration in intact concrete is dependent on the diffusion coefficient. Lowering the diffusion coefficient in concrete (which can be achieved in part by using supplementary cementitious materials such as fly ash or slag) can be highly effective at prolonging the service life of bridge decks.

It is reported by Gergely et al (2006) that the principles of diffusion can be used to reasonably predict the concentration of chloride in reinforced concrete bridge elements. A model that uses Fick's Second Law of diffusion can estimate the concentration of chloride at the depth of the reinforcing steel after a given amount of time if accurate estimates of the material properties (diffusion coefficient) and environmental conditions (chloride loading) are available. This information can be used with estimates of corrosion threshold to make service life predictions based on corrosion induced deterioration.

2.6 Mechanism of Reinforcing Steel Corrosion

2.6.1 General

Concrete normally provides a high degree of protection to the reinforcing steel against corrosion, by virtue of the high alkalinity (pH > 13.5) of the pore solution (Ahmed, 2002). Under high alkalinity steel remains passive. In addition, well-consolidated and properly cured concrete with a low w/c ratio has a low permeability, which minimizes penetration of corrosion inducing agents, such as chloride, carbon dioxide, moisture, etc. to the steel surface. Further, the high electrical resistivity of concrete restricts the rate of corrosion by reducing the flow of electrical current from the anodic to the cathodic sites. At the outset, it must be mentioned that, usually in a properly designed, constructed and maintained structure, there should be little problem of steel corrosion during its design life. Unfortunately, this highly desirable durability requirement is not

always achieved in practice due to which corrosion of reinforcement in concrete has become a commonly encountered cause of deterioration in many reinforced structures.

In general, there are two major factors, which cause corrosion of reinforcement in concrete to proceed to an unacceptable degree. They are: (i) carbonation, and (ii) presence of chloride ions, which may either have been present in the concrete constituents right from the beginning or are introduced into the concrete through ingress during the service life. The quality of concrete, mainly the permeability, nature and intensity of cracks, and the cover thickness, have also a great bearing upon the initiation and sustenance of reinforcement corrosion. Once reinforcement corrosion is initiated, it progresses almost at a steady rate and shortens the service life of the structure, by causing surface cracking and subsequently spalling of the cover concrete due to expansion of the corroding steel. The rate of corrosion directly affects the extent of the remaining service life of a corroding RC structure (Ahmed 2002).

2.6.2 Corrosion Cell

Corrosion of steel embedded in concrete is an electrochemical process. The corrosion process is stated to be similar to the action which takes place in a battery (ACI Committee 222, 1992). The surface of the corroding steel functions as a mixed electrode that is a composite of anodes and cathodes electrically connected through the body of steel itself, upon which coupled anodic and cathodic reactions take place. Concrete pore water functions as an aqueous medium, i.e., a complex electrolyte. Therefore, a reinforcement corrosion cell is formed, as shown in Figure 2-3 (Hansson CM 1984).

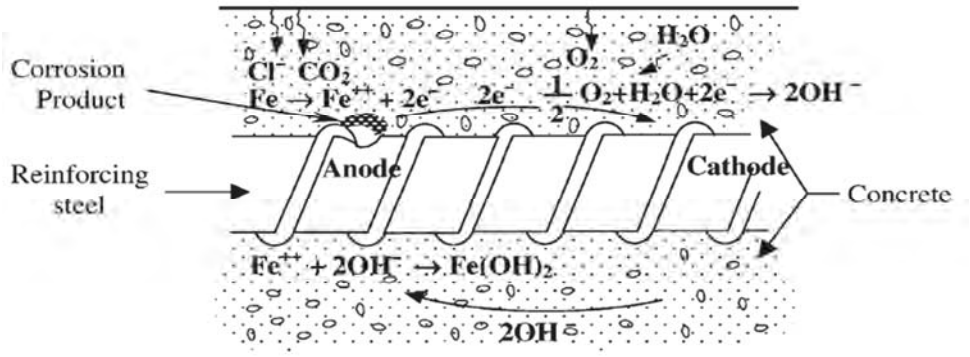

Figure 2-3 Schematic illustration of corrosion of reinforcement in concrete

2.6.3 Anodic and Cathodic Reactions

Reactions at the anodes and cathodes are broadly referred to as 'half-cell reactions'. The 'anodic reaction' is the oxidation process, which results in dissolution or loss of metal whilst the 'cathodic reaction' is the reduction process which results in reduction of dissolved oxygen forming hydroxyl ions. For steel embedded in concrete, the following are the possible anodic reactions depending on the pH of interstitial electrolyte, presence of aggressive anions, and the existence of an appropriate electrochemical potential at the steel surface:

$$3Fe + 4H_2O \rightarrow Fe_3O_4 + 8H^+ + 8e^-$$
$$2Fe + 3H_2O \rightarrow Fe_2O_3 + 6H^+ + 6e^-$$
$$Fe + 2H_2O \rightarrow HFeO^-$$
$$Fe \rightarrow Fe^{2+} + 2e^-$$

The possible cathodic reactions depend on the availability of O_2 and on the pH in the vicinity of the steel surface. The most likely reactions are as follows:

$$2H_2O + O_2 + 4e^- \rightarrow 4OH^-$$
Or
$$2H^+ + 2 \rightarrow H_2$$

2.6.4 Concrete Cracking Process

The durability of reinforced concrete structures is affected by the chloride penetration and susceptibility of the reinforcement to chloride-induced corrosion, when exposed to deicing salts. Once the chloride content at the reinforcement reaches a threshold value and enough oxygen and moisture are present, the reinforcement corrosion will be initiated. Corrosion products then accumulate in the concrete–steel interface transition zone (porous zone). Porous zone is a region around the reinforcement which is formed by:

1. The transition from cement paste to steel
2. Entrapped or entrained air voids around the reinforcing bar
3. Capillary voids in the cement paste through which corrosion products diffuse

The initiation of corrosion starts after the break down of the passive film in the presence of moisture and oxygen, resulting in a formation of expansive corrosion products that expand and occupy more space than the original reinforcing steel volume. When the stress created by the expansive corrosion products is greater than the tensile strength of the concrete the concrete cover cracks and spalling of concrete results. The corrosion cracking process is presented in Figure 2-4 (Weyers et al., 1995).

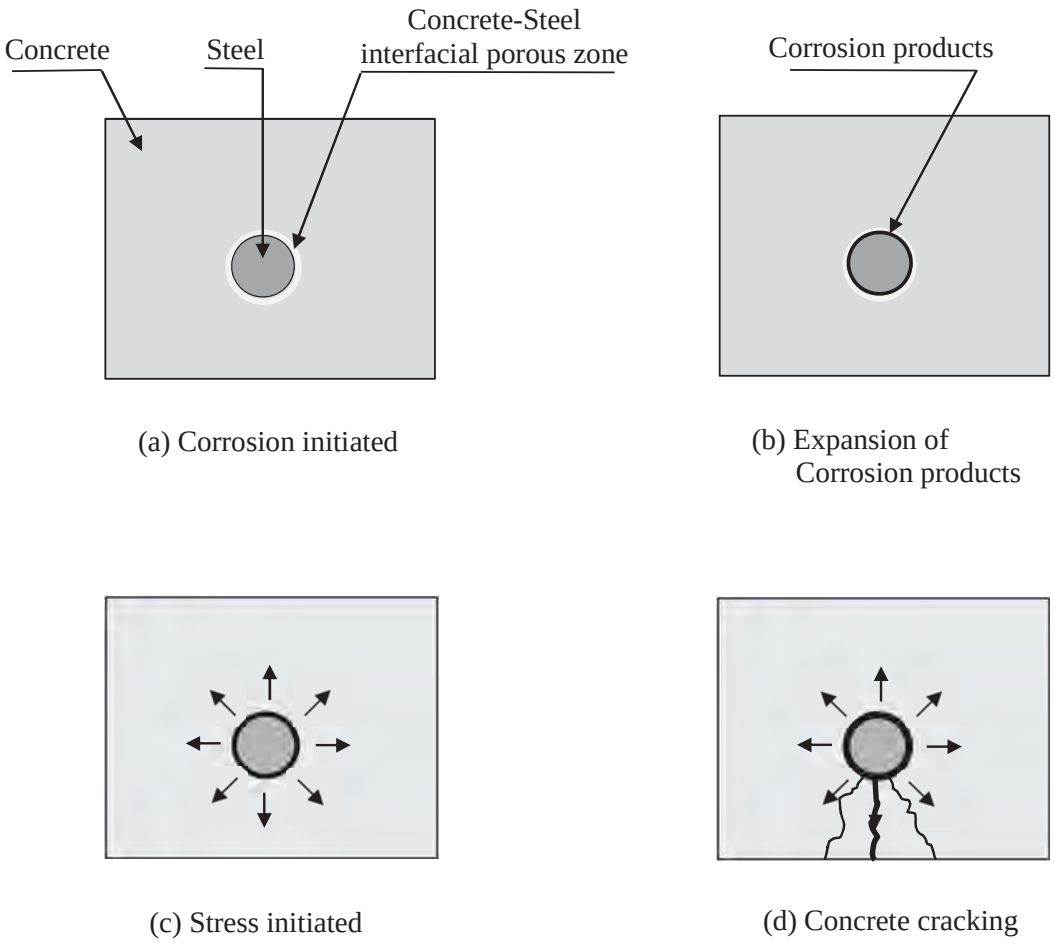

Figure 2-4 A schematic diagram of corrosion cracking processes

2.7 Steel Corrosion and Associated Concrete Damage

Corrosion is an electrochemical process and ordinarily begins at the surface of the steel. (Callister, 1997). Corrosion is the most frequent and serious form of degradation of steel reinforced concrete (Taly, 1998). The corrosion of steel causes deterioration of concrete. The product of steel corrosion, rust, has a volume several times greater than the metallic iron from which it was formed, which causes pressure build-up and cracking in the concrete (Mays, 1992). Young et al. (1998) reported that 0.00004 to 0.0002 inch of corrosion is sufficient to cause

concrete cracking. The resulting cracks often appear in an orientation parallel to the reinforcing steel.

Four main causes for corrosion include carbonation, chloride attack, inadequate concrete cover, and presence of cracks. The effects of corrosion include cracking or spalling, rust staining, corrosion of reinforcing steel, excessive deflection, and ultimately, failure of structural members. Prevention of corrosion must address two factors of environmental factors: those affecting the concrete structure and those affecting the reinforcing steel.

The geometry and type of reinforcing bars can also influence the onset and propagation of corrosion. Mohammed reported that deformed reinforcing bars are more prone to corrosion than plain bars. Kirkpatrick et al. (2001) indicated that typical time to corrosion is approximately 4-6 years for bare reinforcement. The use of various sealers and coatings has also been investigated for preventing deterioration of concrete structures (Ibrahim et al., 1999).

Experimental and modeling work has been conducted to assess and predict the formation of cracks in concrete due to corrosion. Mohammed et al. (2000) conducted experiments to assess the influence of crack width on the rate of corrosion. Mohammed et al. (2000) reported that the simple presence of cracks is more critical than the width of cracks.

Francois and Arligui (1998) conducted 12-year salt fog exposure tests on 10 ft long beams to establish a relationship between cracking in loaded beams and the corrosion of reinforcing steel. Beams were removed from the exposure conditions at various intervals to assess chloride penetration profiles, steel corrosion maps, flexural strength, concrete microstructure, and steel/concrete interfaces. Francois and Arligui (1998) made a distinction between cracks caused by service loads (primary cracks) and cracks caused by rust formation and associated volume changes (secondary cracks). Similar to Mohammed et al. (2000), Francois and Arligui (1998) found that corrosion is not influenced by crack width, which is within the range of cracks produced by service loads, <0.00002 inch crack width. In addition, both w/c ratio of the concrete and load level applied to the structure play more significant roles in defining corrosion onset and propagation than width of cracks. Increased loads produce damage to both the paste/aggregate interface and the steel/concrete interface. After initiation of

corrosion, the surrounding conditions (mostly related to physical and chemical condition of concrete) dominate over the presence of cracks (Mohammed et al., 2000).

Loss of strength due to corrosion is due to a loss in cross section and a degradation of the bond with the concrete. Almusallam et al. (1996) prepared test slabs and induced artificially accelerated corrosion. The slabs were loaded in flexure after varying degrees of corrosion. An initial increase in ultimate strength was observed and attributed to increased frictional bond between the steel and the concrete due to growth of film rust. Almusallam et al. (1996) observed similar modes of failure for low corrosion specimens to control specimens (no corrosion present). Higher degrees of corrosion led to a progressive loss of ductility. At 60% corrosion, the slabs demonstrated equivalent strength to unreinforced slabs (Almusallam et al., 1996). In another study related to mode of failure of corroded sections, Enright and Frangopol (2000) observed that bridges subjected to corrosion may be more vulnerable to shear failure than to flexural failure due to a variety of controlling factors including steel placement, influence of corrosion, and interaction with concrete.

2.8 Critical Chloride Ion Concentration in Concrete Causing Steel Corrosion

The corrosion initiation takes place when a chloride concentration at the reinforcement level reaches a critical level, which is also often referred to as the threshold chloride level (Glass and Buenfeld, 1997; Alonso et al., 2000; Oh et al., 2003; Maheswaran and Sanjayan, 2004; Trejo and Monteiro, 2005; Garces et al., 2005). To initiate corrosion, a threshold concentration of chloride (minimum concentration of chloride necessary to destroy the passive film) is required in excess of the amount immobilized by reaction with C_3A in cement (i.e. bounded).

The threshold concentration of chloride ions to initiate corrosion is complex as it depends on several factors, including the pH value of concrete, the water content, the type of cement, concrete mix proportions, water/cement (w/c) ratio, C_3A content of the cement, blended materials, concentration of hydroxyl ions, relative humidity, the proportion of water soluble chloride, the sulfate content and the temperature (Alonso et al., 2000; Oh et al., 2003; Trejo and Pillai, 2003).

A level of 1.2 to 1.5 lbs/cyd is usually considered a threshold level for uncoated steel in regular reinforced concrete bridge decks (Miki, 1990). Weyers at al. (2006a) maintains that a single critical threshold chloride levels (lbs/cyd) cannot be defined. Rather there exit a range of concentrations that can lead to a state of corrosion of the steel reinforcement. For epoxy coated steel this variability can be expressed by the mean value of 7.85 with a standard deviation of 6.52 and for uncoated reinforcement by the mean value of 4.98 with standard deviation of 4.64.

2.9 Assessment of Bridge Deck Concrete

Assessment of the mechanical properties of bridge deck concrete can be accomplished by conducting destructive testing or by using non-destructive testing methods. Destructive testing provides a direct measurement of mechanical properties but is generally not practical for testing existing infrastructure components. Destructive tests can be conducted on molded cylinders, sampled cores, or molded beams of concrete. Numerous standardized test methods are available for testing concrete strength, durability, permeability, and physical composition (Kosmatka and Panarese, 1988).

A successful nondestructive test is the one that can be applied to concrete structures in the field, and be portable and easily operated with the least amount of cost. Leshchinsky (1991) summarized the following advantages of nondestructive tests, as compared to core testing:

- A reduction in the labor consumption of testing.
- A decrease in labor consumption of preparatory work (such as tedious work associated with determining location and diameters of reinforcement bars).
- A smaller amount of structure damage in testing.
- A lower probability of such structural damage which may cause the need for reinforcement.
- A possibility of testing concrete strength in structures where cores cannot be drilled (thin-walled, densely-reinforced, etc.).
- An application of less expensive testing equipment.

The following section briefly discusses the advantages and disadvantages of common NDT (non-destructive testing) methods. The methods are in situ compressive strength test, corrosion rate measurement, carbonation depth assessment, and estimate of concrete cover.

2.9.1 In-situ Compressive Strength

Assessment of the in situ compressive strength is based on the principle that the rebound of an elastic body depends on the hardness of the surface on which the mass impinges. Hence, the energy absorbed by concrete can be related to its strength. A Schmidt hammer (as per ASTM C 805) normally is being employed for the determination of compressive strength nondestructively. The test method starts by the careful selection and preparation of the concrete surface to be tested. Then, a fixed amount of energy is applied by pushing the hammer against the test surface. The plunger must be allowed to strike perpendicularly to the surface. The angle of inclination of the hammer affects the result. After impact, the rebound number should be recorded. Amasaki (1991) presented the effect of carbonation on the rebound number. Grieb (1958) showed the effect of type of aggregates on the rebound number and hence the estimated strength. Willetts (1958) presented the effect of moisture content of concrete on the results of the rebound hammer test by comparing dry and tested samples. For these reasons, it is necessary to take 10 to 12 readings over the area to be tested because the test is sensitive to the material conditions immediately underneath the plunger (Neville and Brooks, 1994). According to Teodoru (1988), the results obtained are only representative of the outer concrete layer within a thickness of 1.18 – 1.97 inch (30–50 mm) from the surface. Due to the difficulty of acquiring the appropriate correlation data in a given instant, the rebound hammer is most useful for rapidly surveying large areas of similar types of concrete.

2.9.2 Measuring the pH level of Concrete

Carbonation is a process, in which CO_2 reacts with the hydration products of cement and reduces the pH of the concrete pore solution from more than 12 to less than 9. This process promotes the breakdown of the passivity of concrete and initiating the corrosion of reinforcing steel. The concrete carbonation starts by the penetration of CO_2 from air or from water and start reacting to the calcium hydroxide as shown below:

$$Ca(OH)_2 + CO_2 \quad \text{---}> \quad CaCO_3 + H_2O$$

The depth of carbonation can be determined by spraying a solution of 1% of phenolphthalein in 70% ethyl alcohol (CPC-18, 1988). The phenolphthalein solution is colorless but it changes to purple when pH is higher than ≈9. As such, when this solution is sprayed on the common face of the split slices, the carbonated portion remains colorless (i.e., same as the color of concrete) while the non-carbonated portion becomes purple if a deep purple indicator is used. However, if a rainbow indicator is used, a full profile of the pH in the concrete can be found as shown in the Figure 2-5.

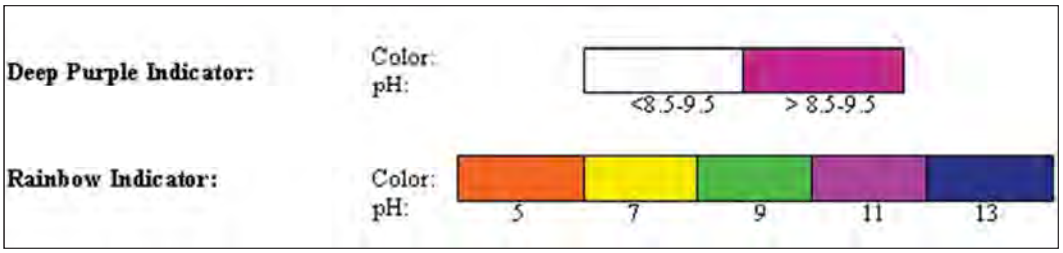

Figure 2-5 Carbonation Depth Measurement of Concrete

2.9.3 Corrosion Risk Assessment by Half-Cell Potential

Rapid, non-destructive techniques such as half-cell potential mapping can detect the localized chloride-induced corrosion of the reinforcement and improve the quality of condition assessment and repair works (ASTM C 876, Elsener 1992 & 2001; Cairns and Melville, 2003; Pradhan and Bhattacherjee, 2009). Electrons flow through the steel to the cathode, driving the half-cell reaction forming hydroxide (OH^-) with the water and oxygen. This principle creates a potential difference that can be measured by the half-cell method. A schematic view of the electric field and the current flow on steel in concrete is presented inFigure 2-6.

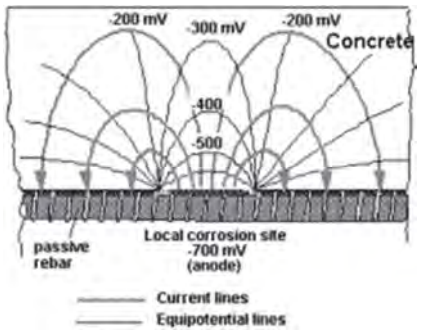

Figure 2-6 Schematic view of the electric field and current flow of an active/passive macrocell on steel in concrete (Elsener 2001)

The susceptibility to reinforcement corrosion, referred to as the half-cell potential, is defined as the voltage measured with respect to a standard electrode. The voltage differential between the reinforcement and the concrete media (as measured on the surface) is defined as the corrosion potential. A reference electrode is connected via a high impedance voltmeter to the steel reinforcement and placed in a grid over the water saturated concrete surface. Typical magnitudes for the half-cell potential of steel reinforcement in concrete measured against a $Cu/CuSO_4$ reference electrode (RILEM TC 154-EMC) are presented in Table 2-2.

Table 2-2 Half-Cell Potential for Different Types of Concrete (RILEM TC 154-EMC)

Concrete Condition	**Half Cell Potential**
Water saturated concrete without O_2	-1000 to -900 mV
Moist, chloride contaminated concrete	-600 to -400 mV
Moist, chloride free concrete	-200 to +100 mV
Moist, carbonated concrete	-400 to +100 mV
Dry, carbonated concrete	0 to +200 mV
Dry, noncarbonated concrete	0 to +200 mV

The main disadvantage of this method is that the potentials measured are sensitive to moisture content, thickness of concrete cover, surface coating, resistivity of concrete, and the type of electrode (Misra and Uomoto 1990).

2.9.4 Corrosion Risk Measurement by Polarization Resistance

The corrosion rate of reinforcement can be estimated from the polarization resistance using the galvanostatic pulse technique. A current pulse (I) is imposed on the reinforcement from a counter electrode placed on the concrete surface. A guard ring confines the current to an area (*A)* of the reinforcement below the central counter electrode. The applied current is usually in the range of 5 to 400 μA and the typical pulse duration is 5 to 10 seconds. The reinforcement is polarized in the anodic direction compared to its free corrosion potential, E_{corr}. The resulting change of the electrochemical potential of the reinforcement is recorded as a function of time using a reference electrode (Ag/AgCl). A typical potential response for reinforcement actively corroding is shown in Figure 2-7.

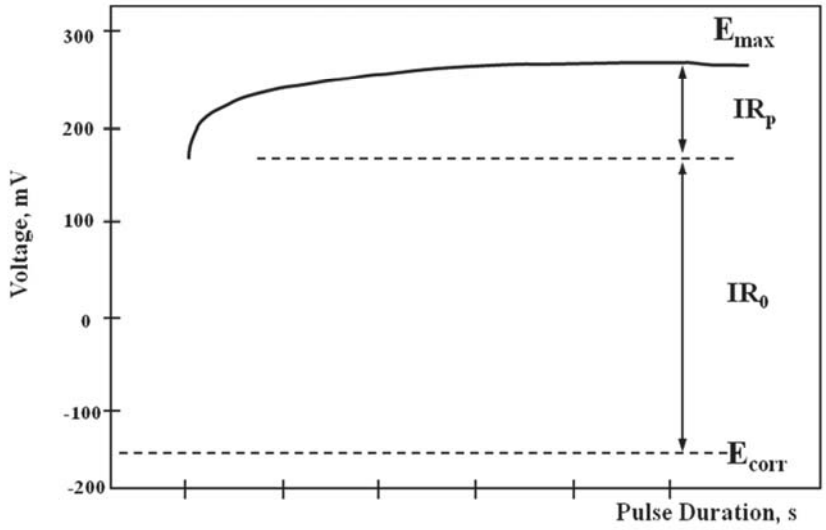

Figure 2-7 A typical response from the GalvaPulse. E_{max}: maximum corrosion potential; IR_0: ohmic potential drop; IR_p: potential due to polarization of the reinforcement; E_{corr}: free corrosion potential.

When the current is applied to the system, there is an ohmic potential drop ($IR_{0)}$ as well as change in potential due to polarization of the reinforcement (IR_p). The polarization resistance of the reinforcement (R_p) is calculated by curve fitting to the transient portion of the potential data. By means of the Stern-Geary equation for active corrosion ($I_{corr} = 26/R_p$) and Faraday's law of electrochemical equivalence, the corrosion rate is estimated as: Corrosion Rate (μm/year) = $11.6\times(I_{corr}/A)$, where A is the confined area (in cm^2) of the reinforcement below the central counter electrode. The factor 11.6 is for uncoated steel. The value of R_0, the electrical resistance of the concrete between the counter electrode and the reinforcement, is also determined. Note that method reports results in metric units.

Glass et al. (1993) have examined the galvanostatic pulse technique as an alternative method of impedance analysis for steel corrosion in mortar under immersed condition and reported this method as a suitable technique for measuring the corrosion rate of steel. A recent research investigation carried out by Sathiyanarayanan et al. (2006) have also recommended the galvanostatic pulse technique as a reliable alternate method for measuring the corrosion rate of steel in concrete. A typical schematic potential transient for a current pulse under galvanostatic condition, presented by Sathiyanarayanan et al., (2006) is depicted in Figure 2-8.

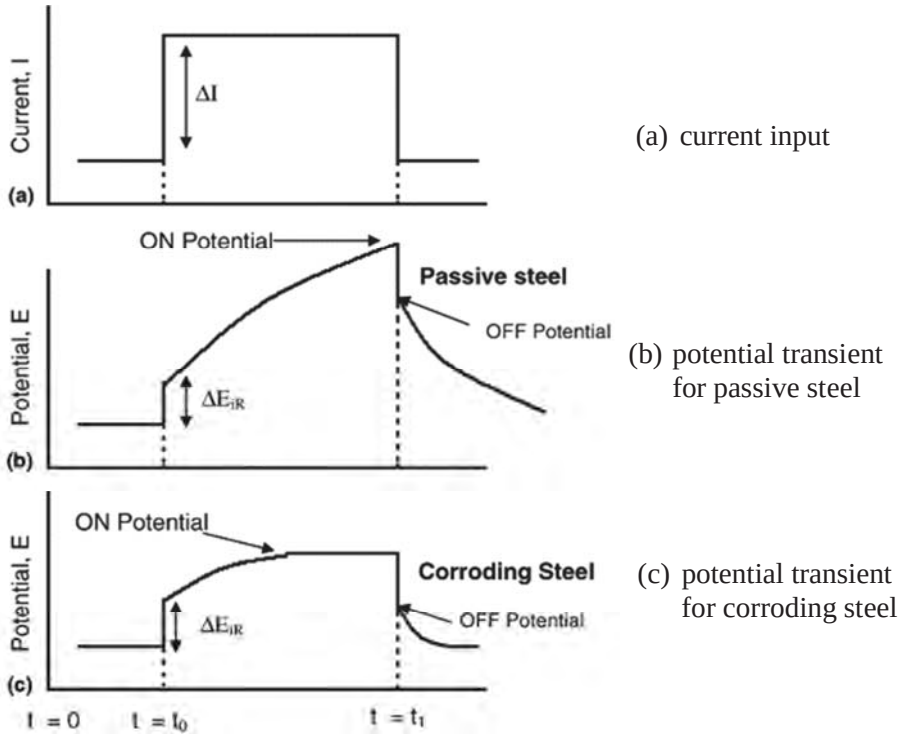

Figure 2-8 Nature of potential transient of steel in concrete for a galvanostatic current pulse

2.10 Diffusion Coefficient of Concrete in Bridge Deck

The ability of concrete to resist the penetration of chloride ions is a critical parameter (Thomas 1998). Prediction model for the ingress of chlorides into concrete should consider the complex combination of several transport processes (Neville 1995; Kropp et al.,1995) that include diffusion, capillary sorption (absorption of water containing chlorides into unsaturated concrete), and permeation (water flow in concrete due to a pressure gradient). However, diffusion of chlorides into a concrete bridge deck exposed to the periodic application of deicing salts can be assumed to be the governing transport mechanism (Cady & Weyers, 1983). Once the chlorides have penetrated the concrete, reached the reinforcement and the concentration is above critical chloride content value, the corrosion of the reinforcement can be initiated (Lounis et al.,

2004). The time-dependent distribution of chloride concentration over the depth of the bridge deck can be obtained from the solution of Fick's second law of diffusion.

Fick's second law of diffusion is a convenient mathematical model to describe the diffusion processes of chloride ingress in a concrete structure. The value of chloride diffusion coefficient in the diffusion equation during the transient transport phase can be regarded as a variable dependent on chloride content varied with time and depth. Assuming that the concrete deck is a homogeneous isotropic semi-infinite medium, and assuming constant boundary condition; the initial chloride (C_i), exposed surface chloride content (C_s) and diffusion coefficient, the chloride content at depth x and time t is given by:

$$C(x, t) = C_i + (C_s - C_i)\ \mathrm{erfc}\left(\frac{x}{\sqrt{4tD}}\right) \qquad \text{(Equation 2-1)}$$

Where,

$C(x, t)$ = chloride content at depth x and time t

C_i = initial chloride content

C_s = chloride content of the exposed concrete surface

D = constant diffusion coefficient

Erfc = error function

Despite its simplicity and extensive use, this model has some shortcomings, because:

- The diffusion coefficient is not a constant but rather depends on time, temperature, and depth because of the heterogeneous nature and aging of concrete (Cady and Weyers 1982; Neville 1995; Kropp et al., 1995); and
- The top surface of the bridge deck is subjected to a continually changing chloride exposure.

The chloride concentration at the deck surface varies with the season, however at some shallow depth near the deck surface (½ inch), the chloride concentration, referred to as near-

surface chloride concentration can be assumed at a quasi-constant maximum chloride content of exposed concrete surface (C_s) (Cady & Weyers, 1982).

The diffusion coefficient values obtained from Equation 2-1 represents the diffusivity of the concrete during sampling. Studies show that diffusion coefficient decreases with time, Thomas et al. (1998) proposed the time dependent diffusion coefficient as:

$$D_t = D_{28}\left(\frac{t_{28}}{t}\right)^m \qquad \text{(Equation 2-2)}$$

Where,

D_t = diffusion coefficient at time t,

D_{28}= diffusion coefficient at time t_{28}, (28 days)

m = diffusion reduction coefficient. (m=0.1 for Portland cement, Thomas et al., 1998)

The relationship is consistent with similar mathematical descriptions proposed by Mangat et al. (1994) and M. Maages et al. Equation 2-2 can be used to determine the diffusivity at any time given the diffusivity at time of sampling.

2.11 Estimation of Time from Corrosion Initiation to Corrosion Cracking in Concrete

Chloride-induced steel corrosion is one of the major problems for steel reinforced concrete structures. The high alkaline environment of concrete forms a passive film on the surface of the embedded steel which normally prevents the steel from further corrosion (Page and Treadaway 1982). However, under chloride attack, the passive film is disrupted or destroyed, and the steel corrosion starts (Townsend et. al., 1981; Verbeck, 1975). In addition to loss of concrete cover, a reinforced-concrete member may suffer structural damage due to loss of bond between steel and concrete and loss of reinforcement cross-sectional area (Mehta, 1973).

The accurate prediction of deterioration and its effect on corrosion-induced cracking is essential for determining the service life of the existing structures. Many studies have developed

corrosion-induced cracking models linking the surface crack width to corrosion and service life (Maaddawy and Soudki, 2007; Al-Harthy and Stewart, 2006; Li et al., 2004; Vu and Stewart, 2005; Stewart and Mullard, 2007)

Researchers intended to model the cracking behavior caused by corrosion using nonlinear fracture mechanics and/or finite element analysis (Molina FJ et al., 1993; Hansen EJ et al., 1999; Pantazopoulou SJ et al., 2001). In the models crack propagation was governed by energy considerations. Although these models represent the cracking behavior in more detail, they do not lend themselves to be used by practicing engineers.

Bazant (1979) suggested a mathematical model to calculate the time between corrosion initiation and corrosion cracking of concrete bridge decks. According to Bazant's model, the time from corrosion initiation to corrosion cracking is mainly dependent on corrosion rate, cover depth, spacing between steel reinforcing bars, diameter of the steel reinforcing bar, and properties of concrete such as tensile strength, modulus of elasticity, Poisson's ratio, and creep coefficient. Liu and Weyers (1998) points out a significant limitation of Bazant's model to be the assumption that all corrosion products create pressure on the surrounding concrete which will predict early corrosion cracking. The work of Bazant was extended by Liu and Weyers (1998). Liu and Weyers modeled the time from corrosion initiation to corrosion cracking based on the amount of corrosion products required to cause cracking of concrete cover. The model includes same parameters used in Bazant's model but it takes into account the time required for corrosion products to fill a porous zone around the steel reinforcing bar before creating an internal pressure on the surrounding concrete. In Liu–Weyers's model, the rate of steel mass loss caused by corrosion was assumed to decrease as time progresses. The rate of steel mass loss was assumed to be directly proportional to the square root of the product of the corrosion current and the time of corrosion exposure. For the same time of corrosion exposure, this assumption significantly underestimates the amount of steel weight loss compared with that obtained by using Faraday's law (Masound SG 2002). Underestimating the rate of steel loss caused by corrosion would result in overestimating the time to corrosion cracking.

As discussed by Maaddawy and Soudki (2007), a Japanese researcher, Morinaga, proposed an empirical equation based on field and laboratory data to predict the time from corrosion initiation to corrosion cracking. According to Morinaga's equation, the time from corrosion initiation to corrosion cracking is function of corrosion rate, concrete clear cover, and steel bar diameter. The empirical equation proposed by Morinaga does not account for the mechanical properties of concrete which would significantly affect the time to corrosion cracking.

The model proposed by Maaddawy and Soudki (2007) presents a simple mathematical model that can be used by practicing engineers and researchers to reasonably predict the time from corrosion initiation to corrosion cracking. This model relates the steel mass loss and the internal radial pressure caused by the expansion of corrosion products developed. The concrete around a corroding steel reinforcing bar is modeled as a thick-walled cylinder with a wall thickness equal to thinnest concrete cover. The concrete ring is assumed to crack when the tensile stresses in the circumferential direction at every part of the ring have reached the tensile strength of concrete. The internal radial pressure at cracking is then determined and related to steel mass. With the help of Faraday's law, the time from corrosion initiation to corrosion cracking is then predicted. The internal radical pressure caused by corrosion (P_{cor}) and time from corrosion initiation to corrosion cracking (T_{cr}) is given in Equation 2-3 and Equation 2-4.

$$P_{cor} = \frac{2M_{loss}E_{ef}\left[\left(1/0.622\rho_r\right)-\left(1/\rho_s\right)\right]}{\pi D\left(1+\nu+\psi\right)\left(D+2\delta_0\right)} - \frac{2\delta_0 E_{ef}}{\left(1+\nu+\psi\right)\left(D+2\delta_0\right)} \qquad \text{(Equation 2-3)}$$

$$T_{cr} = \left[\frac{7117.5\left(D+2\delta_0\right)\left(1+\nu+\psi\right)}{iE_{ef}}\right]\left[\frac{2Cf_{ct}}{D} + \frac{2\delta_0 E_{ef}}{\left(1+\nu+\psi\right)\left(D+2\delta_0\right)}\right] \qquad \text{(Equation 2-4)}$$

Where,

C = clear concrete cover (mm)

D = diameter of steel reinforcing bar (mm)

E_{ef} = effective elastic modulus of concrete

f_{ct} = tensile strength of concrete

I = current density

P_{cor} = internal radial pressure caused by corrosion

T_{cr} = time from corrosion initiation to corrosion cracking

M_{loss} = mass of steel per unit length consumed to produce M_r

M_r = mass of rust per unit length

δ_0 = thickness of porous zone

v = Poisson's ratio (0.18 for concrete)

ρ_s = mass density of steel

ρ_r = mass density of rust

ψ = factor depends on D, C and δ_0

The following are assumptions for this model:

1. There is a porous zone around the steel reinforcing bar which the corrosion products must first fill before the products introduce internal pressure on the surrounding concrete.
2. Corrosion products are formed uniformly around the steel reinforcing bar which results in a uniform expansive stresses around the steel bar.
3. The volume expansion caused by corrosion creates strain only in concrete. It means the strain in steel is neglected.
4. Units are metric.

2.12 Environmental Scanning Electron Microscope Study of Corroded Concrete

Environmental Scanning Electron Microscope (ESEM) is a powerful microscope used to characterize wet, oily, dry, porous and soft materials and produces high-resolution images of a sample surface revealing details less than a nanometer (10^{-9} of a meter) in size with a maximum magnification of more than 500,000 times. Moreover, it has ability to generate localize chemical element analysis by Energy Dispersive Analysis using X-ray (EDAX). Furthermore, specimens can be viewed with no or minimal preparation, in their natural state or in vacuum. Microstructural studies using electron microscopy are very useful in studying the concrete deterioration mechanism, the nature of the damage, and the products of deterioration. A brief account of literature review is presented here.

Lloyd and Heidersbach (1985) described the application of the SEM in postmortem analyses of corrosion and cracking problems in a variety of metal-reinforced systems. Examples were given for the investigation of the failure mode of metals, such as brittle failure, fatigue failure, and ductile failure modes. Examination of corrosion products on the surface of the metal, or cement paste clinging to the rusty metal can reveal the cause of the corrosion. Localized chemical analysis on the rusted bar can give indications as to the time relation between the occurrence of crack and the occurrence of rust.

Ollivier (1985) demonstrated that SEM can be used to study surface micro cracks. He used replica made with a film (acety-cellulose) to get a "print" of the surface to be studied. The film was slightly dissolved in methyl acetate and then put on the surface to be printed. The replica was then observed by the SEM. It was demonstrated that observation of the network of micro cracks on the external surface of concrete is possible with a higher resolution.

Sarkar et al. (1992) investigated mortar cut from the excavated wall and foundation of Champ-de-Mars, Montreal, which date back to the seventeenth century, using XRDA, SEM/EDXA, and optical microscopy. SEM/EDXA detected prismatic calcium carbonate crystals indicative of pronounced carbonation, grain periphery discoloration and aggregate corrosion indicative of alkali-aggregate reaction, and secondary ettringite attributable to the more recent application of de-icing salts above ground. XRD analysis showed the presence of an argillaceous component. It is suggested that the original composition probably comprised calcined lime mixed with burnt clay, the latter used to generate pozzolanic activity. Marusin (1993) carried out extensive studies using SEM/EDXA, and suggested that at least some of the concrete failures, which were regarded as caused by alkali-silica reaction, were actually caused by delayed ettringite formation (DEF).

It is reported by Yuan and Ji, 2009 that the interfacial transition zone (ITZ) between un-corroded steel bar and concrete shows characteristic of high porosity. The high porosity in the ITZ offers space for expansion of corrosion products. During the corrosion process, the corrosion products diffuse into the ITZ, and the ITZ transforms into the corrosion products layer consisting of concrete and corrosion product, and the expansive pressure is developed. Before concrete

cover cracking, the corrosion products layer is distributed on the side facing the concrete cover only; nearly no corrosion is found at the side away from the concrete cover. It is observed from the sample specimen pictures, the typical porous zone thickness is in the range of 0.0254-0.0505 inch (30-60 μm). The majority of the instrumentation reports results in metric units (such as μm) and throughout this report dual units will be reported on this property..

Wong et al. (2010) reported in their investigation that corrosion of steel in reinforced concrete produces soluble corrosion products that can migrate or diffuse through the cement paste. This study observed that the corrosion products can be deposited in air voids, in the outer and inner hydration products and in rims and relicts of reacted slag. A distinct boundary between the affected and unaffected paste areas can be seen in BSE (back scattered electron) images, indicating the extent of the penetration front. The corrosion products penetrate the aggregate-paste ITZ as well as the 'bulk' paste farther away. The affected paste areas have higher analysis totals, and Fe and O contents, but are depleted in Ca. The latter indicates that dissolution of portlandite and partial decalcification of the C–S–H gel have occurred. This increases the local porosity and diffusivity, which then facilitate corrosion product transport. However, it is also reported by the authors that when the pores become filled or blocked by solid corrosion products, subsequent products are forced to accumulate at the steel–concrete interface, inducing expansive pressure that leads to bond failure and cracking of the concrete cover.

Other interesting applications include the investigation into the cause of warping of precast panels by Shayan (1985), the study by Sarkar (1992) of the deterioration of building materials, concrete, brickwork, and rendering mortars, of various old buildings as old as 60 years, and the interesting study by Shayan and Quick (1992) on the cracking of prestressed, steam-cured concrete sleepers revealing the formation and combined action of alkali-aggregate reaction products and secondary ettringite.

2.13 Summary

It has been found from the literature that the threshold chloride concentration is an important parameter. Initiation time for the corrosion of steel depends largely on the level of chloride ions present in the concrete at the reinforcement level. Furthermore, cracks provide an

indication of the deterioration of bridge decks. An inter relationship exists between the crack initiation and the onset of rust development in the steel. However, corrosion may also occur without visual evidence on the concrete surface such as cracking or stain. Deterioration in terms of spalling and delamination, are largely dependent on environmental loads associated with the freeze/thaw and the use of deicing salt (chloride exposure). The use of multiple NDT methods combined with visual inspection and coring are effective in assessing the bridge deck performance.

Fick's second law of diffusion is considered to be a convenient mathematical model to describe the diffusion processes of chloride ingress in a concrete structure. The value of chloride diffusion coefficient in the diffusion equation during the transient transport phase can be regarded as a variable dependent on chloride content varied with time and depth. These values can be used to calculate the time taken for chloride concentration to reach critical value at the level of the reinforcement.

It is also found from the literature that Maaddawy and Soudki's model can be used to predict the time from corrosion initiation to corrosion cracking. The thickness of the porous zone, which is determined by ESEM (Environmental scanning electron microscope), is an important parameter in determining time from corrosion initiation to corrosion cracking in the model.

CHAPTER 3: METHODOLOGY OF LABORATORY TESTS

3.1 Introduction

The experimental program was designed to provide an investigation of the performance and durability of bridge decks constructed using a concrete with and without introduced chloride and normal reinforcement under different environmental exposure conditions. A total of 20 specimens were constructed for this purpose. Sixteen specimens were constructed using the chloride introduced concrete mix design and four specimens were constructed using the non-chloride introduced mix. Several destructive and non-destructive tests were conducted at different stages of the environmental conditioning to identify risk of spalling, and the influence of various types of environmental exposures on the structural behavior including the ultimate flexural load carrying capacity. The environmental exposure conditions included: service load exposure, freeze-thaw exposure, saltwater exposure, and repeated load cycles.

3.2 Overview

A summary flow chart for the experimental program is shown in Figure 3-1. The chart includes the chronological application of the environmental exposure conditions, the number of specimens assigned for each exposure, the duration of each exposure, and the different types of destructive and nondestructive tests conducted at various stages of the test program.

All of the specimens were subjected to a predefined service load application before any environmental conditioning. The purpose of this load application was to create cracks, along the bottom side of all of the specimens, representing a possible serviceability condition. These cracks allow water and oxygen to penetrate to the reinforcement location during the freeze/thaw and saltwater exposures.

The various types of environmental exposure conditioning and the number of specimens designated for each exposure are shown in Table 3.1. Four specimens, two from each mix type, were designated as control specimens. These specimens were not subjected to any freeze-thaw, saltwater, or repeated load exposure.

Eight specimens, constructed from the chloride introduced mix design, were subjected to a combined effect of saltwater exposure and repeated load (termed saltwater specimens). Two saltwater specimens were exposed to saltwater for 3,000 hours and also exposed to a total of 1,000,000 cycles of repeated load; two saltwater specimens were exposed to saltwater for 6,000 hours and exposed to a total of 2,000,000 cycles of repeated load; two saltwater specimens were exposed to saltwater for 8,000 hours and exposed to a total of 2,000,000 cycles of repeated load; and the last two saltwater specimens were exposed to saltwater for 10,000 hours and exposed to a total of 3,000,000 cycles of repeated load.

Six specimens from the chloride induced concrete mix design and two specimens from the non-chloride induced concrete mix design were subjected to a combined effect of freeze/thaw cycles and repeated load (termed freeze/thaw specimens). Five freeze/thaw specimens (three from the chloride mix and two from the non-chloride mix) were exposed to 300 freeze/thaw cycles and exposed to a total of 1,000,000 cycles of repeated load. The final three freeze/thaw specimens were exposed to 600 freeze/thaw cycles and exposed to a total of 2,000,000 cycles of repeated load.

Non-destructive tests using GalvaPulse, CANIN and SilverSchmidt concrete hammer were performed on all specimens at given intervals throughout the test program. GalvaPulse was used to evaluate the corrosion rate of the steel reinforcement. CANIN was used to evaluate the half-cell electrical potential of the reinforcement. The SilverSchmidt hammer was used to evaluate the surface hardness. Each specimen was subject to static as well as repeated load test at various stages of the environmental exposure program. Also, Rapid Chloride Test was used to determine the chloride content on concrete powder samples taken from selected specimens before and after the specimens were exposed to the environmental loads. At the end of the exposure tests, all of the specimens were loaded to failure in a four point loading configuration.

Moreover, after the ultimate load test was performed, an environmental scanning electron microscope (ESEM) was used to determine the corrosion state of the reinforcement and the concrete porous zone thickness between the reinforcement and the surrounding concrete. The ESEM test was performed on 3in. × 3in. × 1.5in. samples cut from the specimens.

Each specimen was identified by the type of environmental exposure condition and the duration of the exposure. The first letter of the labels identified the kind of environmental exposure; control specimens were labeled “C”, while saltwater specimens were labeled “S” and freeze/thaw specimens were labeled “F”. The next letter of the label identified the type of the specimen; specimens constructed with the chloride mix were labeled “WC”, while specimens constructed with the non-chloride mix were labeled “WO”. For the freeze/thaw specimens, the number after the letters “WO” or “WC” identified the number of freeze/thaw cycles in hundreds. For the saltwater specimens, the number after the letter “WC” identified the time for the saltwater exposure in hundreds of hours. The final number in the specimen label identified the specimen number in the group. For example, sample S-WC-30-1 means saltwater specimen #1 with chloride mix subjected to 3000 hours of saltwater ponding.

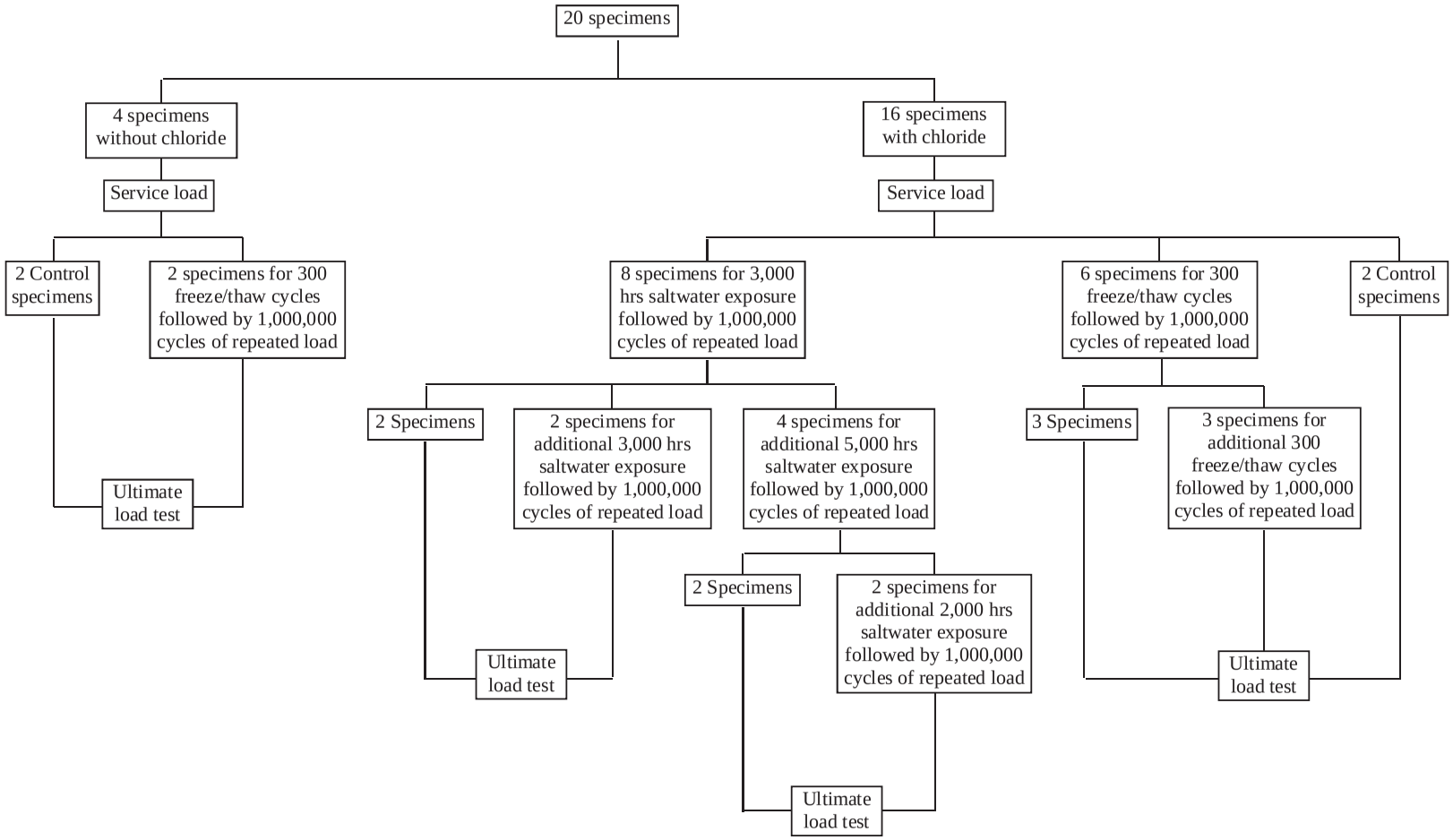

Figure 3-1 Summary flow chart for the experimental test program

Table 3-1 Specimens labeling and the types of exposure conditioning

Environmental Exposure Condition	Labels	Sequence of Environmental Exposure Conditioning
Control	C-WO-1 C-WO-2 C-WC-1 C-WC-2	Service Load
3000 Hours Saltwater	S-WC-30-1 S-WC-30-2	Service Load 3,000 hours of saltwater 1,000,000 cycles of repeated load
6000 Hours Saltwater	S-WC-60-1 S-WC-60-2	Service Load 3,000 hours of saltwater 1,000,000 cycles of repeated load 3,000 hours of saltwater 1,000,000 cycles of repeated load
8000 Hours Saltwater	S-WC-80-1 S-WC-80-2	Service Load 3,000 hours of saltwater 1,000,000 cycles of repeated load 5,000 hours of saltwater 1,000,000 cycles of repeated load
10,000 Hours Saltwater	S-WC-100-1 S-WC-100-2	Service Load 3,000 hours of saltwater 1,000,000 cycles of repeated load 5,000 hours of saltwater 1,000,000 cycles of repeated load 2,000 hours of saltwater 1,000,000 cycles of repeated load
300 Cycles Freeze/Thaw	F-WO-3-1 F-WO-3-2 F-WC-3-1 F-WC-3-2 F-WC-3-3	Service Load 300 freeze/thaw cycles 1,000,000 cycles of repeated load
600 Cycles Freeze/Thaw	F-WC-6-1 F-WC-6-2 F-WC-6-3	Service Load 300 freeze/thaw cycles 1,000,000 cycles of repeated load 300 freeze/thaw cycles 1,000,000 cycles of repeated load

3.3 Test Specimens

The specimens were constructed to have similar depth and span as the typical bridge decks on steel girders as used by the Michigan Department of Transportation (MDOT). The materials used to design the concrete mix met the MDOT Standard Specifications for Construction section 701.03.

3.3.1 Materials

The MDOT bridge deck concrete mix used for constructing the specimens was D-MR (limestone aggregate, air entrainment, and water reducing admixture) obtained from a single truck mixer. Test cylinders and rectangular prisms were also constructed from the same concrete mix design. The cylinders were used to evaluate the compressive strength and the rectangular prisms were used to evaluate the flexural strength of the concrete at various stages of the test program. The mix design had a water-cement ratio of 0.41. The sand used in the mixture was 2NS Smelter Bay and the coarse aggregate used was 6AA Limestone Manitoulin Dolomite. The Limestone Manitoulin Dolomite was selected due to its superior resistance to abrasion and to freeze-thaw cycles, and air entrainment. The cement – sand – coarse aggregate ratio by weight was 1.00 – 1.74 – 2.65 (658 lbs. - 1148 lbs. - 1741 lbs.). The mixture included 0.8 oz./cwt./cubic yard of air entraining admixture, 5.5 oz./cwt./cubic yard of water reducing admixture and 7.0 oz./cwt./cubic yard of mid-range water reducing admixture.

The chloride introduced concrete mix had 10 lbs./cubic yard of chloride. In order to get the chloride mix 48.75 lbs of 32% calcium chloride solution was used. The relationship between the chloride and the calcium chloride solution is as follows; a calcium chloride solution of 32% was used, and proportion of chloride in 1 mole of calcium chloride is 64%, thus the total chloride added to 1 cyd of concrete is 48.75 lbs * 0.32 * 0.64 = 9.984 lbs of chloride.

The air content, as determined by using ASTM C231/ C231M, was 6.0% for the non-chloride introduced concrete mix and 6.2% for the chloride introduced concrete mix. The measured slump, as determined by using ASTM C143/ C143M-98, was 5.25 in. for the non-chloride mix and 6.5 in. for the chloride mix.

Uncoated reinforcement bars were used for all specimens. The main reinforcement for both the top and bottom of the specimens was #5 bars. This size conforms to the minimum slab reinforcement requirements of the Michigan Department of Transportation (MDOT Bridge Design Manual section 7.04.01). The secondary reinforcement for both bottom and top reinforcement bars was #4 bars. The nominal yield strength of the reinforcement was 60 ksi with a modulus of elasticity (Young's modulus) of 29,000 ksi.

3.3.2 Specimens Geometry and Fabrication

Bridge Deck Beam Specimens

Specimens were fabricated to represent typical Michigan bridge deck sections. Twenty identical specimens were constructed using conventional removable wooden forms. Box-shaped wooden forms were made using 0.75 in. thick plywood and wooden stiffeners with a cross-section of 2.0 in. x 4.0 in. The dimensions and reinforcement details for specimens are presented in Figure 3-2. The specimen's dimensions were 9 in. depth, 18 in. width and 74 in. length.

The bottom reinforcement was extended 1.5 in. to one edge of each specimen and stainless steel screw (1.0 in. long with a diameter of 0.25 in.) was attached to each extended reinforcement bar. The extended 1.5 in. length of bottom reinforcement was coated with epoxy to avoid inadvertent development of corrosion. The stainless steel screw was used to enable the measurement of the corrosion rate and the potential in the reinforcement using GalvaPulse and CANIN instruments, respectively. The detail of the stainless steel screw is shown in Figure 3-2(c) and Figure 3-3.

The top and bottom longitudinal reinforcement layers consisted of three #5 bars with a center-to-center spacing of 7.5 in. The top and bottom transverse reinforcement bars were #4 bars with 8.5 in. center-to-center spacing. The thickness of the clear concrete cover for the longitudinal reinforcement was 3 in. for the top and 1.5 in. for the bottom and ends. The top longitudinal reinforcement was bent with a radius of 2.25 in. to form a hook in order to provide sufficient development length. Twenty cages were assembled using 0.08 in. diameter steel wire to tie the reinforcement bars together as shown in Figure 3-4 and Figure 3-6.

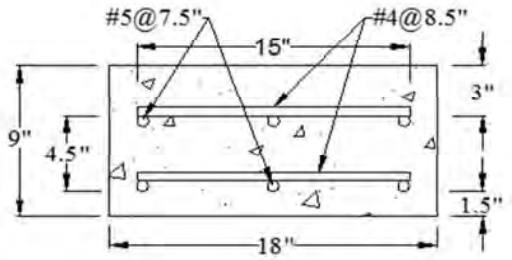

(a) Cross section

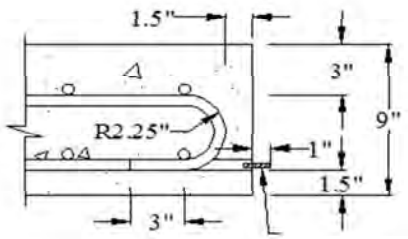

(c) Detail A

Stainless steel screw

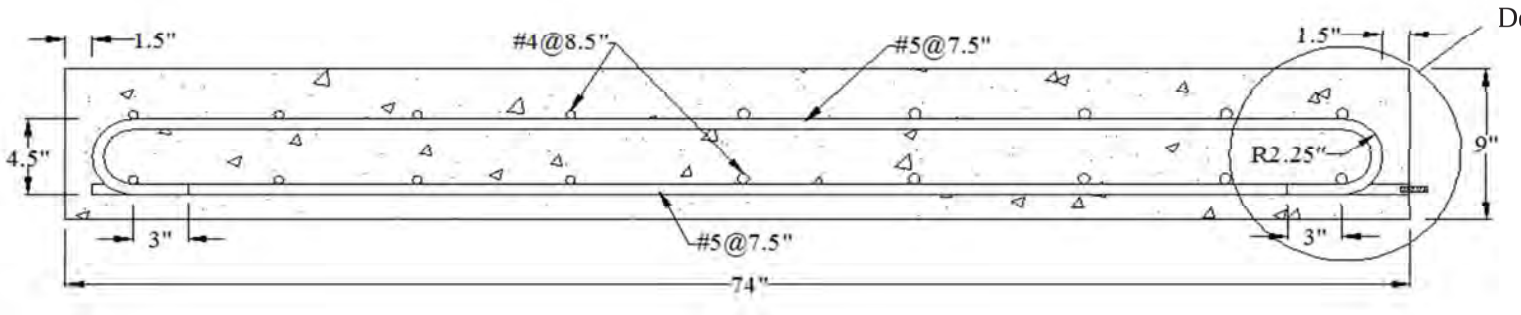

(b) Elevation

Figure 3-2 Dimensions and reinforcement details for specimens

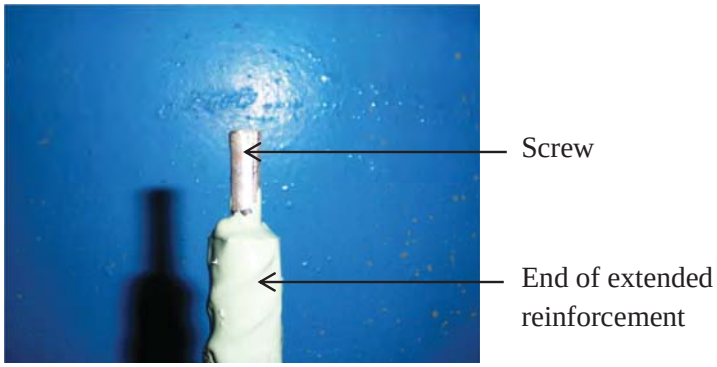

Figure 3-3 Stainless steel screw connected to bottom reinforcement

Figure 3-4 Reinforcement tied together with steel wire

Steel chairs were used to maintain the vertical and lateral distances for the reinforcement cage as well as to ensure the clear cover (Figure 3-5). Three chairs of 1.5 in. height were placed under the bottom reinforcement layer at 17 in. apart. Four additional chairs were placed inside each form to maintain the lateral portion of the cages.

Thermocouples were installed in the specimens to monitor the temperature of the specimens during the environmental exposures. Each specimen was instrumented with two

thermocouples located at the core of the specimen. These thermocouples were placed at the specified location before casting concrete as shown in Figure 3-7. In addition, the specimens that were exposed to freeze/thaw cycles were instrumented with thermocouples on the top surface.

Figure 3-5 Steel chair

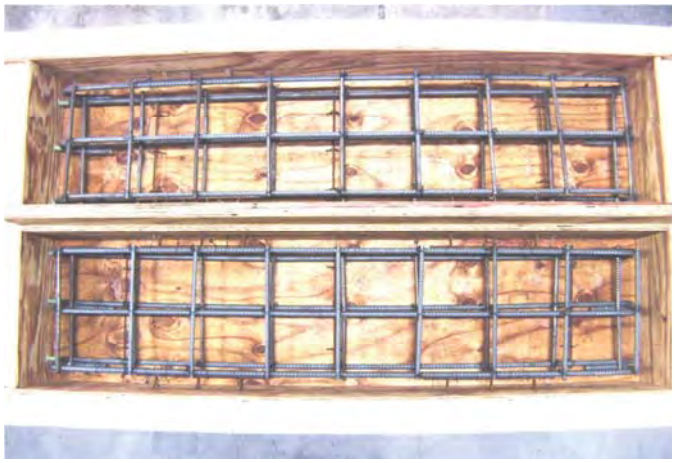

Figure 3-6 Complete forms with the cages

Figure 3-7 Thermocouples located at core of the specimen before casting concrete

Cylinders and Rectangular Prisms

Fifteen cylinders made from the chloride introduced concrete mix and another fifteen cylinders made from the non-chloride introduced concrete mix were prepared to assess the compressive strength gain at various ages of the concrete. The diameter of the cylinders was 6 in. and the height was 12 in. All cylinders were submerged in water until they were taken out for compressive strength test at either 1, 3, 7, 28 or 90 days.

Six rectangular prisms made from the chloride introduced concrete mix and another six prisms made from the non-chloride mix were prepared to evaluate the 28-day flexural strength of the concrete. The dimensions of the prisms were 6 in. x 6 in. x 22 in. and all the prisms were submerged in water until the time of testing.

3.4 Environmental Exposures

The environmental exposure tests were designed to subject the specimens to conditions that simulate possible exposure conditions for bridge deck slabs in Michigan. All specimens were subjected to an initial load to introduce pre-cracks. Four specimens were used as control specimens and the remaining 16 specimens were subjected to the following two categories of environment conditionings: 1) freeze/thaw exposure and repeated load cycles, 2) saltwater exposure and repeated load cycles (also refer to Table 3.1 and Figure 3-1).

3.4.1 Service Cracking Load Test

As mentioned above, the specimens were subjected to cracking load level ensuring that hairline cracks were induced before the concrete deck specimens were exposed to the environmental load. The loading setup was a positive moment load configuration to induce cracking in the bottom regions of the specimens. Cracks with crack widths ranging from 0.004 in. to 0.01 in. were created to simulate cracks that could potentially exist in the service state. Sides of the specimens were covered with a thin mix of water and flour to achieve a whitish surface so that cracks could be visually observed and measured.

Positive Moment Load Setup

The positive moment load setup consisted of a four-point loading system as shown in Figure 3-8. The distance between the left and right supports was 63.0 in. The overhang of each specimen was 5.5 in. away from both supports. The vertical and horizontal alignments of the load setups were verified prior to initiation of the service load application. Supports for the setup were designed to provide a hinged support at one end and a roller support at the other end of the specimen.

Each specimen was instrumented with 2 linear potentiometers at the left and right midspan edges to monitor vertical displacement. The load was applied using a 50 kip actuator. A data acquisition system was used to collect the load-displacement response of a specimen during test (Figure 3-9).

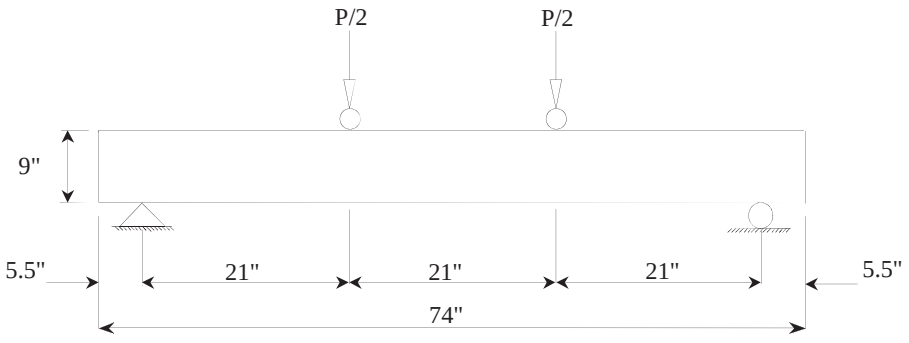

Figure 3-8 Positive moment load setup

(a) Actuator applying load on the specimen

(b) Controllers and data acquisition

Figure 3-9 Actuators, controllers, and data acquisition

Application of Cracking Load

A series of loads starting from 2 kips to 16 kips at increments of 2 kips were applied to the specimens to create cracks on the bottom side. A constant loading and unloading rate of 0.02 in. per minute was used. Load increased with increasing displacement initially, which was followed by constant load with increasing displacement indicating the development of cracking in the specimens. Presence of multiple cracks in the specimens having a width range of 0.004 in. to 0.01 in. was observed at loads of 14 kips and 16 kips (Figure 3-10).

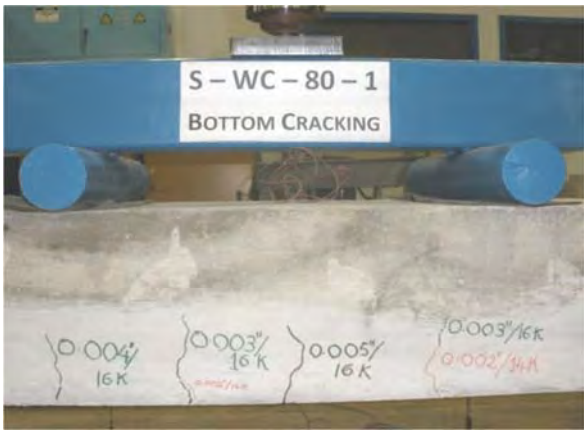

Figure 3-10 Cracks along the bottom of specimen

3.4.2 Freeze/Thaw Cycles

In this test program, eight bridge deck specimens, two specimens from the non-chloride mix and six from the chloride mix, were subjected to freeze/thaw exposure. Five specimens, two specimen with non-chloride mix and six with chloride mix, were exposed to a total of 300 freeze/thaw cycles and the remaining three specimens made from the chloride mix were exposed to a total of 600 freeze/thaw cycles (see Table 3.1). The specimens were subjected to the freeze/thaw cycles in a large (25.0 ft x 13.0 ft x 15.5 ft) walk-in environmental chamber (Figure 3-11). The eight specimens were placed inside a holding tank in the chamber. The holding tank had dimensions of 14.0 ft. x 4.5 ft. x 2.75 ft.

Figure 3-11 Freeze/Thaw Chamber

Thermocouples were extended from the core of each specimen and connected to a data acquisition system located outside the chamber. In the holding tank, the specimens were separated by wooden spacers to allow uniform exposure to all surfaces of each specimen as shown in Figure 3-12. Air ducts and ply-woods were used to improve circulation of air in the holding tank.

(a) Placement of specimens in holding tank (b) Spacers on first layer of specimens

Figure 3-12 Placement of freeze/thaw specimens in the holding tank

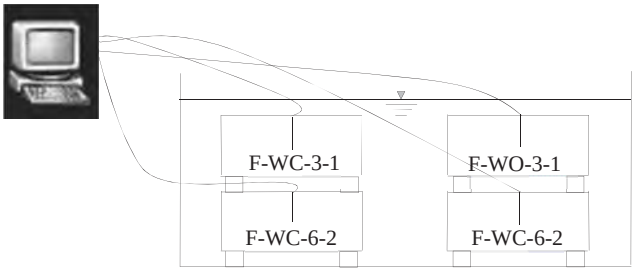

Figure 3-13 Arrangement of freeze/thaw specimens in holding tank

The freeze/thaw exposure was applied according to ASTM C 666/C 666M – 03 "Standard Test Method for Resistance of Concrete to Rapid Freezing and Thawing" with two deviations. First, the cycle time was increased due to the large thermal inertia (size) of the specimens. Second, the specimens did not remain completely submerged for the entire cycle. In the modified procedure, the specimens were subjected to a 3-stage cycle: freezing period, thawing period, and soaking period. The total duration of each freeze/thaw cycles was approximately 7 hours and 48 minutes. The dry freezing period had a duration of approximately

3 hours and 48 minutes and was induced using flowing air cooled to approximately –76 ºF. The dry thawing period of the cycle had a duration of approximately 2 hours and 12 minutes. and was induced using flowing air, heated to approximately 140 ºF. The soaking period of the cycle had a duration of approximately 1 hour and 48 minutes and consisted of soaking the specimens in water at a temperature of approximately 40 ºF. Exact durations of the freezing and thawing periods were controlled to reach core temperatures of the specimens of 0ºF and 40ºF for freezing and thawing, respectively. The variations of temperatures with time during the modified freeze/thaw test procedure are provided in Figure 3-14.

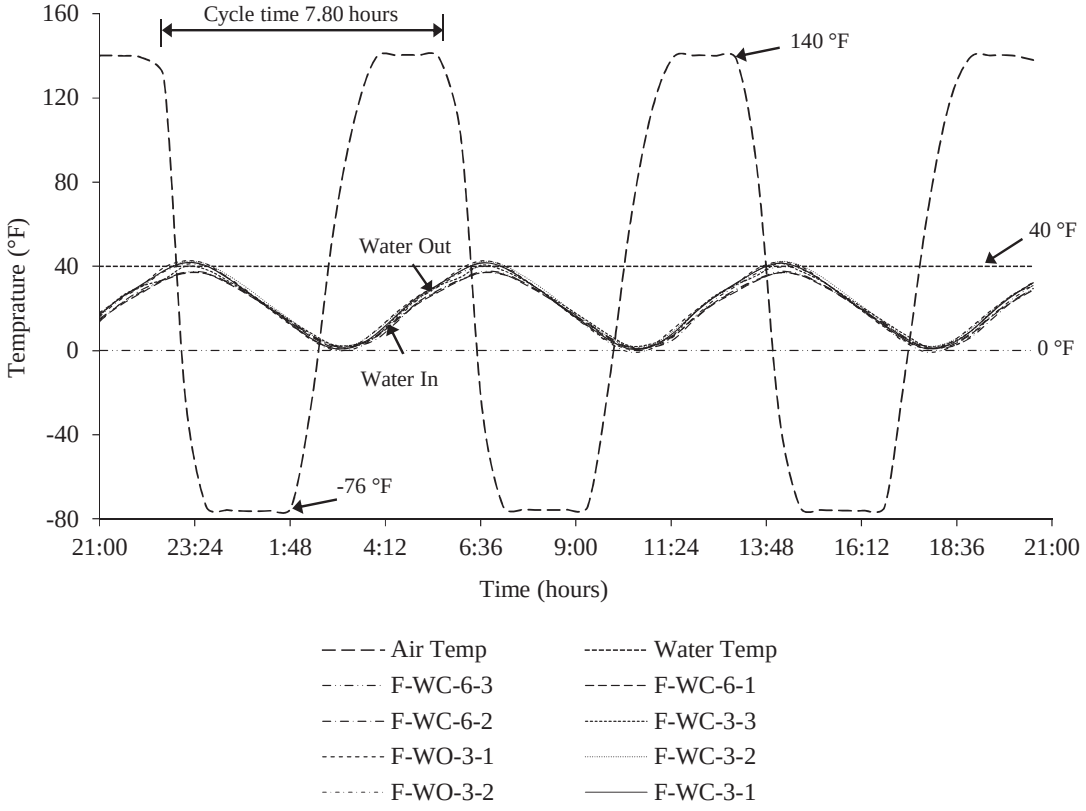

Figure 3-14 Temperature variations for freeze/thaw cycles

All of the bridge deck specimens were removed from the holding tank subsequent to completion of the 300 freeze/thaw cycles. Non-destructive tests (NDT) were then performed on all eight specimens. Following the NDT tests, the eight specimens were subjected to 1,000,000 repeated load cycles. The repeated load cycles are described in detail in Section 3.4.4. The 300-cycle freeze/thaw specimens were then subjected to ultimate load test. The ultimate load test is discussed in Section 3.6.

The remaining freeze/thaw specimens were returned to the holding tank as shown in Figure 3-15. These specimens were subjected to an additional 300 freeze/thaw cycles, and hence a total of 600 freeze/thaw cycles. The specimens were removed from the holding tank at 400 cycles, 500 cycles and 600 cycles of freeze/thaw for NDT. Subsequently, the specimens were subjected to 1,000,000 repeated load cycles and to the ultimate load test.

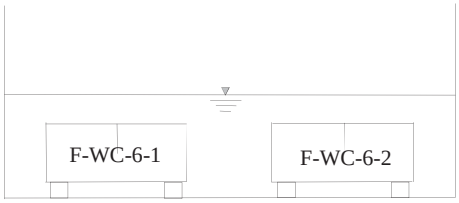

Figure 3-15 Holding tank inside the environmental chamber with the 600-cycle freeze/thaw specimens

3.4.3 Saltwater Exposure

The saltwater exposure simulates the application of deicing salts on the bridge decks during the winter months. In this test program, eight bridge deck specimens were exposed to saltwater: two specimens were subjected to 3,000 hours of saltwater exposure; two specimens were subjected to 6,000 hours of saltwater exposure; two specimens were subjected to 8,000 hours of saltwater exposure; and two specimens were subjected to 10,000 hours of saltwater exposure.

The 3.5 percent saltwater ponding solution contained primarily NaCl in addition to other ions. The salt was mixed with the water to obtain a specific gravity of approximately 1.025. The

consistency of the salt solution concentration was monitored indirectly by measuring the specific gravity of the solution, which was maintained at 1.025 ± 0.005.

The specimens were exposed to saltwater in 2 tanks (A and B) with four specimens in each. The holding tanks had dimensions of 10.0 ft. x 4.0 ft. x 5.0 ft. The specimens in a single tank were separated using wooden spacers to allow saltwater exposure to the entire surface of each specimen. The saltwater solution was added to the tanks to entirely cover all of the specimens as shown in Figure 3-16 and Figure 3-17. Submersible pumps were used in the tanks to promote the circulation of the saltwater. Plastic tarps were placed over the tanks to limit growth of algae. The specific gravity and the temperature of the solution were measured weekly throughout the test program.

Specimens S-WC-30-1 and S-WC-30-2 were exposed to saltwater for 3,000 hours. Subsequently, they were removed from the saltwater solution and subjected to 1,000,000 cycles of repeated load following non-destructive tests. Finally, the two specimens were subjected to the ultimate load test.

Specimens S-WC-60-1 and S-WC-60-2 were exposed to saltwater for 6,000 hours. The specimens were removed from the saltwater solution after the first 3,000 hours of exposure and subjected to 1,000,000 cycles of repeated load following non-destructive tests. The specimens were then returned to the saltwater tank and subjected to the remaining 3,000 hours of exposure. At the end of the 6,000 hours in saltwater solution, the specimens were removed and subjected to an additional 1,000,000 cycles of repeated load. Finally, the two specimens were tested for ultimate load.

Specimens S-WC-80-1, S-WC-80-2, S-WC-100-1 and S-WC-100-2 were exposed to saltwater for 3,000 hours. The specimens were then removed from the saltwater solution and subjected to 1,000,000 cycles of repeated load following non-destructive tests. Subsequently, the specimens were returned to the saltwater tank and subjected to additional 5,000 hours of exposure. At the end of the 8,000 hours in saltwater solution, specimens were removed and subjected to additional 1,000,000 cycles of repeated load following non-destructive tests. The ultimate load capacity was determined for the two specimens S-WC-80-1 and S-WC-80-2. The

specimens S-WC-100-1 and S-WC-100-2 were returned to the saltwater tank and subjected to another 2,000 hours of exposure to complete a total of 10,000 hours of saltwater exposure. Finally, the ultimate load capacity was determined for the two specimens followed by concrete powder sampling to determine the chloride content.

(a) Placement of specimens

(b) Final arrangement of specimens before filling tank with saltwater

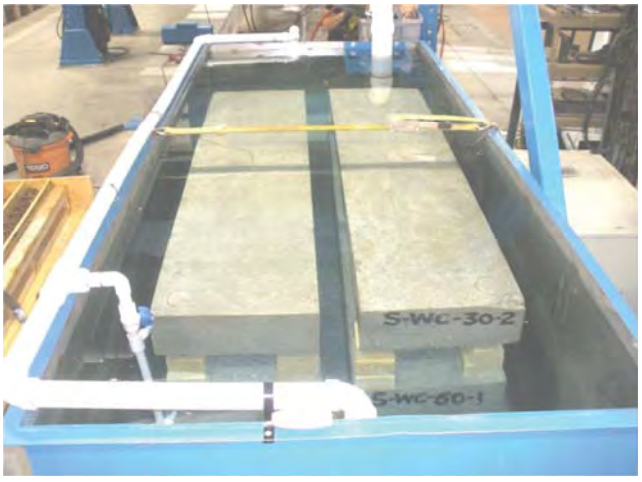

(c) Specimens in tank after filling with saltwater

Figure 3-16 Placement of specimens inside saltwater tanks

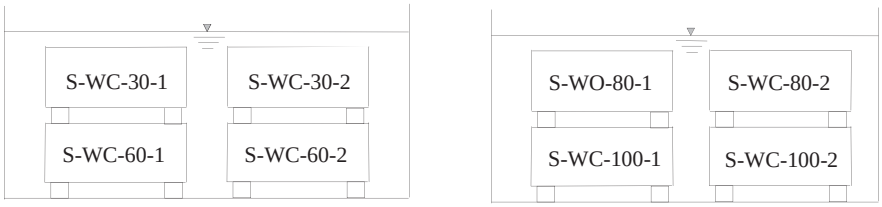

(a) Saltwater tank A (b) Saltwater tank B

Figure 3-17 Arrangement of saltwater exposure specimens

3.4.4 Repeated Load Cycles

Repeated load cycles simulate live loads that act on the bridge decks. Note that the specimens were not tested to fatigue failure. The research team and the MDOT technical advisory group determined the parameters of the test. In this test program, 1,000,000 repeated loads were applied in sets of 250,000 cycles. The rest time between sets were typically 2 hours in which time a quasi-static load test was performed. Repeated load cycles were applied in combination with either freeze/thaw exposure or saltwater exposure tests. The load was applied using the same load configuration as used during pre-cracking and is also shown in Figure 3-18. The distance between the left and right supports was 63.0 in. Each of the left and right loads was equal to half of the total load (P/2). The loads were applied at the third distances of the span L (at 21.0 in. and at 42.0 in.). There was a 5.5 in. overhang at each support.

The amplitude of the cyclic load was taken as 25% of the computed ultimate load carrying capacity of 52 kips. This corresponded to load amplitudes of 13.0 kips. A minimum amplitude of 2.5 kips and a maximum amplitude of 15.5 kips were maintained. The minimum load amplitude above 0 kip was maintained for safety reasons. The repeated load cycles were applied with a frequency of 3.0 Hz. A load spectrum showing the upper and lower limits is shown in Figure 3-19. A static load test at every 250,000 cycles of repeated load was also conducted using the same load configuration (Figure 3-18).

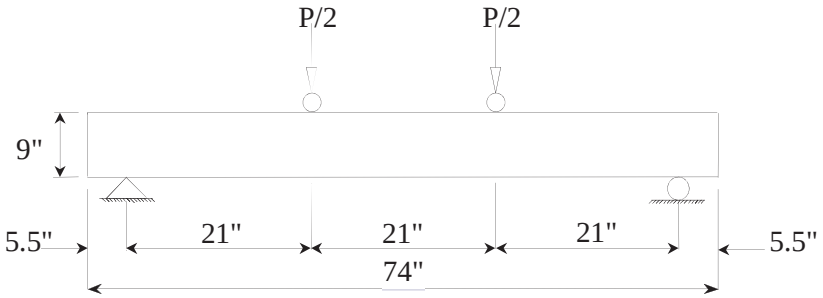

Figure 3-18 Test set-up for repeated load cycles

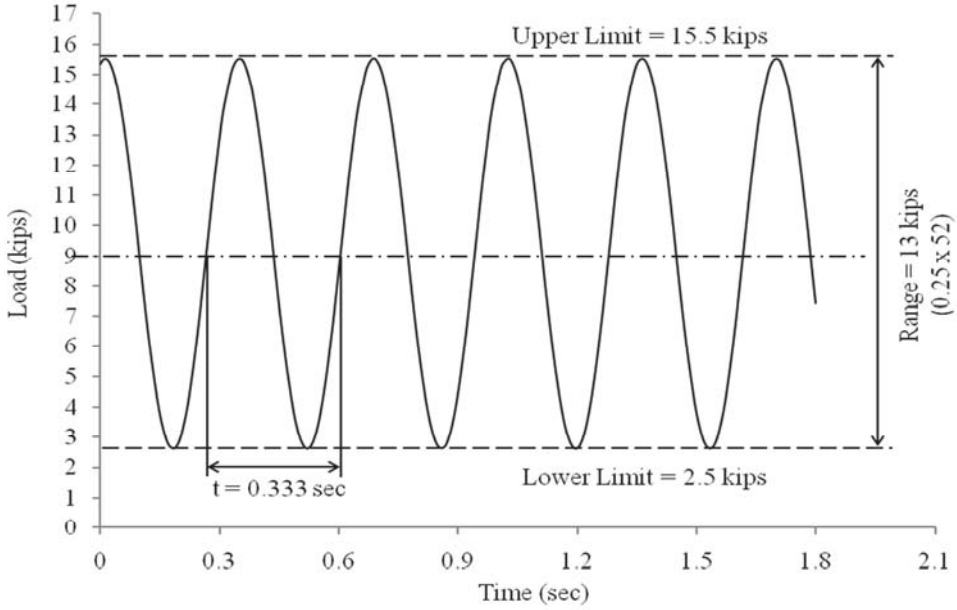

Figure 3-19 Load spectrum of the repeated load application

3.5 Non-destructive test procedures

Non-destructive tests are test methods used to examine or investigate the material integrity of an object without impairing the usefulness of the structure. For this test program, four different non-destructive test methods were used: rebound hammer test, half-cell potential test, galvanostatic pulse technique and rapid chloride test. The testing procedures of each of these test method are described below.

3.5.1 Rebound Hammer Test

The instrument used for the non-destructive rebound hammer test is an integrated electronic SilverSchmidt (Figure 3-20) which was used to estimate the in-situ compressive strength from the concrete surface hardness. The concrete test hammer measures rebound coefficient (Q- value) of a spring loaded mass impacting against the concrete surface, where Q = 100*(Energy restored) / (Energy input). The procedure to conduct the rebound hammer test involved marking specific impact points on the selected concrete surfaces using a template provided with the instrument. In this test program, 10 impact points were used at three different locations on surface of each specimen. Holding the plunger against the concrete surface in a horizontal position, pre-loading the spring followed by a release applies an impact pressure at the points of interest. The corresponding Q-value was then stored and the concrete surface hardness value was found at the end of one set of measurement series (i.e. at end of 10 points of measurement) at the specific location.

(a) SilverSchmidt Hammer

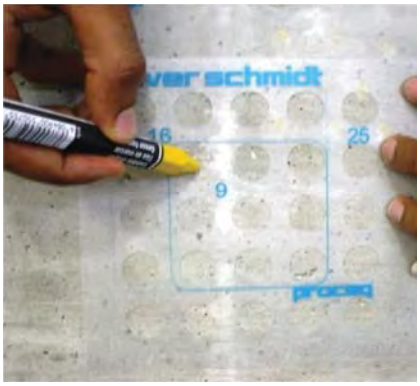

(b) Marking impact points

(c) Q- value after one impact

(d) Reading showing the compressive strength after 10 impacts

Figure 3-20 SilverSchmidt instrument

3.5.2 Half-Cell Potential Test

The instrument CANIN, with a $Cu/CuSO_4$ half-cell reference electrode, is a system for measuring potential fields over the surface of reinforced concrete elements. If certain potential gradients occur, (changes in value per unit of length) a distinction can be made between locations with corroding steel reinforcement and those without. The preparation procedure involves filling the rod electrode with saturated $CuSO_4$ solution. The half-cell potential is measured between the extended/exposed lower reinforcement and the concrete surface. Placing the rod electrode against the concrete surface will complete the circuit and enable the potential data to be collected. Potential readings were measured at 6 in. spacing along each of the bottom main reinforcement and the average output was recorded from each specimen.

(a) $Cu/CuSO_4$ half-cell electrode

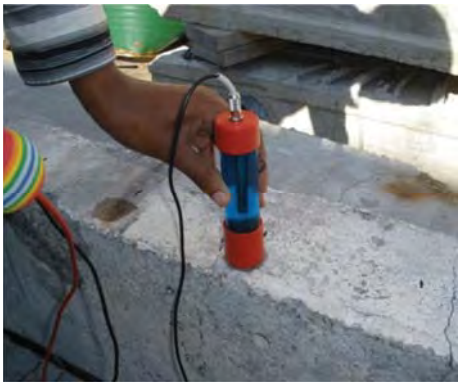

(b) Placing rod electrode against concrete surface

(c) Measuring potential using CANIN

Figure 3-21 CANIN instrument

3.5.3 Corrosion Rate Test

The GalvaPulse instrument, which uses galvanostatic pulse measurement, was used to measure the corrosion rate at the time of testing. The GalvaPulse instrument setup involved connecting the corrosion rate display device (PSION) to the stainless steel screw attached to the bottom main reinforcement by means of clamping pliers and cable. The Ag/AgCl electrode was then connected to the PSION.

A large circular sponge and center sponge were attached to the electrode to insure the conductivity between the concrete surface and the electrode. The electrode was then pressed firmly against the concrete surface at the testing point and the electrode was kept completely

steady for 10 seconds till one measurement completed. The record was then stored in the PSION. This procedure was repeated at every 8 inches along each of the bottom main reinforcements. The average corrosion rate value was then recorded from each specimen.

(a) Ag/AgCl Electrode PSION

(b) PSION

(c) Measuring corrosion rate

Figure 3-22 GalvaPulse instrument

3.5.4 Rapid Chloride Test (RCT)

Rapid chloride test (RCT) was used to measure the acid soluble chloride content in the concrete elements. The chloride content could be measured by immersing an RCT electrode in a

concrete powder mixed with the RCT extraction liquid. The main components of the RCT kit (Figure 3-23) were RCT electrode, electrometer (used to display the voltage reading), electrode wetting agent (EWA), different calibration liquids (clear, purple, green and pink calibration liquids), RCT extraction liquid and RCT calibration sheet. The procedure involved collecting concrete dust sample of roughly 0.16 oz. by rotary drilling. In order to have a representative value of the chloride content, several samples were collected from different locations on the surface of the specimens. A sample of 0.0528 oz. concrete powder was then placed in the extraction liquid and shaken for 5 minutes before measuring the solution voltage (mV) using the RCT electrode and electrometer.

The RCT electrode was first calibrated by filling it with electrode wetting agent and immersing it into the clear (containing 0.005% Cl ions), purple (containing 0.02% Cl ions), green (containing 0.05% Cl ions) and pink (containing 0.5% Cl ions) calibration liquids consecutively in order to obtain the corresponding voltage readings from the electrometer. These values were plotted on the calibration sheet to produce the conversion curve used to determine the percentage of Cl ion in the prepared concrete powder solution. A typical conversion curve used is indicated in Figure 3-24. After the RCT electrode surface was cleaned with distilled water, it was again refilled with EWA and used to measure the voltage of several concrete powder solutions.

(a) RCT calibration liquids

(b) RCT electrometer and electrode

(d) RCT Extraction liquid with electrode

(c) EWA and Distilled water

(e) RCT 500 kit

Figure 3-23 RCT 500 instrument

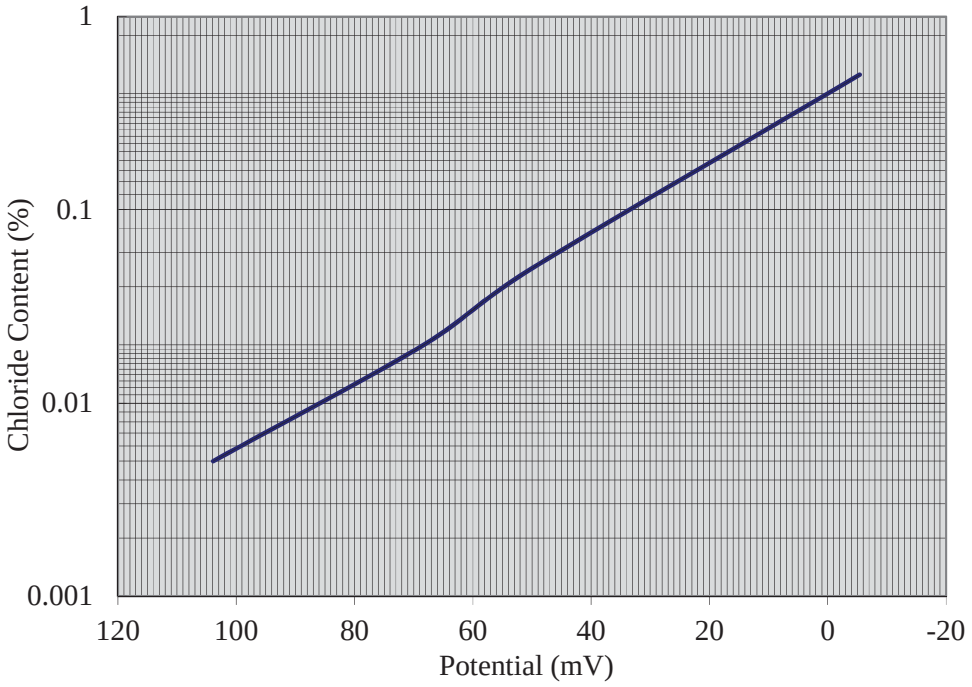

Figure 3-24 RCT conversion curve

3.6 Ultimate Load Tests

The ultimate load test was performed to evaluate if the environmental exposure and the repeated loads had affected the load carrying capacity of the specimens. The load set-up used for the ultimate load test was four-point loading which was the same set-up used for repeated load cycles (Figure 3-8 and Figure 3-9). A 50 kip actuator with displacement rate of 0.02 inches per minute was used for the ultimate load test of each specimen. The observed ultimate failure modes were either flexural mode or combined flexural/shear mode (Figure 3-25). A typical load-displacement curve is shown in Figure 3-25.

a. Load set-up b. Flexure/shear mode of failure

Figure 3-25 Setup of specimen for ultimate load test

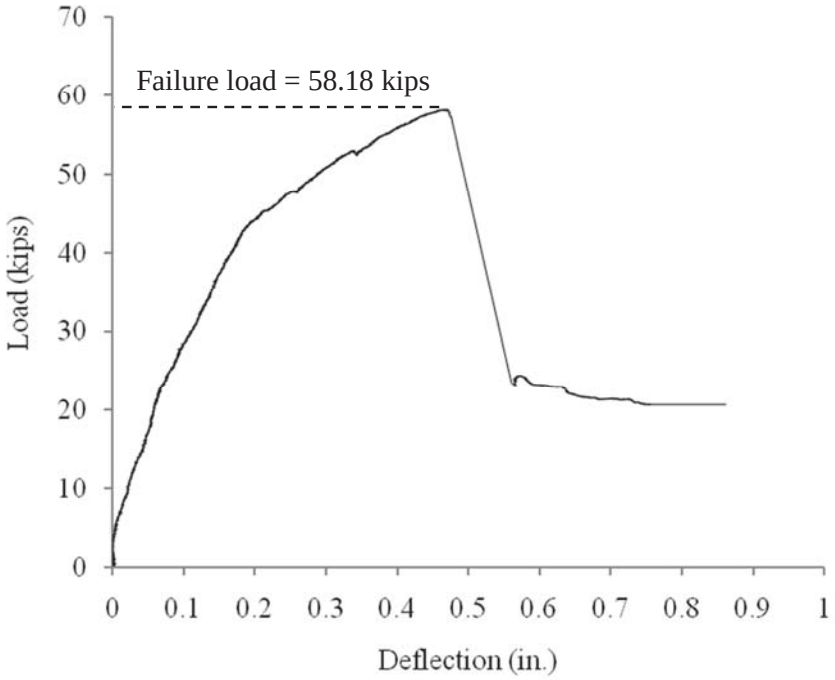

Figure 3-26 Typical load-deflection curve for ultimate load test

3.7 Environmental Scanning Electron Microscope (ESEM)

ESEM (environmental scanning electron microscope) which is shown in Figure 3-27 is a powerful microscope used to characterize wet, oily, dry, porous and soft materials. It can produce high-resolution images of a sample surface revealing details less than a nanometer (10^{-9} of a meter) in size. Furthermore, it has the ability to generate localized chemical element analysis (EDAX- Energy Dispersive Analysis using X-ray).

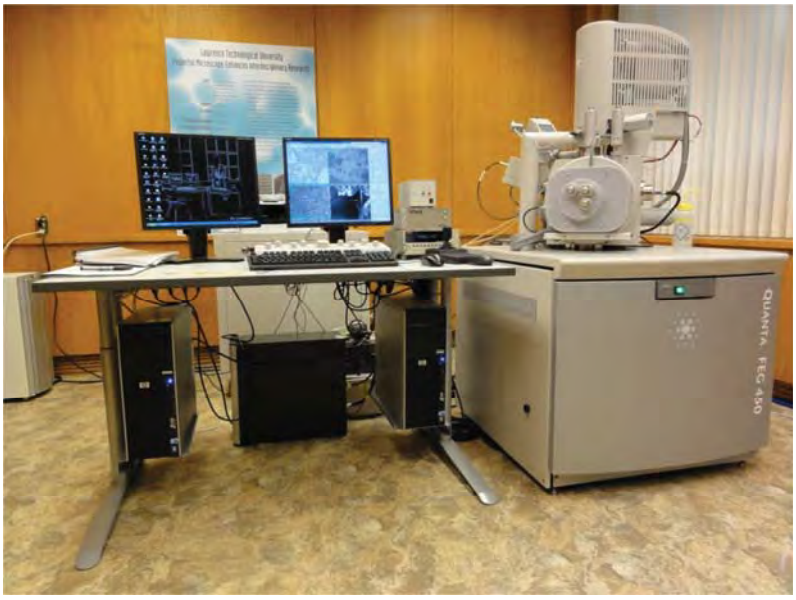

Figure 3-27 Environmental electron scanning microscope

3.7.1 Objectives of Using ESEM

The objectives of using ESEM in this particular project are to determine porous zone thickness between the steel reinforcement and the surrounding concrete (which is an important parameter for mathematical corrosion cracking model) and to determine the corrosion state of the steel reinforcement embedded in the concrete. ESEM analysis was conducted on the field investigated bridge cores and selected representative laboratory specimens.

3.7.2 Laboratory Specimens Selection

One specimen was selected from each test group as listed in Table 3-1. The specimens selected were: control beams with and without chloride, C-WO and C-WC; 3000 hours saltwater with chloride, S-WC-30; 6000 hours saltwater with chloride, S-WC-60; 8000 hours saltwater with chloride, S-WC-80; 10,000 hours saltwater with chloride, S-WC-100; 300 cycles freeze-thaw with and without chloride, F-WO-3 and F-WC-3; 600 cycle freeze-thaw with chloride, F-WC-6.

3.7.3 Sample Preparation

Three samples of size 3 in. × 3 in. × 1.5 in. were cut, using a diamond hand saw, from the two ends and the middle of each specimens. In total, 27 samples were prepared for image analysis using the ESEM. Pictures depicting the sample locations in the specimen, cutting of samples and a prepared sample are presented from Figure 3-28 through Figure 3-30. Furthermore field investigated bridge cores were cut into 1.5 in. thickness and diameter of 4 in. as shown in Figure 3-31.

Figure 3-28 Cutting of samples with concrete diamond hand saw

Figure 3-29 Sample locations in the specimen

Figure 3-30 Sample of size 3in. × 3in. × 1.5in. taken from a specimen

Figure 3-31 Sample preparation of bridge cores taken during field sampling.

3.7.4 Measuring the Porous Zone Size by ESEM

Porous zone size, which represents the interface between the steel reinforcement and concrete of the samples, were measured from secondary electron (SE) imagining. Secondary electron (SE) mode provides high-resolution imaging of fine surface morphology. Inelastic electron scattering caused by the interaction between the sample's electrons and the incident electrons results in, the emission of low-energy electrons from near the sample's surface. The topography of surface features influences the number of electrons that reach the secondary electron detector from any point on the scanned surface. This local variation in electron intensity creates the image contrast that discloses the surface morphology.

Multiple images using secondary electron (SE) at a magnification of 1000× were taken along the periphery of the steel reinforcement and concrete interface. Porous zone size measurements were taken on the images and the average value was denoted as the porous zone

size of the corresponding sample. A representative image showing the porous zone for the specimen C-WO is presented in Figure 3-32.

Figure 3-32 Porous zone of C-WO (1000x)

3.7.5 Determining the Corrosion State by ESEM

Corrosion states of the samples were evaluated using backscattered electron (BE) imaging, which gives better contrast for different atomic masses. Backscattered electrons are produced by the elastic interactions between the sample and the incident electron beam. Higher atomic mass material appears brighter than lower atomic mass material in a backscattered electron image.

Figure 3-33 shows backscattered electron images of non-corroded and corroded reinforcement on representative specimens. It can be observed from the images that the non-corroded reinforcement appears brighter due to the higher atomic mass, and the corroded reinforcement appears darker due to the lesser atomic mass of the corrosion product. Corrosion product may be hydrated ferric oxide.

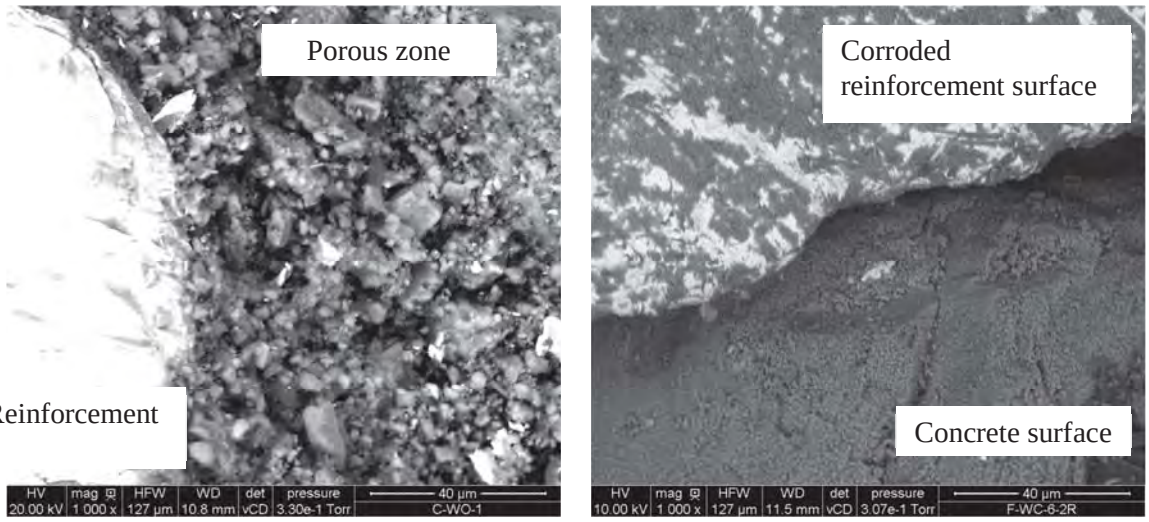

(a) non-corroded reinforcement (b) corroded reinforcement

Figure 3-33 Representative backscattered electron image (Magnification of 1000x)

3.7.6 Energy Dispersive Analysis using X-ray (EDAX)

Energy dispersive analysis by x-ray (EDAX) identifies and counts the impinging X-rays based upon the characteristic energy levels of the elements. By using this qualitative analysis, the corrosion state of the steel reinforcement was determined for all the samples using spot scanning at excitation energy of 20 kV.

In this manner, EDAX evaluation was performed for each sample and three spots were chosen, on the reinforcement, on the porous zone and on the concrete surface. Typical plots of element compositional analysis of the reinforcement, porous zone and concrete surface are presented in Figure 3-34 through Figure 3-36. Note the spike in oxygen present on the reinforcement surface and perimeter indicating presence of corrosion products.

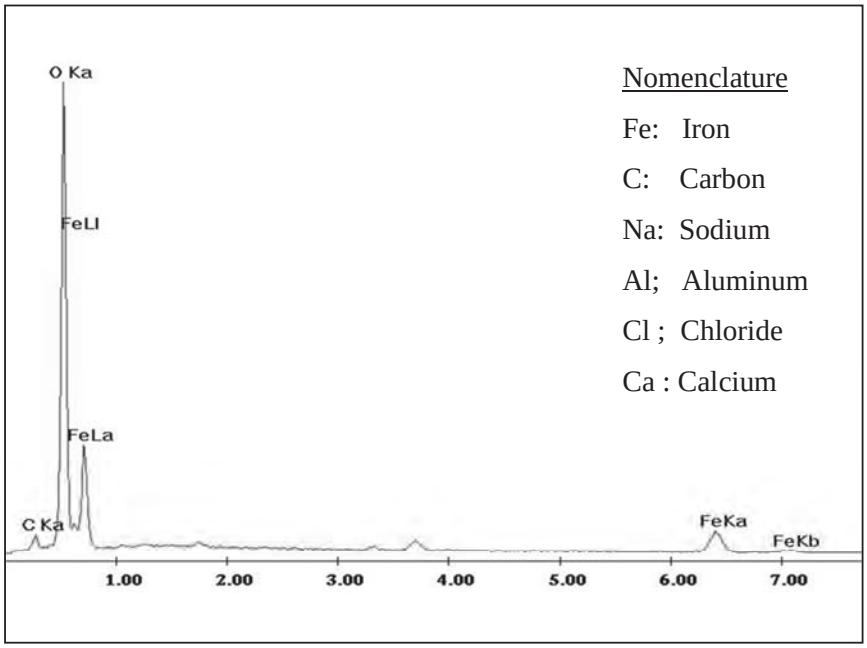

Figure 3-34 Typical plot showing the element composition analysis on reinforcement surface

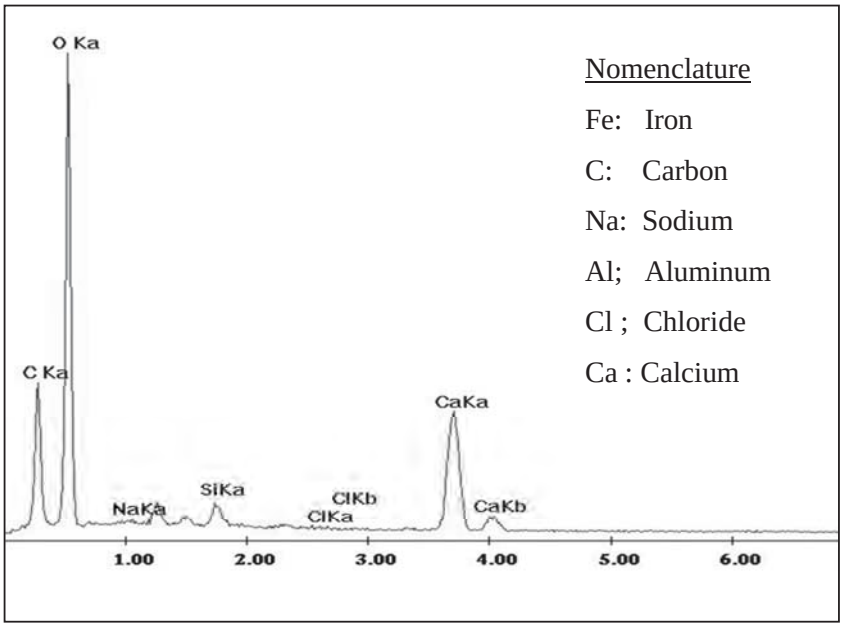

Figure 3-35 Typical plot showing the element composition analysis on concrete surface

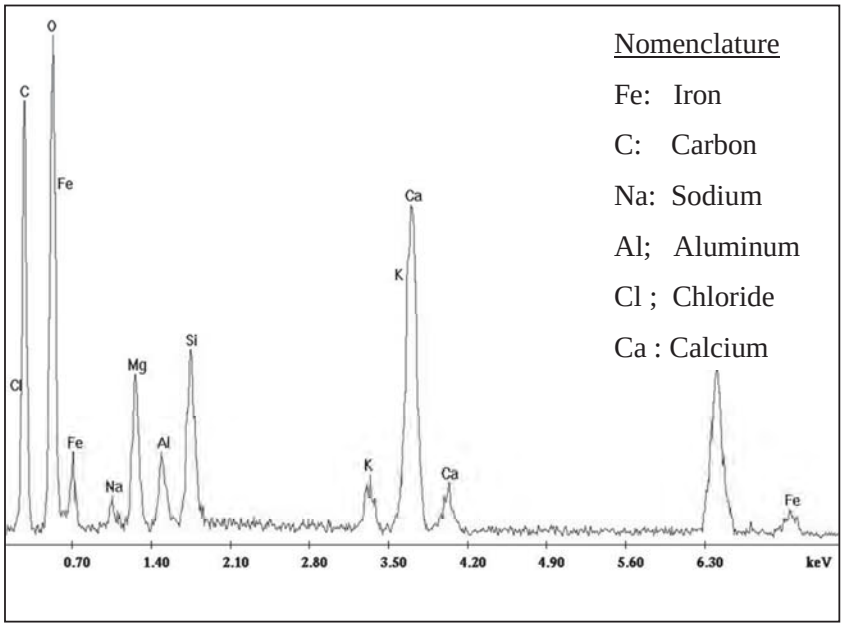

Figure 3-36 Typical plot showing the element composition analysis on porous zone

CHAPTER 4: METHODOLOGY OF FIELD INVESTIGATION

4.1 Introduction

Field investigation, associated non-destructive test (NDT) and coring were conducted on three bridges located in Oakland County, Michigan. The bridges were all constructed with a 9 in. standard bridge deck supported by steel bridge girders. The selection of the bridges was based on the MDOT's National Bridge Inspection Rating matrix. The deck rating of the three bridges, included in this study, was poor or below (NBI rating of 4 or below) per November 2009. However, the surface rating was at good, fair and poor indicating deterioration on the bottom surface of the deck. Site visits confirmed the deterioration of the bottom surface ranging from cracking, leaching, rust stains, spalling and exposed corroded reinforcement. For the detailed field investigations, the Lawrence Technological University research team performed the visual inspection and non-destructive tests while, MDOT personnel provided the traffic control and retrieved cores from the concrete deck slabs.

The bridges were visually inspected and NDT data were collected from three representative areas of the bridge decks. These test areas were accessed from below the bridge deck. Concrete cores and powder were collected from the bridge decks and were taken to Center for Innovative Material and Research (CIMR) for further evaluation.

4.2 Objective of Field Investigation

The objective of field investigation is to identify performance based thresholds and procedures to identify concrete bridge decks experiencing high risk for falling concrete and to conduct field exploration and sampling to determine the concrete properties and condition, and steel condition that are highly influences falling concrete.

4.3 Field Investigation

4.3.1 Selection of Bridges

The details of the bridge selected for field investigation, coring and associated non-destructive test (NDT) are presented in Table 4-1. The table includes the MDOT structure number, year of construction, year of lane added, year of concrete overlay as well as the NBI

deck and surface rating. Deck rating reflects the overall general condition of the deck; the rating includes the underside of the deck and the wearing surface. However, the condition of the railings, sidewalks, curbs, expansion joints and deck drains is not considered in this rating.

Table 4-1 Selected bridges for field investigation, coring and associated NDT

MDOT structure number	Facility carried & featured intersection	Constructed	Lane added	Shallow overlay	Deck rating*	Surface rating*
63174-S05-1	I-75 NB over 14 Mile Road	1963	1970	1994	4 (poor)	8 (good)
63022-S02-3	I-96 WB over Milford Road	1957	1965	1994	4 (poor)	5 (fair)
63022-S01	I-96 WB over Kent Lake Road	1948	1967	1989	3 (serious)	4 (poor)

*Deck and surface rating per NBI subcategory 58, 58A & 58B

4.3.2 Coring Procedure

The bridge deck coring was a multi-step process: identifying coring locations, coring full depth of bridge deck, collecting the core from below the bridge, plugging and filling the holes.

Identifying coring locations

Coring locations were selected to represent the general condition of the bridge taking into account limitations imposed by the scope of traffic control, site conditions, and the time interval work was allowed to be conducted. In most cases, cores were taken from the tail span to facilitate retrieving the core after drilling and prevent the full depth core from dropping on the roadway.

Coring full depth of the bridge deck

The coring equipment consisted of a core drill with diamond–impregnated bits attached to a core barrel for obtaining cylindrical core specimens. The full depth cores were taken using a core barrel with an 4.0 in. outer diameter in diameter and a length allowing drilling through the thickness of the deck slab (8 to 10 in.). The coring procedure is shown in Figure 4-1. The drilled cores were collected from below the deck.

Plugging and filling

Procedures were established for preparing the holes for plugging and subsequently filling the holes with concrete mixture. Prior to filling the full depth core hole, a shelf for support of the core plug reinforcement was created by adjacent coring to a depth of 2 in. using a 4 in. diameter core barrel. The core reinforcement was needed to hold the patch in place. The core reinforcement was bent offsite to form a loop shape with 2 in. legs and placed in the core hole. A plastic plug form was placed at the bottom of the hole by tying to the core reinforcement. The procedures from coring to plugging of the resulting hole are presented in Figure 4-1. The reinforced hole was then filled using ready-mix concrete “DURAPATCH HIWAY” which sets in 10 minutes. Then the concrete was consolidated using a steel rod.

(a) Coring by MDOT personnel

(b) Collecting core from underneath the bridge

(c) Resulting hole in concrete deck

(d) Concrete core taken from bridge deck

(e) Bottom view of plug

(f) Reinforcement detail in the core hole

Figure 4-1 Coring procedure

4.3.3 Visual Inspection

The selection of the areas for detailed NDT and coring was based on the general condition of each bridge deck as determined by visual inspection. The types of deterioration

assessed were cracking of the bottom surfaces of the bridge decks, presence of traces of rust, salt or other deicing agents, extent of spalling and condition of exposed reinforcement if any.

General physical characteristics and overall condition of the cores were evaluated by visual inspection. The reinforcing steel was assessed for presence of rust and extent of rust. The concrete was assessed for quantity, size, and alignment of cracking; size of voids; size of honeycombing (if any). Moreover, the cores were assessed for consistency of the concrete condition along the depth.

4.3.4 Non-destructive Test (NDT)

Non-destructive testing (NDT) is used to assess the condition of concrete and reinforcement bar without inducing further significant damage to the deck slab. The NDTs equipment used were: Profometer (locating reinforcement bar), SilverSchmidt (in-situ hardness test), CANIN (corrosion potential measurement) and RCT (rapid chloride content test)

For non-destructive testing, a minimum of three areas A1, A2 and A3, approximately 54 in. x 80 in. each, were selected on the bottom surface of the deck of each bridge. The areas were selected to represent the overall condition of the bridge deck and to examine the difference in the condition of the deck due to the difference in deicing practices such as priority deicing of deceleration lanes and ramps. Areas A1 and A2 were typically on located on or adjacent to the right lane, while area A3 was located on or adjacent to the left lane.

Test grids of 4 in. x 18 in. were mapped on each area (Figure 4-2). The bottom steel reinforcement bars were located using the Profometer. The reinforcement was exposed by drilling a ½ in. diameter hole to complete the circuit for the half-cell potential measurements using the CANIN system. The surface, on areas marked out for potential measurements, were water saturated for improved conductivity. Moreover, in-situ hardness was measured by Silverschmidt. Chloride content and pH values were determined by taking concrete powder samples and cores from the bridges. The powder samples were taken from the bottom surface of the deck in a minimum of 6 random areas to a distance of 4 in. from the bottom deck surface. Mapped grids underneath the bridges and exposing reinforcement bar by drill bit are shown in Figure 4-2 and Figure 4-3, respectively.

Figure 4-2 Grids used for NDT

Figure 4-3 Exposing reinforcement bar

4.3.4.1 Profometer (Locating Reinforcement Bar)

The Profometer is used to locate reinforcement, to determine reinforcement diameter and concrete cover on site. The measuring method is based on the pulse-induction technique. It has a universal probe (Figure 4-4 b) that detects the location of the reinforcement along with display device that displays concrete cover, diameter and location of reinforcement (Figure 4-4 a). The

scan car is a movable device that carries the probe and measures the distance traveled (Figure 4-4 c). The supporting rod supports and guides the scan car while rolling along the deck detecting reinforcement (Figure 4-4 d). The process of locating the reinforcement underneath a bridge deck using Profometer is shown in Figure 4-5.

(a) Display device

(b) Universal probe

(c) Scan car

(d) Supporting rod

Figure 4-4 Components of Profometer

Figure 4-5 Locating a reinforcement bar with Profometer underneath bridge deck

4.3.4.2 SilverSchmidt (In-situ hardness test)

An integrated electronic SilverSchmidt Hammer was used to determine the in-situ hardness of concrete. The hammer measures rebound coefficient (Q-value) of a spring loaded mass impacting against the concrete surface. Impact is triggered at end position and the corresponding Q-value is stored and with reference to a conversion curve, the rebound value is used to determine the in-situ hardness of concrete deck in units of stress such as psi. The in-built conversion curve is used to convert the Q values into in-situ hardness. Thirty points were marked for specific impact points in each test area, and the corresponding rebound coefficients were measured. The SilverSchmidt kit, marking of data points and measuring in-situ hardness on concrete surface are shown in Figure 4-6 and Figure 4-7, respectively.

Figure 4-6 SilverSchmidt kit

(a) Marking of data points

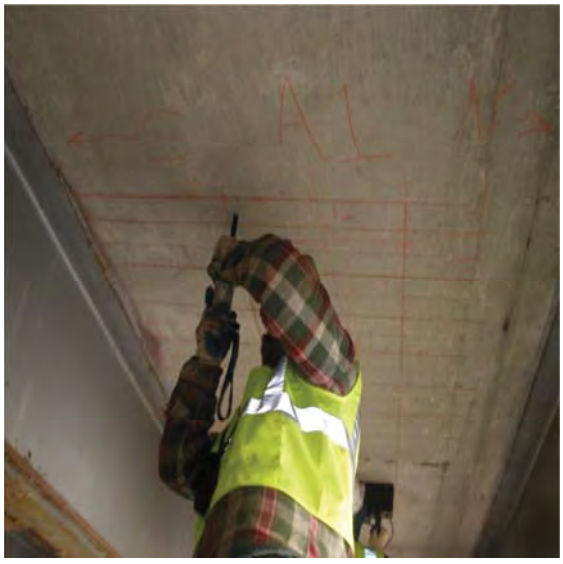

(b) Rebound measurement

Figure 4-7 Measuring of in-situ hardness from the bottom of the deck

4.3.4.3 CANIN (Corrosion Potential Measurement)

The development of reinforcement corrosion is an electrochemical process. The surface of the corroding steel functions as a mixed electrode that is composed of anodes and cathodes electrically connected through the body of the steel itself, upon which a coupled anodic and cathodic reaction takes place. A potential field can be measured on the concrete surface by the use of an electrode, known as a half-cell, and a high-impedance voltmeter. Half-cell potential also called open-circuit potential, rust potential or corrosion potential is measured at several discrete points and is used as a qualitative index for ascertaining the chance of the reinforcement being corroded. Interpretation of the half-cell potential test result is carried out per the ASTM C876 'Standard Test Method for Half-Cell Potentials of Uncoated Reinforcing Steel in Concrete", which is presented in Table 4-2 below.

Table 4-2 Interpretation of half-cell potential values as per ASTM C876

Potential difference (mV)	**Chance of corrosion**
< -500	Visible evidence of corrosion
-350 to -500	95%
-200 to -350	50%
> -200	5%

The components of CANIN includes a display device, a rod electrode filled with copper (II) sulfate solution, foam rubber (sponge) attached at the end of the rod electrode, a cable coil which is attached to the reinforcement, and a display device. The components are presented below in Figure 4-8. An example of the measuring corrosion potential using the CANIN system from underneath the bridge deck is shown in Figure 4-9.

Potential measurement was taken from a total of 24 points in each test area: A1, A2, A3, B1, B2, and B3. In this manner, a minimum of 72 data points were collected for each of the bridges investigated.

a) Display device

b) Copper (II) Sulfate

c) Rod electrode

d) Foam rubber (sponge)

e) Cable coil

f) Wheel electrode

Figure 4-8 Components of CANIN

Figure 4-9 Measuring corrosion potential underneath bridge deck with CANIN

4.3.4.4 RCT (Rapid Chloride Content Test)

One of the mechanisms for corrosion initiation to takes place is, when a chloride concentration at the reinforcement level reaches a critical level, which is also often referred to as the threshold or critical chloride level. A level of 1.2 to 1.5 lb/cyd is considered a threshold level for bare steel in regular reinforced concrete bridge decks (Miki, 1990).

The RCT (rapid chloride content test) system is used to accurately and quickly determine the chloride ion content from powder samples of concrete obtained on-site or in the laboratory. The test results were used for:

- Establishing the chloride ion profile through the deck thickness.
- Diagnosing a structure for corrosion activity, in combination with other test systems such as the GalvaPulse, the CANIN and the Rainbow Indicator.
- Measuring the chloride ion content of concrete or its constituents.

The components of the RCT equipment are presented below in Figure 4-10 which includes calibration liquids, electrode wetting agent, distilled water, RCT electrode and electro meter. Samples of concrete powder (Figure 4-12) were taken from the bottom of the bridge decks with a rotary drill (Figure 4-11). Twelve to eighteen concrete powder samples from different depths, weighing on average 0.32 oz., were collected in each test area A1, A2, A3, B1, B2 and B3. The powder samples were obtained by drilling from a maximum depth of 4 in. from the bottom deck surface. In addition, concrete powder samples were taken, through the full depth, of cores obtained from the bridges as presented in Figure 4-13 and Figure 4-14.

The samples of concrete powder obtained were dissolved by shaking for 5 minutes into extraction liquid (Figure 4-15) which removes interfering ions, e.g. sulfide ions, and extracts the chloride ions in the sample. A calibrated electrode was submerged into the solutions and the potential is measured in voltage (Figure 4-16). The potential (mV) was recorded, and the chloride content was determined using a calibration curve (Figure 4-17). The calibration curve is determined using a potential reading of a calibration liquid of 0.005%, 0.020%, 0.05% and 0.500% chloride content.

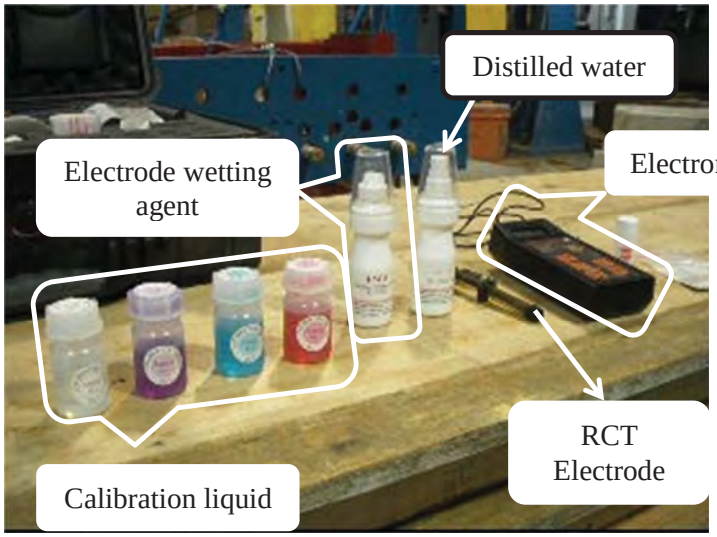

Figure 4-10 RCT 500 components

Figure 4-11 Collecting of concrete powder from the bottom deck

Figure 4-12 Concrete powder taken from Area A2 at 2 cm depth from the bottom

Figure 4-13 Collecting of concert powder from full depth of cores

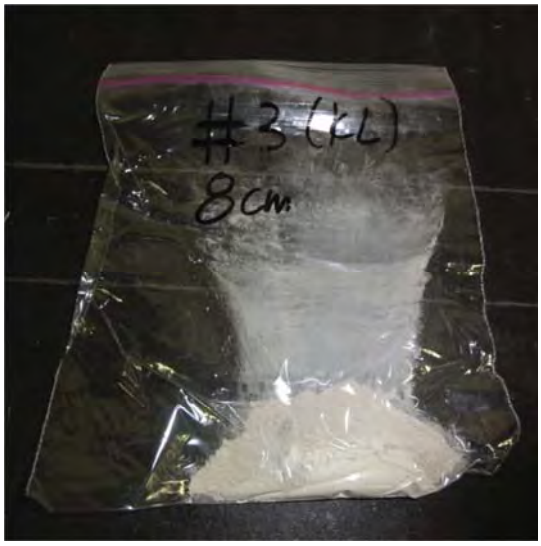

Figure 4-14 Concrete powder taken from core at a depth of 8cm

Figure 4-15 Concrete Powder sample mixed in the extraction solution

Figure 4-16 Voltage reading (mV) of concrete powder solution

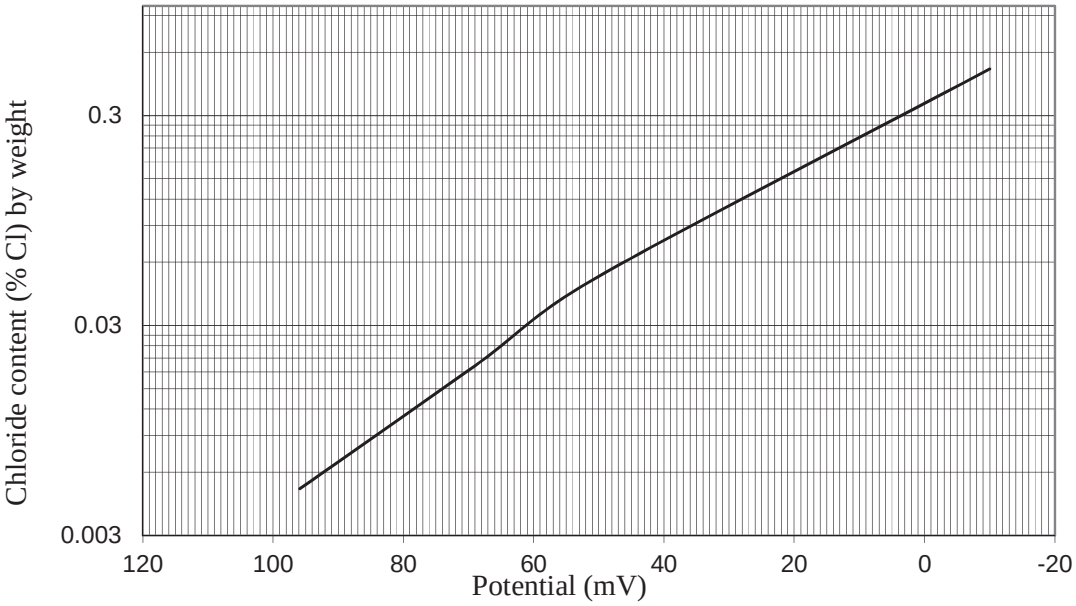

Figure 4-17 Calibration graph, potential (mV) versus chloride content by weight (% Cl ion)

4.3.4.5 Deep Purple and Rainbow Indicator (pH Value Test)

Deep Purple and Rainbow Indicator are used to determine the pH value of the concrete samples. pH values at or below 9.5 of concrete is typically linked to commencement of steel corrosion (Berkely KGC et al.,1990). Each core is sprayed with the indicator, and allowed to dry. The approximate pH of the core is indicated by the color change. The phenolphthalein indicator is 1% of phenolphthalein in 70% ethyl alcohol (CPC-18, 1998). This solution is colorless but it changes to purple when pH is higher than 9. A full pH profile of the concrete can be found with the Rainbow Indicator system where different colors are indicated for different pH values. The pH value associated with different color is presented for Deep Purple Indicator and Rainbow Indicator in Figure 4-18.

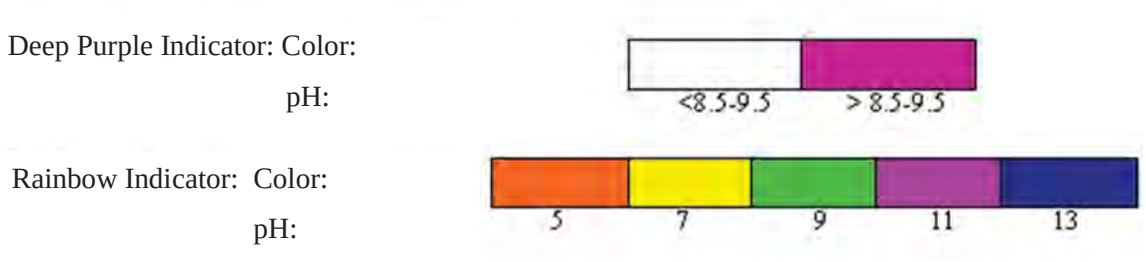

Figure 4-18 Corresponding color and pH value for Deep Purple Indicator and Rainbow Indicator

The potential state of reinforcement corrosion at various pH levels is presented below in Table 4-3 (Berkely KGC et al. 1990). The critical pH value which is associated with commencement of steel corrosion is given to be less than 9.5 and a pH of less than 7 in a reinforced concrete is considered to be under severe corrosion conditions.

Table 4-3 State of reinforcement corrosion at various pH levels (Berkely KGC et al. 1990)

pH of concrete	**State of reinforcement corrosion**
Below 9.5	Commencement of steel corrosion
At 8.0	Passive film on the steel surface disappears
Below 7	Catastrophic corrosion occurs

4.4 Bridge Evaluations

The analysis of data from each bridge investigation and associated retrieved cores are presented in the following section. For each bridge, two sections are presented: Field investigation and evaluation of cores. The field investigation section includes visual inspection of the condition of the deck concrete and reinforcement, structural description of the bridge deck and history, and coring locations. The bridge locations are highlighted on the Oakland County map (Figure 4-19).

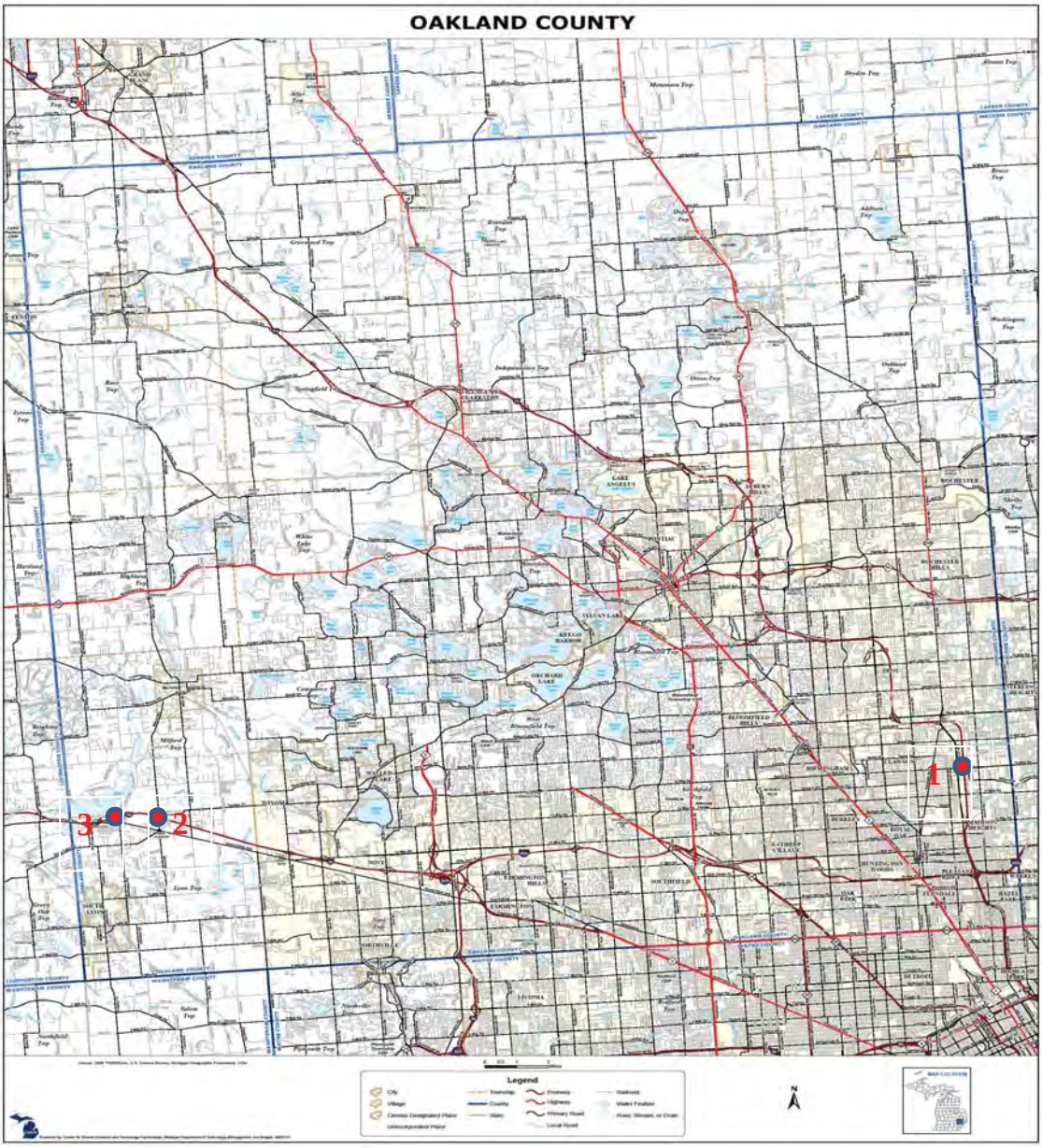

1. 63174-S05-1 carrying I-75 NB over 14 Mile Road
2. 63022-S02-4 carrying I-96 WB over Milford Road
3. 63022-S01 carrying I-96 WB over Kent Lake Road

Figure 4-19 Oakland County Map
(Source: Michigan Center for Geographic Information)

4.4.1 Bridge 63174-S05-1 carrying I-75 NB over 14 Mile Road

The bridge was constructed in 1963 and a lane was added in 1970. This three span and four lane structure has a total length of 155.8 ft. with a maximum central span of 87.9 ft. The width of the deck slab is 64.3 ft. Steel girders are supported on two abutments and three piers. Three areas A1, A2 and A3, (Figure 4-21) representing the general bridge deck condition were selected for non-destructive testing. Moreover, four cores were taken from the leftmost lane (A3) of the bridge for further laboratory investigation. An overview of the intersection and the area of interest are presented in Figure 4-20.

Figure 4-20 Intersection of 63174-S05-1 carrying I-75 NB over 14 M Road
Source: Google Earth

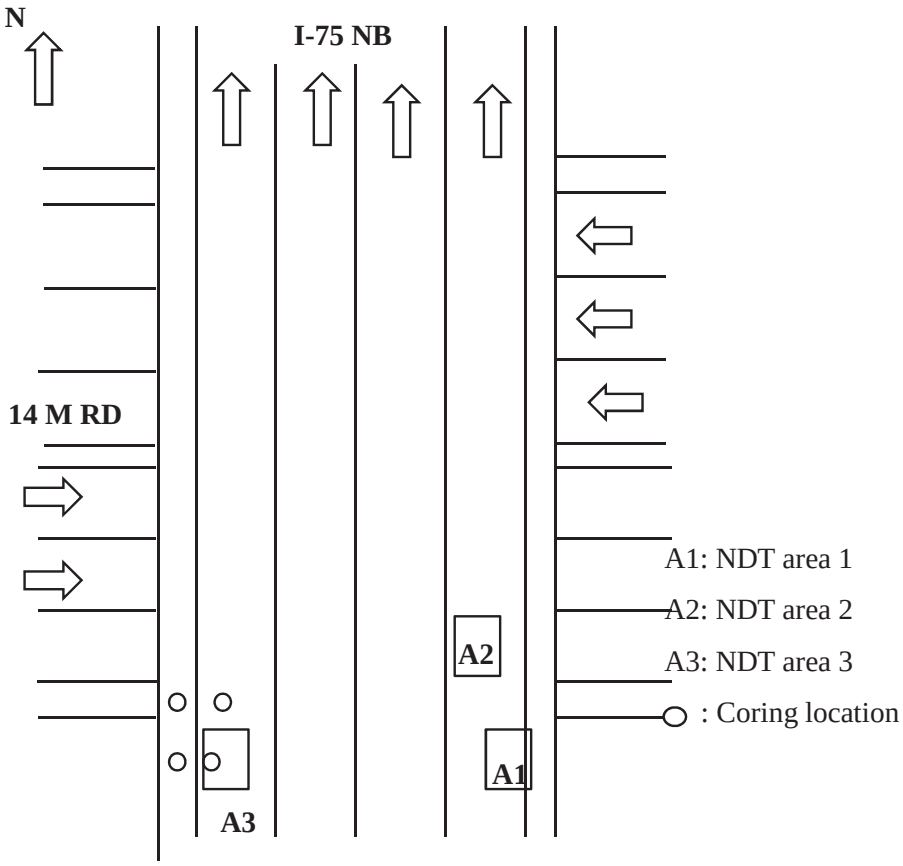

Figure 4-21 NDT and coring areas of 63174-S05-1 carrying I-75 NB over 14 M Road

Visual inspection

Good surface concrete condition was observed on the wearing surface of the deck as presented in Figure 4-22(a). Traces of corrosion and cracks at the bottom the decks were observed on the tail span (Figure 4-22 (b)). The bottom of the deck had cracks propagated along transverse and longitudinal direction as shown in

Figure 4-22(c) and Figure 4-22(d). The deck underside beneath the left lane was covered with plywood to protect the roadway from falling concrete chunks (Figure 4-22(e)). Moreover, exposed reinforcement and deteriorated concrete was observed on the bridge barrier Figure 4-22(f).

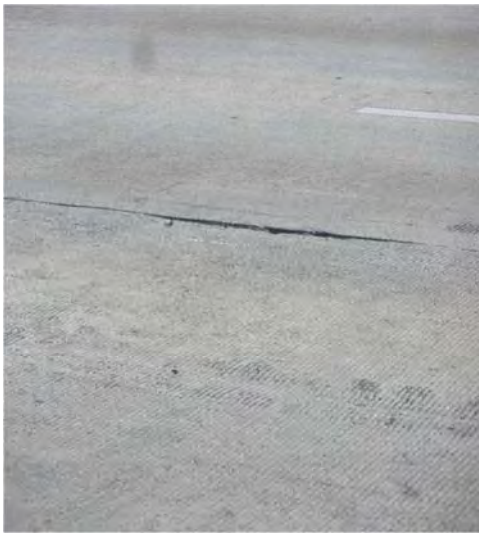

(a) Generally good concrete condition on the wearing surface

(b) Rust traces and cracks (tail span)

(c) Transverse bottom cracks (Scale ≈ 1:20) (tail span)

(d) Longitudinal bottom cracks and corrosion traces (Scale ≈ 1:20) (tail span)

(e) Bottom view of 63174-S05-1 carrying I-75 NB over 14 Mile Road

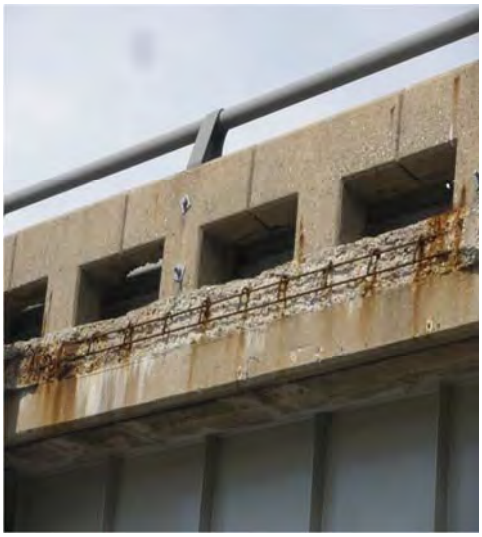

(f) Exposed and deteriorated concrete on the barrier

Figure 4-22 Visual evaluation of 63174-S05-1 carrying I-75over 14 Mile Road

Evaluation of cores

Four concrete cores were taken from the bridge deck. Visual inspection of the cores indicated a different concrete type on the top 3 in, consistent with the historical records of a shallow overlay in 1970. Air voids were encountered in the original concrete deck. The heights of the cores were not significantly different; they all were around 9 in. and 4 in. in diameter. The four cores are shown below in Figure 4-23. Each core was carefully inspected and illustrated as follows, and the corresponding photos are presented in Figure 4-24 through Figure 4-27.

Figure 4-23 63174-S05-1 carrying I-75 NB over 14 Mile Road cores

Core 1

- Height: 9 in.
- Diameter: 4 in.
- Reinforcement at a depth of 2 in. and 6 in. from bottom surface
- No major crack
- 3 in. overlay with different aggregate size
- No significant rust on the reinforcement

Figure 4-24 Core 1 of 63174-S05-1 carrying I-75 NB over14 Mile Road

Core 2

- Height: 9 in.
- Diameter: 4 in.
- No reinforcement
- No major crack
- 3 in. overlay with different aggregate size

Figure 4-25 Core 2 of 63174-S05-1 carrying I-75 NB over 14 Mile Road

Core 3

- Height: 9 in.
- Diameter 4 in.
- Reinforcement at 4.75 in. and 5.5 in. from the bottom surface
- 3 in. overlay with different aggregate size
- No significant rust on the reinforcement
- No major crack

Figure 4-26 Core 3 of 63174-S05-1 carrying I-75 NB over 14 Mile Road

Core 4

- Height: 9 in.
- Diameter: 4 in.
- Reinforcement at 5 in., 4.5 in and 6.25 in from bottom surface
- 3.5 in. overlay with different aggregate size
- No significant rust on the reinforcement
- No major crack

Figure 4-27 Core 4 of 63174-S05-1 carrying I-75 NB over 14 Mile Road

4.4.2 Bridge 3022-S02-4 carrying I-96 WB over Milford Road

This 15^{o} skew bridge was constructed in 1957, an additional lane was added in 1965 and the entire deck had a shallow overlay in 1994. The bridge has three spans, four lanes, and a total length of 170.9 ft. with a central maximum span of 55.8 ft. The width of the deck slab is 68.9 ft, with a 15^{o} skew. Steel girders are supported on two abutments and three piers. Area of interest of the bridge is shown in Figure 4-28 and the three areas (A1, A2 & A3) selected for non-destructive testing are presented in Figure 4-29. Due to MDOT budget constraints, traffic control restrictions and coordination issues with construction projects in the area cores were not retrieved from this bridge.

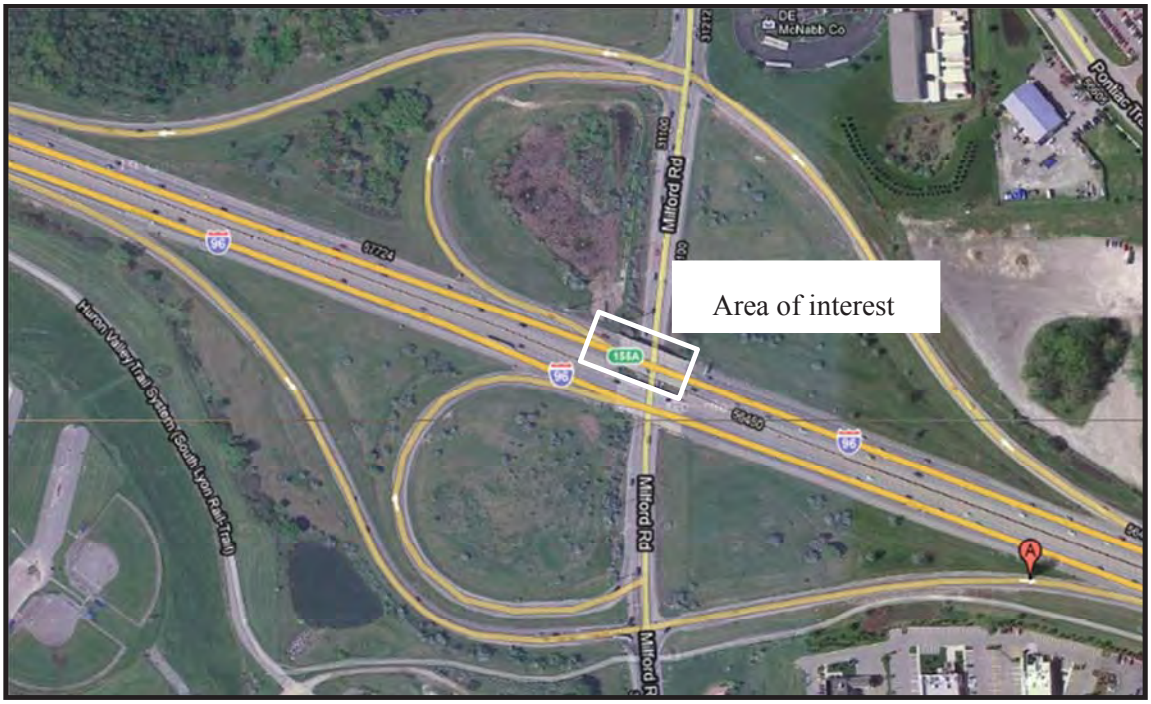

Figure 4-28 Intersection of 3022-S02-4 carrying I-96 WB over Milford Road
Source: Google earth

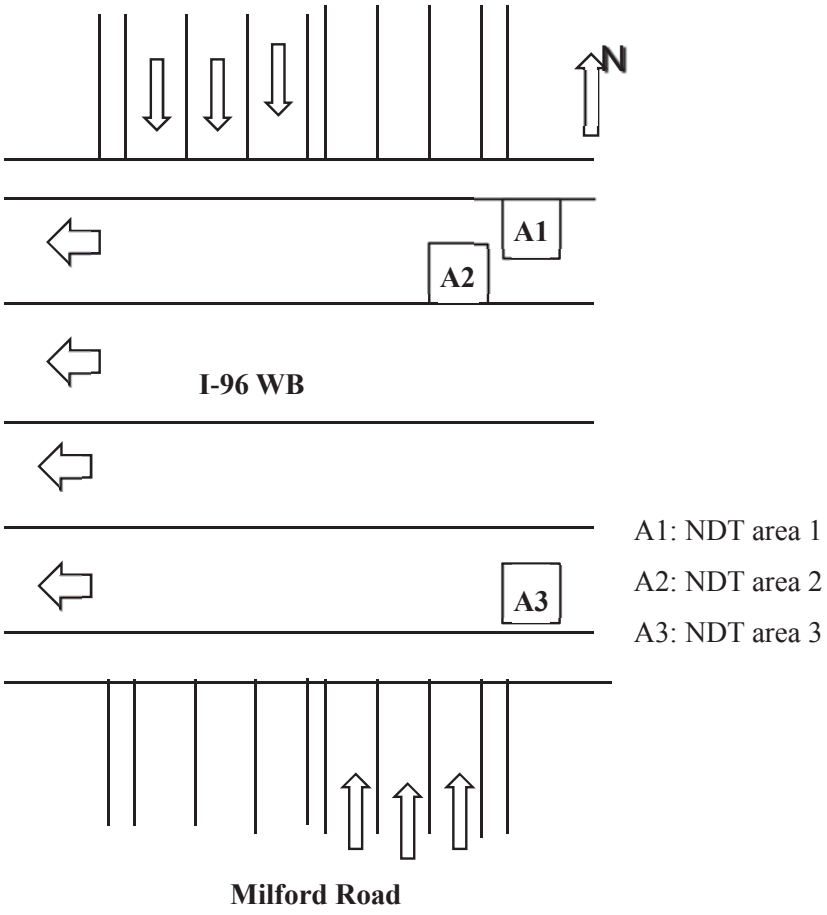

Figure 4-29 NDT areas of 63022-S02-4 carrying I-96 over Milford Road

Visual inspection

In general, the top and the bottom concrete deck surfaces were in good condition over the roadway, whereas poorer conditions existed over the tail spans. A small portion of the bottom deck was covered with plywood (Figure 4-30(a)). And small areas of transverse and longitudinal cracks, traces of rust and deicing salt were observed (Figure 4-30(b) and Figure 4-30(c)). Deteriorated concrete deck and exposed reinforcement bars existed on the bottom deck of the tail span as shown in Figure 4-30(d).

(a) Bottom view of 63022-S02-4 carrying I-96 WB over Milford Road

(b) White traces and cracks (tail span)

(c) Cracks and corrosion traces (tail span, WB)

(d) Deteriorated concrete and exposed reinforcement bar (tail span, WB)

Figure 4-30 Visual evaluation of 63022-S02-4 carrying I-96 WB over Milford Road

4.4.3 Bridge 63022-S01 carrying I-96 WB over Kent Lake Road

This 36^{o} skew bridge was constructed in 1948, an additional lane was added in 1967 and the entire deck had a shallow overlay in 1989. This four span and six lane structure has a total length of 178.8 ft. with a maximum central span of 49.9 ft. The width of the deck slab is 116.1 ft. Steel girders are supported on two abutments and four piers. Area of interest of the bridge is shown in Figure 4-31.

This bridge was visited twice for NDT purposes. A total of six areas were selected for non-destructive testing. NDT was carried out in areas A1, A2 and A3 during the first visit and NDT of areas B1, B2 and B3 was performed during the second visit. Due to the high traffic volumes and the ongoing roadwork ½ mile further west of the bridge, coring was performed during a third visit on a Sunday morning. NDT areas and coring locations are presented in Figure 4-32

Figure 4-31 Intersection of 63022-S01 carrying I-96 WB over Kent Lake Road
Source: Google earth

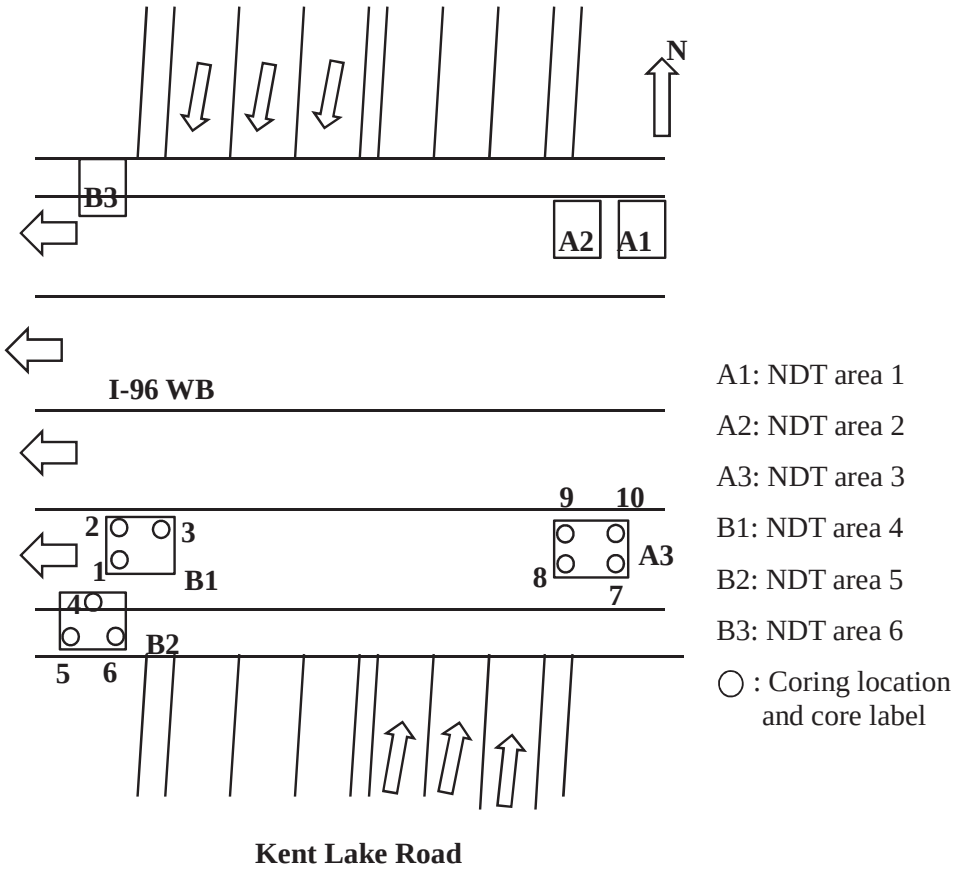

Figure 4-32 NDT areas of 63022-S01 carrying I-96 WB over Kent Lake

Visual inspection

This 63 years old bridge exhibited deteriorated concrete conditions across the majority of the bottom deck. Significant portions of the bottom deck over the roadway were covered with plywood to protect travelers below from falling concrete chunks (Figure 4-33(a)). Rust stains and effluorescence were observed (Figure 4-33(b)) and exposed reinforcement bars were noticed on the tail span (Figure 4-33(c) and Figure 4-33(d)).

(a) Plywood cover on most part of the bottom deck of 63022-S01 carrying I-96 over Kent Lake Road

(b) Crack and effluorescence (tail span,WB)

(c) Deteriorated concrete and exposed reinforcement (under plywood)

(d) Corroded reinforcement (tail span, WB)

Figure 4-33 Visual evaluation of 63022-S01 carrying I-96 over Kent Lake Road

Evaluation of cores

Ten cores were obtained from the deck and are presented in Figure 4-34. Visual inspection of the cores verified 1 in to 1.75 in. shallow overlay. Voids were encountered on the original concrete. The cores were 4 in diameter and at least 8 in depth. The cores obtained from the bridge are shown below in Figure 4-34. The individual cores are presented in Figure 4-35 through Figure 4-44.

Figure 4-34 63022-S01 carrying I-96 over Kent Lake Road cores
(Cores 1, 2, 3, 7, 8, 9 and 10 were from the right lane;
Cores 4, 5 and 6 were from the interior shoulder)

Core1

(a) Core 1 (b) Rust on the reinforcing bar

Figure 4-35 Core 1 of 63022-S01 carrying I-96 over Kent Lake Road

- Height 8.5 in.
- Diameter 4 in.
- 1 in. overlay with different aggregate size
- Reinforcement was observed at 2.0 in. and 4.0 in. from the bottom surface
- Rust was observed on the perimeter of the reinforcement and the adjacent porous zone

Core 2

(a) Core 2 (b) Rust on the reinforcing steel

Figure 4-36 Core 2 of 63022-S01 carrying I-96 over Kent Lake Road

- Height 8.75 in.
- Diameter 4 in.
- 1.75 in. overlay with different aggregate size
- Reinforcement at 2.75 in. and 1.75 in. from the bottom surface
- Rust was observed on the perimeter of the reinforcement and the adjacent porous zone

Core 3

(a) Core 3 (b) Rust on the reinforcing steel

Figure 4-37 Core 3 of 63022-S01 carrying I-96 over Kent Lake Road

- Height 8.75 in.
- Diameter 4 in.
- 1.75 in. overlay with different aggregate size
- Reinforcement at 2.75 in. and 1.75 in. from the bottom surface
- Rust was observed on the perimeter of the reinforcement and the adjacent porous zone

Core 4

(b) Core 4 (b) Rust on the reinforcing steel

Figure 4-38 Core 4 of 63022-S01 carrying I-96 over Kent Lake Road

- Height 8.75 in.
- Diameter 4 in.
- 1.75 in. overlay with different aggregate size
- Reinforcement was observed at 3.5 in. from the top surface
- Rust was observed on the perimeter of the reinforcement and the adjacent porous zone

Core 5

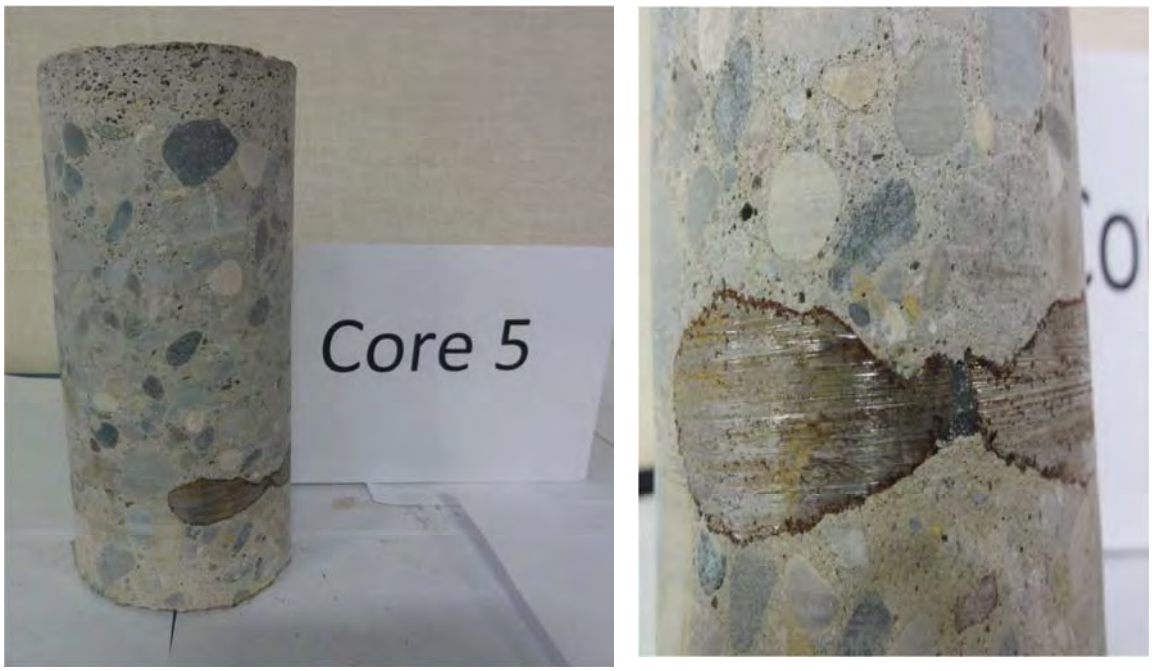

(a) Core 5 (b) Rust on the reinforcing steel

Figure 4-39 Core 5 of 63022-S01 carrying I-96 over Kent Lake Road

- Height 8.25 in.
- Diameter 4 in.
- 1.75 in. overlay with different aggregate size
- Reinforcement at 4.0 in. and 1.75 in. from bottom surface
- Rust was observed on the perimeter of the reinforcement and the adjacent porous zone

Core 6

(a) Core 6 (b) Rust on the reinforcing steel

Figure 4-40 Core 6 of 63022-S01 carrying I-96 over Kent Lake Road

- Height 8.5 in.
- Diameter 4 in.
- 1.75 in. overlay with different aggregate size
- Reinforcement at 2.3 in. and 4.0 in. from bottom surface
- Rust was observed on the perimeter of the reinforcement and the adjacent porous zone

Core 7

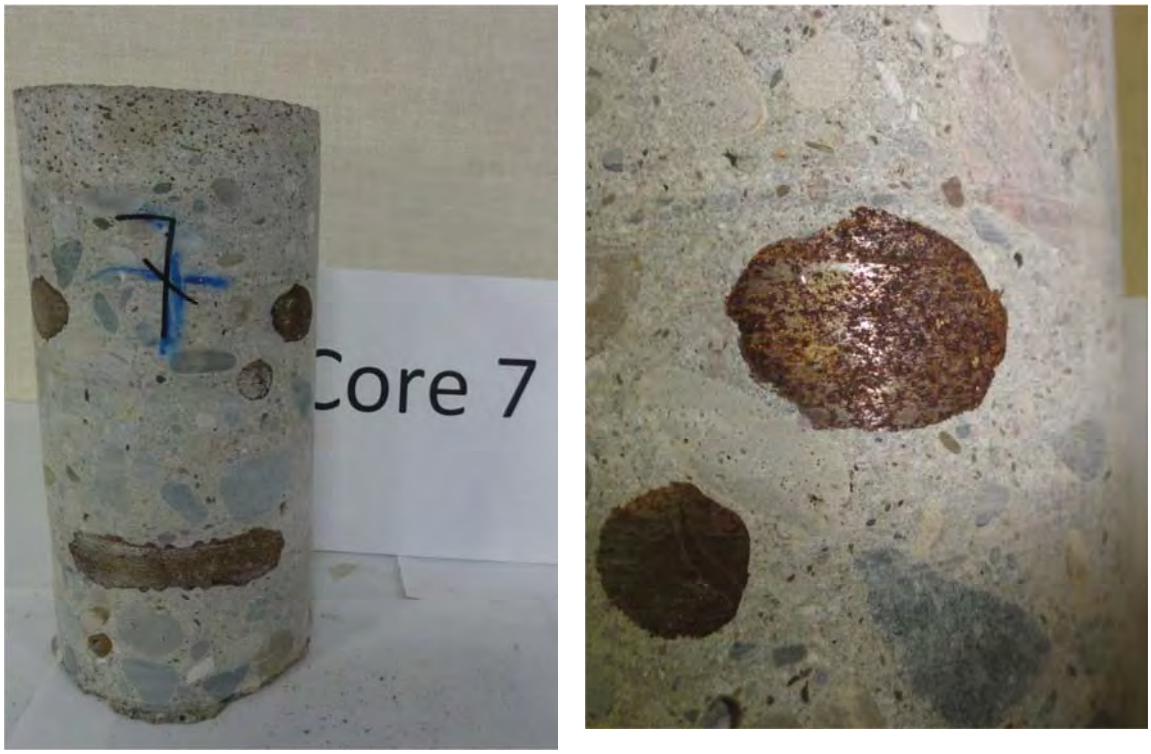

(a) Core 7 (b) Rust on the reinforcing steel

Figure 4-41 Core 7 of 63022-S01 carrying I-96 over Kent Lake Road

- Height 8.0 in.
- Diameter 4 in.
- 2.0 in. overlay with different aggregate size
- Reinforcement at 4.75 in., 5.75 in., 5.25 in., 4.75 in., and 2.0 in. from bottom surface
- Rust was observed on the perimeter of the reinforcement and the adjacent porous zone

Core 8

(a) Core 8 (b) Rust on the reinforcing steel

Figure 4-42 Core 8 of 63022-S01 carrying I-96 over Kent Lake Road

- Height 8.25 in.
- Diameter 4 in.
- 1.75 in. overlay with different aggregate size
- Reinforcement at 2.5 in., 2.75 in., and 6.25 in. from bottom surface
- Rust was observed on the perimeter of the reinforcements

Core 9

(a) Core 9

(b) Cracks on the core propagating from bottom surface to mid height

(c) Cracks on core propagating from bottom to mid height

(d) Crack on deck propagating from bottom surface to mid depth

Figure 4-43 Core 9 of 63022-S01 carrying I-96 over Kent Lake Road

- Height 8.25 in.
- Diameter 4 in.
- 1.25 in. overlay with different aggregate size
- No reinforcement
- Cracks of size approximately 0.085 in. propagated from bottom surface of the deck to mid height

Core 10

(a) Core 10

(b) Cracks on the core propagating from bottom surface

Figure 4-44 Core 10 of 63022-S01 carrying I-96 over Kent Lake Road

- Height 8.25 in.
- Diameter 4 in.
- 1.25 in. overlay with different aggregate size
- Reinforcement at 6 in. form top surface
- Rust was observed on the perimeter of the reinforcements
- Cracks of size approximately 0.075 in. propagated from bottom surface of the deck

CHAPTER 5: RESULTS AND DISCUSSIONS OF LABORATORY INVESTIGATION

5.1 Introduction

Results and discussions of the laboratory experimental program are presented in this chapter. First, results related to the compressive and flexural strength of the concrete mixes are presented. Next, the results and discussions of the exposure tests and load tests for the laboratory deck slab specimens are presented. Results and discussions of half-cell potential tests, corrosion rate tests, surface hardness tests, and repeated loading tests for specimens constructed from the chloride introduced concrete mix are discussed followed by the results and discussions for the specimens constructed from the non-chloride introduced concrete mix. The details of the deployed experimental methods are presented in Chapter 3.

5.2 Compressive Strength of Concrete

The concrete compressive strength was determined on cylinders according to ASTM C39/ C39M-09. Results of the compressive strength tests are presented in Table 5-1 and the development of compressive strength with time is shown in Figure 5-1. The 28-day average compressive strength was 4,900 psi for the non-chloride introduced concrete mix and 6,070 psi for the chloride introduced concrete mix.

(a) Cylinder before test (b) Cylinder after test

Figure 5-1 Cylinders during compressive strength test

Table 5-1 Compressive strength test results for cylinders

Age (days)	Number of Cylinders	Compressive Strength (Non-Chloride Introduced Mix) (psi)			Compressive Strength (Chloride Introduced Mix) (psi)		
		Measurement Data	Standard Deviation	Average	Measurement Data	Standard Deviation	Average
1	3	2,440 2,730 2,860	217	2,670	3,610 3,520 3,530	48	3,550
3	3	3,560 3,340 3,410	114	3,440	4,410 4,330 4,640	164	4,460
7	3	4,150 3,950 3,810	175	3,970	4,990 4,980 5,150	95	5,040
28	3	4,860 4,800 5,030	121	4,900	6,130 6,350 5,730	316	6,070
90	3	4,940 5,290 5,280	201	5,170	7,010 6,890 6,770	119	6,890

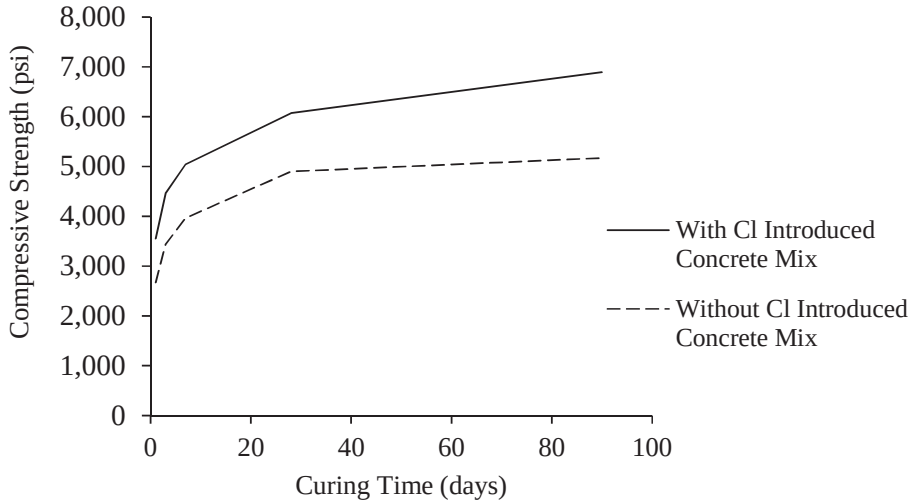

Figure 5-2 Compressive strength development with time

5.3 Flexural Strength of Concrete

The 28-day flexural strength of the concrete was determined in accordance with ASTM C78/ C78M-10, and the results are presented in Table 5-2. The average 28-day flexural strength was 740 psi for the chloride introduced mix and 755 psi for the non-chloride introduced mix.

(a) Prism before test (b) Prism after test

Figure 5-3 Rectangular prisms during flexural strength test in four-point loading setup

Table 5-2. 28-day flexural strength test results for rectangular prisms

Number of Prisms	Flexural Strength (Non-Chloride Introduced Mix) (psi)			Flexural Strength (Chloride Introduced Mix) (psi)		
	Measurement Data	Standard Deviation	Average	Measurement Data	Standard Deviation	Average
6	765 755 765 730 745 780	18	755	690 760 750 740 820 685	50	740

5.4 Cracking Load Test

All 20 deck slab specimens were subjected to a flexural load at the beginning of the test program to cracks having widths between 0.004 in. and 0.01 in (Figure 3-2, Figure 3-8, and Figure 3-10). The range of the pre-cracked widths was selected based on permissible width criteria for severe environments. The service cracking load test is performed with a positive moment (bottom cracking) application. The load-displacement curves for the service cracking load tests for all the specimens are presented in Figure 5-4. The static loading continued past the onset of flexural cracks until the average cracks widths ranged between 0.004 in. and 0.01 in. All specimens experienced cracking at loads between 16 kips and 17 kips as shown in Figure 5-4.

The theoretical cracking load was determined with the 28-day flexural strength. Good agreement was found between the observed and the theoretical cracking loads. The theoretical prediction for the cracking load was 16.5 kips for specimens constructed from the chloride induced mix. The theoretical prediction for the cracking load was 16.9 kips for specimens constructed from the non-chloride induced mix.

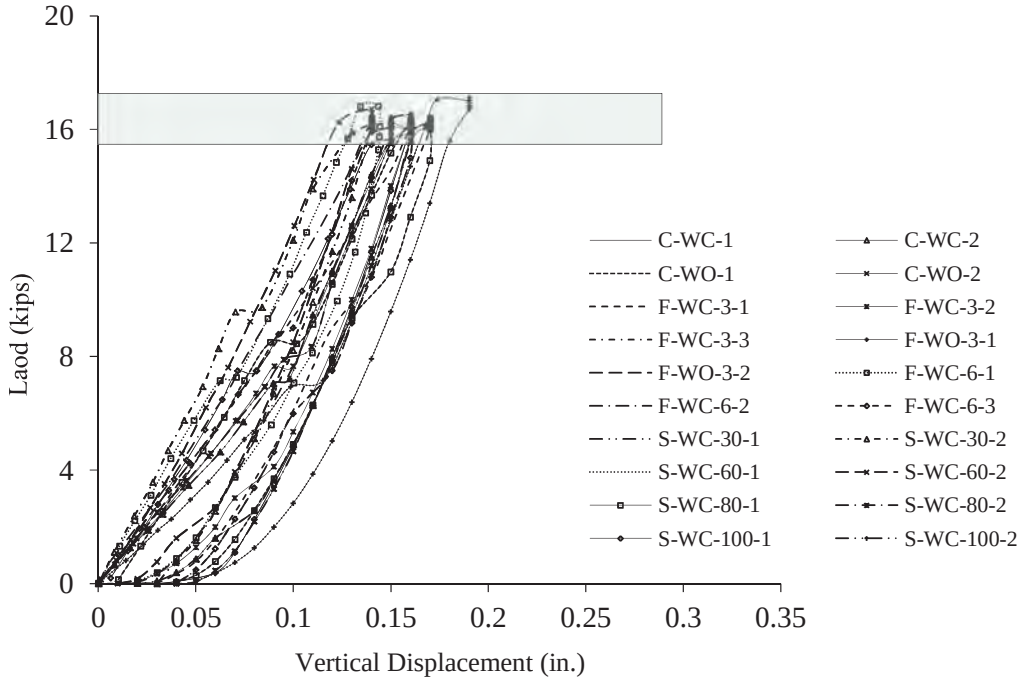

Figure 5-4 Load-displacement curves for positive moment application for all specimens

5.5 NDT Test for Specimens Constructed from Chloride Introduced Concrete Mix

The NDT test results after the environmental exposures are presented in this section for the deck slab specimens constructed from chloride introduced concrete mix. Results from half-cell potential and corrosion rate tests are presented. Results from surface hardness test are presented in Section 5.7. Static load and ultimate load tests are then presented to evaluate the influence of various exposure conditions on the structural behavior of the specimens in Section 5.8 and 5.9, respectively.

5.5.1 Half-Cell Potential Test Results

Half-cell potential tests were conducted on the bottom surface of each specimen at twelve locations along the bottom main reinforcement. The results of these potential tests for the groups

defined as control specimens, freeze-thaw (F-T) specimens and saltwater (S-W) specimens are presented in Table 5-3, Table 5-5 and Table 5-6, respectively.

Control Specimens

Two control specimens constructed from the chloride introduced concrete mix were not exposed to freeze-thaw exposures, saltwater exposures or repeated load tests. Half-cell potential of the control specimens were measured after six months, twelve months and eighteen months, and are presented in Table 5-3. A graphical representation of the average of the measured half-cell potentials is shown in Figure 5-5. The potential of these control specimens were inversely proportional to the age of the specimens. According to ASTM C876, the half-cell potential values can be related to the chances of corrosion in the embedded reinforcement as given in Table 4-2.

Table 5-3 Average half-cell potential values for control specimens

Specimen Name	**Half-Cell Potential* (mV)**			**Chance of Corrosion**
	6 months	**12 months**	**18 months**	
C-WC-1	-170	-139	-120	5% / 5% / 5%
C-WC-2	-160	-134	-75	5% / 5% / 5%

*Average values of 36 (12 locations x 3 bars) data point measurements obtained from CANIN instrument

Table 5-4 Interpretation of half-cell potential values as per ASTM C876

Potential difference (mV)	**Chance of Corrosion**
< -500	Visible evidence of corrosion
-350 to -500	95%
-200 to -350	50%
> -200	5%

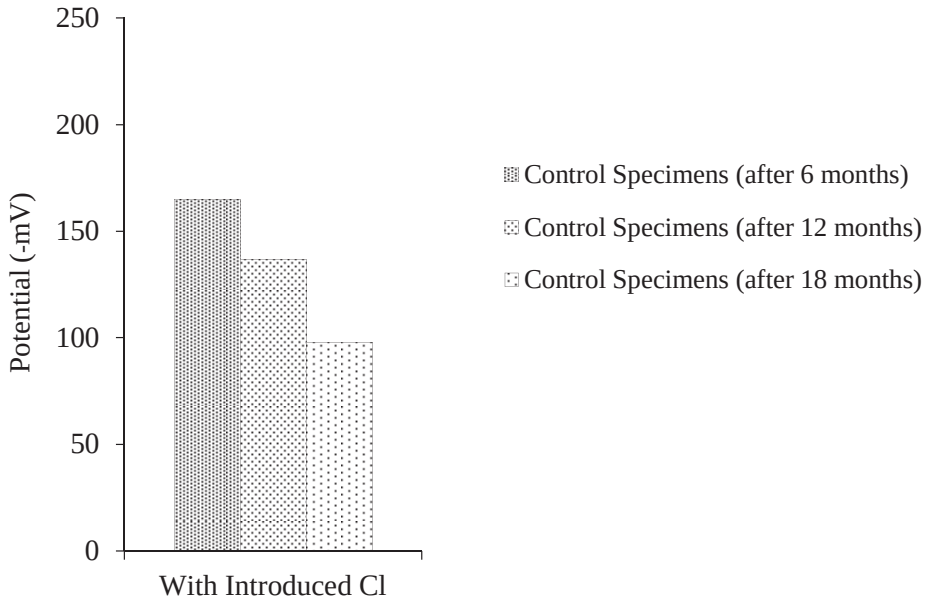

Figure 5-5 Half-cell potential values for control specimens

Freeze-Thaw Specimens

Six specimens constructed from the chloride introduced concrete mix were exposed to freeze-thaw cycles. Half-cell potential test on all six freeze-thaw specimens were conducted at the end of 300 freeze-thaw cycles. In addition, the half-cell potentials were measured at the end of 400, 500 and 600 freeze-thaw cycles on three specimens. Results of the average half-cell potential values are presented in Table 5-5. It can be observed that the potential was increasing with increasing freeze-thaw exposure. A graphical representation of these results is shown in Figure 5-6.

Table 5-5 Average half-cell potential values for freeze-thaw exposed specimens

Specimen Name	Half-Cell Potential* (mV)			
	300 cycles	400 cycles	500 cycles	600 cycles
F-WC-3-1	-210	-	-	-
F-WC-3-2	-270	-	-	-
F-WC-3-3	-340	-	-	-
F-WC-6-1	-330	-320	-380	-387
F-WC-6-2	-345	-338	-355	-363
F-WC-6-3	-290	-348	-370	-380

- Not applicable

*Average values of 36 (12 locations x 3 bars) data point measurements obtained from CANIN instrument

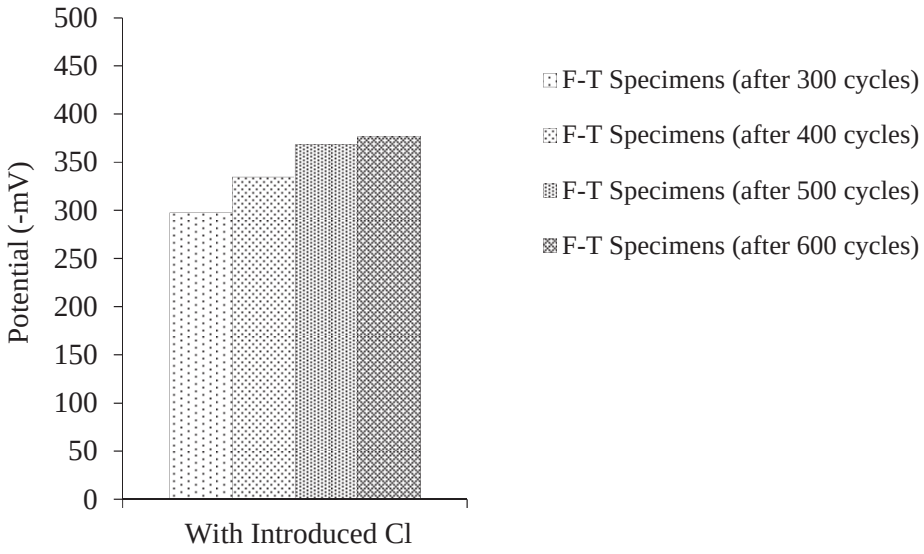

Figure 5-6 Half-cell potential values for freeze-thaw exposed specimens

Moreover, according to ASTM C876, as indicated in Table 4-2, the chance of the reinforcement being corroded after 300 and 400 freeze-thaw cycles was 50% while it was 95% after 500 and 600 freeze-thaw cycles.

Saltwater Specimens

Eight specimens constructed from the chloride introduced concrete mix were exposed to saltwater. The half-cell potentials of all eight saltwater specimens were measured at the end of 3,000 hours of saltwater exposure. Further, half-cell potential measurements were carried out on two specimens at the end of 6,000 hours, on four specimens at the end of 8,000 hours and on two specimens at the end of 10,000 hours of saltwater exposure. Results of the average half-cell potential values are presented in Table 5-6. A slight increase in the potential was observed with increasing duration of saltwater exposure. A graphical representation of the results is shown in Figure 5-7.

Table 5-6 Average half-cell potential values for saltwater exposed specimens

Specimen Name	**Half-Cell Potential* (mV)**				**Chance of Corrosion**
	3,000 hours	**6,000 hours**	**8,000 hours**	**10,000 hours**	
S-WC-30-1	-345	-	-	-	50%
S-WC-30-2	-320	-	-	-	50%
S-WC-60-1	-265	-303	-	-	50% / 50%
S-WC-60-2	-245	-284	-	-	50% / 50%
S-WC-80-1	-295	-	-305	-	50% / 50%
S-WC-80-2	-290	-	-305	-	50% / 50%
S-WC-100-1	-270	-	-315	-324	50% / 50% / 50%
S-WC-100-2	-280	-	-290	-318	50% / 50% / 50%

- Not applicable

*Average values of 36 (12 locations x 3 bars) data point measurements obtained from CANIN instrument

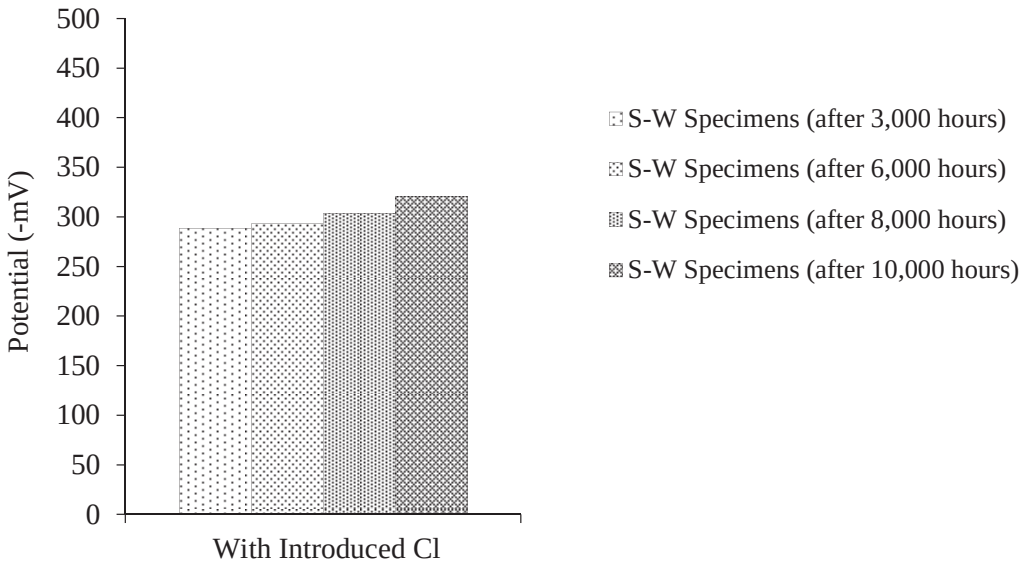

Figure 5-7 Half-cell potential values for saltwater exposed specimens

5.5.2 Corrosion Rate Test Results

Corrosion rate tests were conducted on the bottom surface of each specimen at six locations along the bottom main reinforcements. The results of these corrosion rate tests for control specimens, freeze-thaw specimens and saltwater specimens are presented in Table 5-7, Table 5-8 and Table 5-9, respectively.

Control Specimens

Two control specimens constructed from the chloride introduced concrete mix were not exposed to freeze-thaw exposures, saltwater exposures or repeated load tests. Corrosion rate of the control specimens were measured at six months, twelve months and eighteen months, and the results are presented in Table 5-7. A graphical representation of the average measured corrosion rate is shown in Figure 5-8. It can be observed that the corrosion rate of these control specimens were inversely proportional to the age of the specimens. This decrease in the corrosion rate can be attributed to the self-desiccations (internal drying of the concrete as the free water is used in

the continuous hydration process) in the concrete specimens. Moreover, at the end of eighteen months, an average relative humidity of 73% was measured in the control specimens while 92% average relative humidity was recorded for the freeze-thaw and saltwater specimens.

Table 5-7 Average corrosion rate for control specimens

Specimen Designation	Corrosion Rate* (μm/year)		
	6 months	12 months	18 months
C-WC-1	27	19	12
C-WC-2	36	18	10

*Average values of 18 (6 locations x 3 bars) data point measurements obtained from GalvaPulse instrument.
(1 μm/year – 0.0394 mils/year).

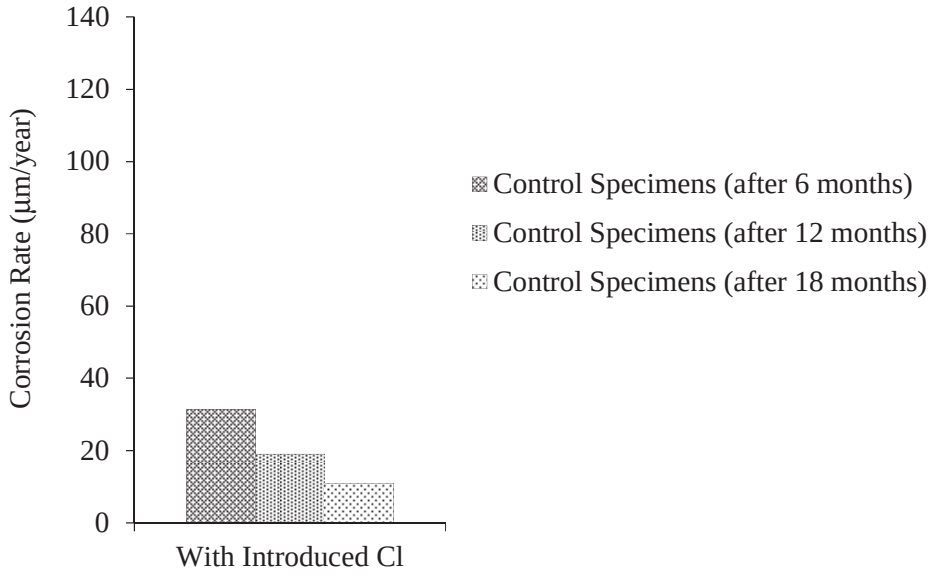

Figure 5-8 Corrosion rate for control specimens

Freeze-Thaw Specimens

Six specimens constructed from the chloride introduced concrete mix were exposed to freeze-thaw. Corrosion rate tests on all freeze-thaw specimens were conducted at the end of 300 freeze-thaw cycles. In addition, the corrosion rates were measured at 400, 500 and 600 freeze-thaw cycles on three specimens. Results of the average corrosion rate are presented in Table 5-8. It can be observed that the corrosion rate was increasing with increasing freeze-thaw exposure. A graphical representation of these results is shown in Figure 5-9.

Table 5-8 Average corrosion rate for freeze-thaw exposed specimens

Specimen Designation	**Corrosion Rate* (μm/year)**			
	300 Cycles	**400 Cycles**	**500 Cycles**	**600 Cycles**
F-WC-3-1	79	-	-	-
F-WC-3-2	85	-	-	-
F-WC-3-3	83	-	-	-
F-WC-6-1	77	91	100	120
F-WC-6-2	83	106	115	133
F-WC-6-3	88	120	125	111

- Not applicable

*Average values of 18 (6 locations x 3 bars) data point measurements obtained from GalvaPulse instrument. (1 μm/year – 0.0394 mils/year).

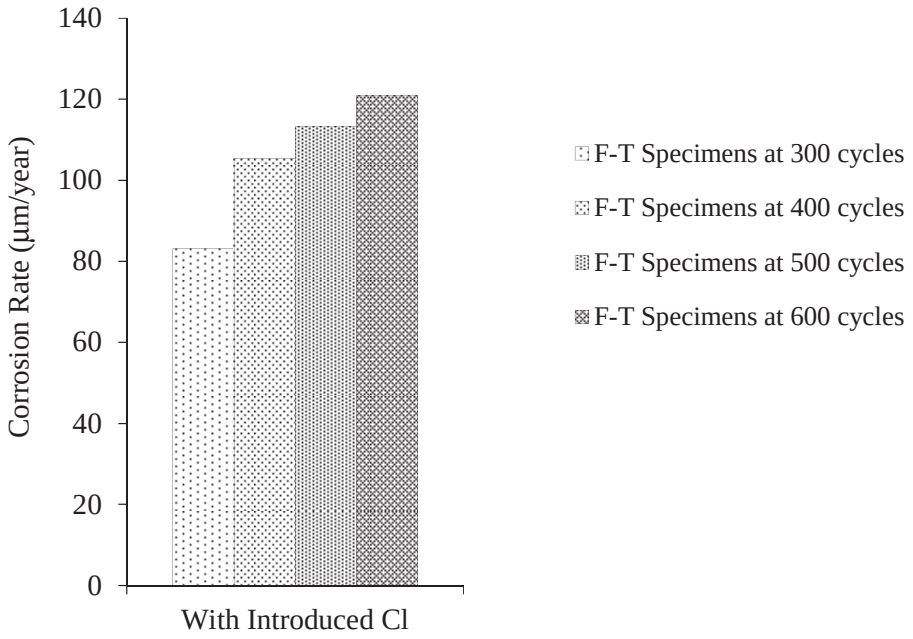

Figure 5-9 Corrosion rate for freeze-thaw exposed specimens. (1 µm/year – 0.0394 mils/year).

Saltwater Specimens

Eight specimens constructed from the chloride introduced concrete mix were exposed to saltwater. The corrosion rates of all saltwater specimens were measured at the end of 3,000 hours of saltwater exposure. Further, corrosion rate measurements were carried out on two specimens at the end of 6,000 hours, on four specimens at the end of 8,000 hours and on two specimens at the end of 10,000 hours of saltwater exposure. Results of the average corrosion rate are presented in Table 5-9. It is observed that the corrosion rate increased with respect to the duration of S-W exposure. A graphical representation of the results is shown in Figure 5-10.

Table 5-9 Average corrosion rate for saltwater exposed specimens

Specimen Designation	Corrosion Rate* (μm/year)			
	3,000 Hours	6,000 Hours	8,000 Hours	10,000 Hours
S-WC-30-1	43	-	-	-
S-WC-30-2	57	-	-	-
S-WC-60-1	52	63	-	-
S-WC-60-2	49	61	-	-
S-WC-80-1	50	-	61	-
S-WC-80-2	52	-	57	-
S-WC-100-1	44	-	87	99
S-WC-100-2	43	-	76	84

- Not applicable

*Average values of 18 (6 locations x 3 bars) data point measurements obtained from GalvaPulse instrument. (1 μm/year – 0.0394 mils/year).

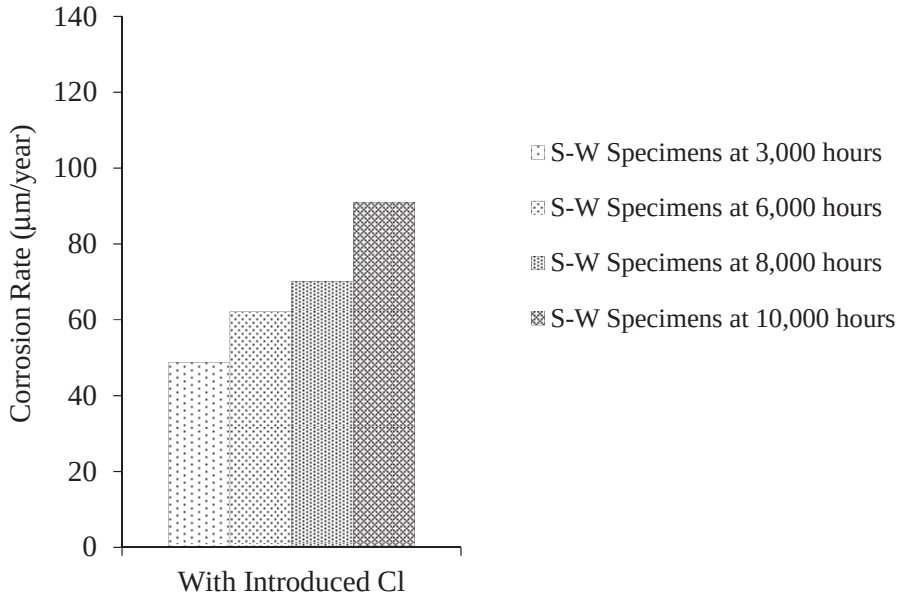

Figure 5-10 Corrosion rate for saltwater exposed specimens. (1 μm/year – 0.0394 mils/year).

5.6 NDT Test for Specimens Constructed from Non-Chloride Introduced Concrete Mix

The NDT test results of the environmental exposure are presented in this section for the deck slab specimens constructed from non-chloride introduced concrete mix. Results from half-cell potential and corrosion rate tests are presented. Results from surface hardness test are presented in Section 5.7. Static load and ultimate load tests are then presented to evaluate the influence of various exposure conditions on the structural behavior of the specimens in Section 5.8 and 5.9, respectively.

5.6.1 Half-Cell Potential Test Results

Half-cell potential tests were conducted on the bottom surface of each specimen at twelve locations along the reinforcement. The results of these potential tests for control specimens and freeze-thaw specimens are presented in Table 5-10 and Table 5-11, respectively.

Control Specimens

Two control specimens constructed from non-chloride introduced concrete mix were not exposed to freeze-thaw exposures, saltwater exposures or repeated load tests. Half-cell potential of the control specimens were measured at the end of six months, twelve months and eighteen months, and are presented in Table 5-10. A graphical representation of the average of the measured half-cell potentials of the specimens is shown in Figure 5-11.

Table 5-10 Average half-cell potential values for control specimens

Specimen Name	Half-Cell Potential* (mV)			Chance of Corrosion
	6 months	12 months	18 months	
C-WO-1	-120	-94	-45	5% / 5% / 5%
C-WO-2	-125	-89	-65	5% / 5% / 5%

*Average values of 36 (12 locations x 3 bars) data point measurements obtained from CANIN instrument

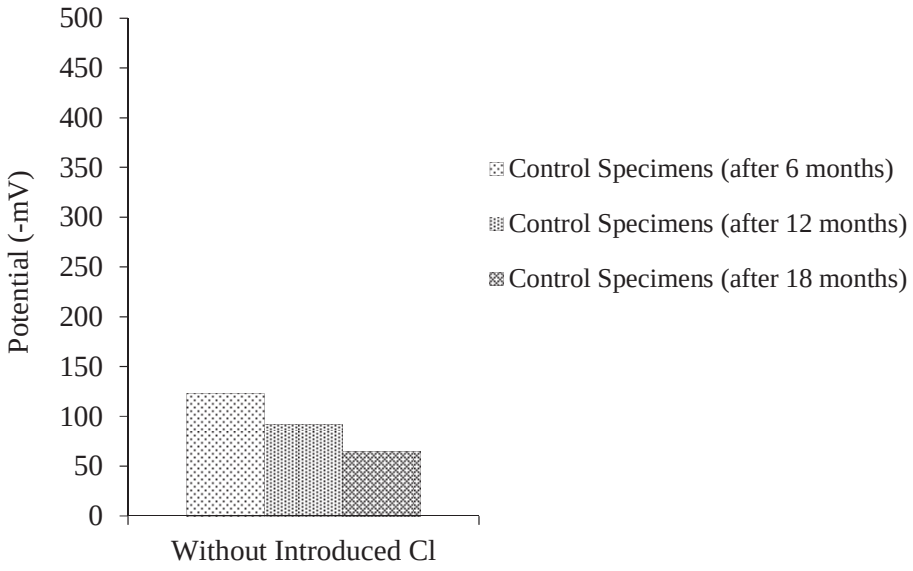

Figure 5-11 Half-cell potential values for control specimens

Freeze-Thaw Specimens

Two specimens constructed from the non-chloride introduced concrete mix were exposed to 300 freeze-thaw cycles. Half-cell potential test on both freeze-thaw specimens were conducted at the end of the 300 freeze-thaw cycles. Results of the average half-cell potential values are presented in Table 5-11.

Table 5-11 Average half-cell potential values for freeze-thaw specimens

Specimen Designation	Half-Cell Potential* (mV)	Chance of Corrosion
	300 Cycles	
F-WO-3-1	-145	5%
F-WO-3-2	-150	5%

*Average values of 36 (12 locations x 3 bars) data point measurements obtained from CANIN instrument

5.6.2 Corrosion Rate Test Results

Corrosion rate tests were conducted on the bottom surface of each specimen at six locations along the bottom main reinforcements. The results of these corrosion rate tests for control specimens and freeze-thaw specimens are presented in Table 5-12 and Table 5-13 respectively.

Control Specimens

Two control specimens constructed from the non-chloride introduced concrete mix were not exposed to freeze-thaw exposures, S-W exposures or repeated load tests. Corrosion rate of the control specimens were measured at the end of six months, twelve months and eighteen months, and the results are presented in Table 5-12. A graphical representation of the average measured corrosion rates is shown in Figure 5-12.

Table 5-12 Average corrosion rate for control specimens

Specimen Designation	Corrosion Rate* (μm/year)		
	6 months	12 months	18 months
C-WO-1	19	15	9
C-WO-2	19	12	6

*Average values of 18 (6 locations x 3 bars) data point measurements obtained from GalvaPulse instrument. (1 μm/year = 0.0394 mils/year)

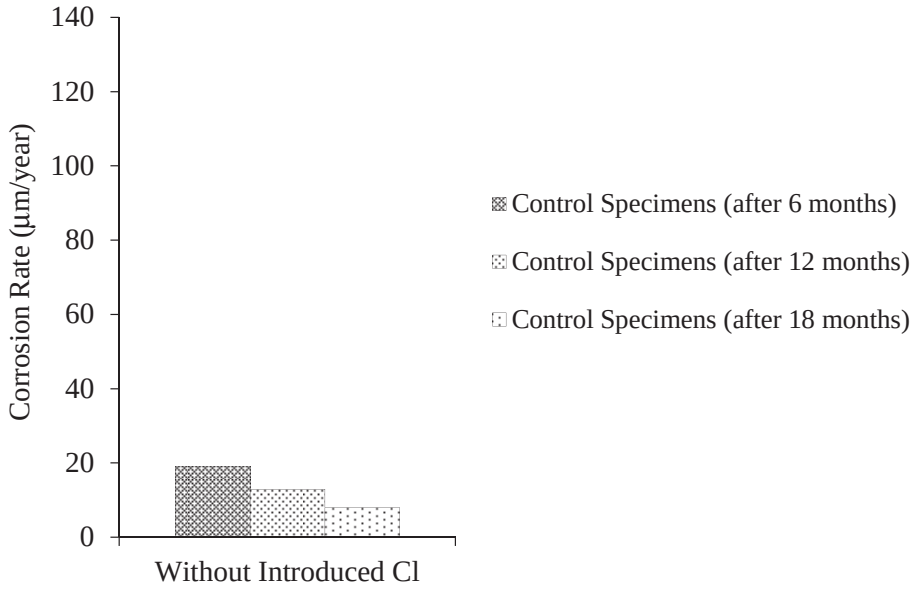

Figure 5-12 Corrosion rate for control specimens. (1 μm/year – 0.0394 mils/year).

Freeze-Thaw Specimens

Two specimens constructed from the non-chloride introduced concrete mix were exposed to 300 freeze-thaw cycles. Corrosion rate tests on both freeze-thaw specimens were conducted at the end of 300 freeze-thaw cycles. Results of the average corrosion rate are presented in Table 5-13.

Table 5-13 Average corrosion rate for freeze-thaw exposed specimens

Specimen Designation	Corrosion Rate* (μm/year)
	300 Cycles
F-WO-3-1	24
F-WO-3-2	13

*Average values of 18 (6 locations x 3 bars) data point measurements obtained from GalvaPulse instrument.
(1 μm/year = 0.0394 mils/year)

5.7 Surface Hardness Test Results

Surface hardness tests were conducted on the surface of each specimen at three different locations. The results of these hardness tests for control specimens, freeze-thaw specimens and saltwater specimens are presented in Table 5-14, Table 5-15 and Table 5-16, respectively.

Control Specimens

There were four control specimens: two specimens constructed from the chloride introduced concrete mix and two specimens constructed from the non-chloride introduced concrete mix. The four control specimens were not exposed to freeze-thaw exposure, saltwater exposure or repeated load tests. Hardness tests of the control specimens were conducted at the end of six months, twelve months and eighteen months. The test results along with standard deviations and coefficient of variations are presented in Table 5-14. It can be observed from the coefficient of variations, COV, that the concrete surface hardness was similar for the two mixes at the three different ages (i.e. at six, twelve and eighteen months of age).

Table 5-14 Results of hardness test of control specimens

Specimen Designation	After 6 months				After 12 months				After 18 months			
	Hardness (psi)	Average (psi)	Standard Deviation	COV (%)	Hardness (psi)	Average (psi)	Standard Deviation	COV (%)	Hardness (psi)	Average (psi)	Standard Deviation	COV (%)
C-WO-1	8,370	8,590	324	3.8	9,830	10,120	478	4.6	11,370	11,650	302	2.6
	8,920				10,380				11,920			
	8,570				10,030				11,570			
C-WO-2	8,450				10,040				11,570			
	9,100				10,690				12,220			
	8,150				9,740				11,270			
C-WC-1	9,950	10,100	277	2.7	10,640	10,880	253	2.3	11,590	11,790	260	2.2
	10,250				10,940				11,890			
	10,450				11,140				12,090			
C-WC-2	10,050				10,910				11,790			
	9,600				10,460				11,340			
	10,300				11,160				12,040			

Freeze-Thaw Specimens

There were eight freeze-thaw specimens: six specimens constructed from the chloride introduced concrete mix and two specimens constructed from the non-chloride introduced concrete mix. Hardness tests were conducted on each freeze-thaw specimens at the end of 300 freeze-thaw cycles. In addition, hardness tests were carried out at the end of 400, 500 and 600 freeze-thaw cycles on three specimens. The test results are presented in Table 5-15(a) and Table 5-15(b). The values of the coefficient of variations, COV, shows that the concrete surface hardness was similar for the two mixes at the four different level of exposure (i.e. at 300, 400, 500 and 600 freeze-thaw cycles).

Table 5-15 Results of hardness test freeze-thaw specimens

(a) Results after 300 and 400 cycles

Specimen Designation	After 300 Cycles				After 400 Cycles			
	Hardness (psi)	Average (psi)	Standard Deviation	COV (%)	Hardness (psi)	Average (psi)	Standard Deviation	COV (%)
F-WO-3-1	8,320 8,820 8,670	8,490	223	2.6	-	-	-	-
F-WO-3-2	8,600 8,250 8,250							
F-WC-3-1	10,580 11,130 11,080	10,300	732	7.1	-	-	-	-
F-WC-3-2	9,170 10,320 9,470							
F-WC-3-3	9,680 9,030 9,180							
F-WC-6-1	10,270 9,970 10,670				11,720 11,420 12,120	11,744	381	3.2
F-WC-6-2	11,130 10,580 11,630				12,000 11,450 12,500			
F-WC-6-3	10,470 10,770 10,220				11,480 11,780 11,230			

- Not applicable

(b) Results after 500 and 600 cycles

Specimen Designation	After 500 Cycles				After 600 Cycles			
	Hardness (psi)	Average (psi)	Standard Deviation	COV (%)	Hardness (psi)	Average (psi)	Standard Deviation	COV (%)
	12,170				12,410			
F-WC-6-1	11,870				12,110			
	12,570				12,810			
	12,370				12,580			
F-WC-6-2	11,820	12,218	342	2.8	12,030	12,494	329	2.6
	12,870				13,080			
	12,080				12,460			
F-WC-6-3	12,380				12,760			
	11,830				12,210			

- Not applicable

Saltwater Specimens

Eight specimens constructed from chloride introduced concrete mix were exposed to saltwater. The hardness tests were conducted on each specimen at the end of 3,000 hours of exposure. Further, hardness tests were carried out on two specimens at the end of 6,000 hours, on four specimens at the end of 8,000 hours and on two specimens at the end of 10,000 hours. The test results are presented in Table 5-16(a), Table 5-16(b) and Table 5-16(c). It can be observed that the results of concrete surface hardness among the S-W specimens measured at the end of 3,000 hours were similar with a COV of 6.8%. Further, the same observation can be made among the saltwater specimens measured at the end of 6,000 hours, 8,000 hours and 10,000 hours of exposure.

Table 5-16 Results of hardness test of saltwater specimens

(a) Results after 3,000 hours of saltwater exposure

Specimen Designation	After 3,000 hours			
	Hardness (psi)	Average (psi)	Standard Deviation	COV (%)
S-WC-30-1	9,170 9,970 9,020	10,007	681	6.8
S-WC-30-2	8,920 9,970 9,770			
S-WC-60-1	8,820 10,220 9,220			
S-WC-60-2	10,150 9,600 11,000			
S-WC-80-1	10,750 10,950 11,250			
S-WC-80-2	10,370 10,420 10,120			
S-WC-100-1	9,590 9,640 9,490			
S-WC-100-2	10,350 10,600 10,800			

- Not applicable

(b) Results after 6,000 hours of saltwater exposure

Specimen Designation	After 6,000 hours			
	Hardness (psi)	Average (psi)	Standard Deviation	COV (%)
S-WC-60-1	10,040 11,440 10,440	11,245	840	7.5
S-WC-60-2	11,750 11,200 12,600			

- Not applicable

(c) Results after 8,000 and 10,000 hours of saltwater exposure

Specimen Designation	After 8,000 hours				After 10,000 hours			
	Hardness (psi)	Average (psi)	Standard Deviation	COV (%)	Hardness (psi)	Average (psi)	Standard Deviation	COV (%)
S-WC-80-1	11,810 12,010 12,310	11,873	242	2.0	-	-	-	-
S-WC-80-2	11,770 11,820 11,520							
S-WC-100-1	11,400 11,450 11,300	11,428	145	1.3	12,640 12,690 12,540	12,563	150	1.2
S-WC-100-2	11,240 11,490 11,690				12,270 12,520 12,720			

- Not applicable

5.8 Repeated Load Cycle Test Results

Following the methodology presented in Section 3.4.4, repeated loads using a four-point bending load setup were applied on each specimen at intervals of 250,000 cycles. The repeated load cycle applied a lower load limit of 2.5 kips and upper load limit of 15.5 kips. Static load test was conducted on each specimen at the end of every 250,000 load cycles. Typical plots showing the load-deflection response at the end of 3,000 hours of saltwater exposure is presented in Figure 5-13. It can be observed that the response at an interval of 250,000 cycles of repeated load is similar and remains, as expected, in the elastic range.

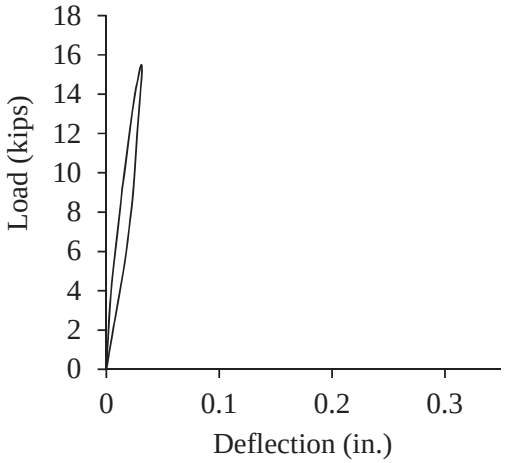

(a) Load-deflection response after 250,000 repeated load cycles

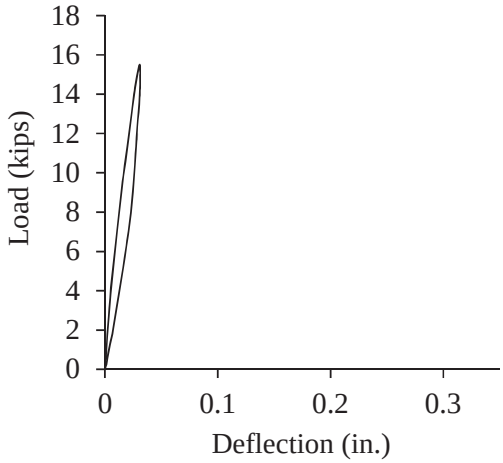

(b) Load-deflection response after 500,000 repeated load cycles

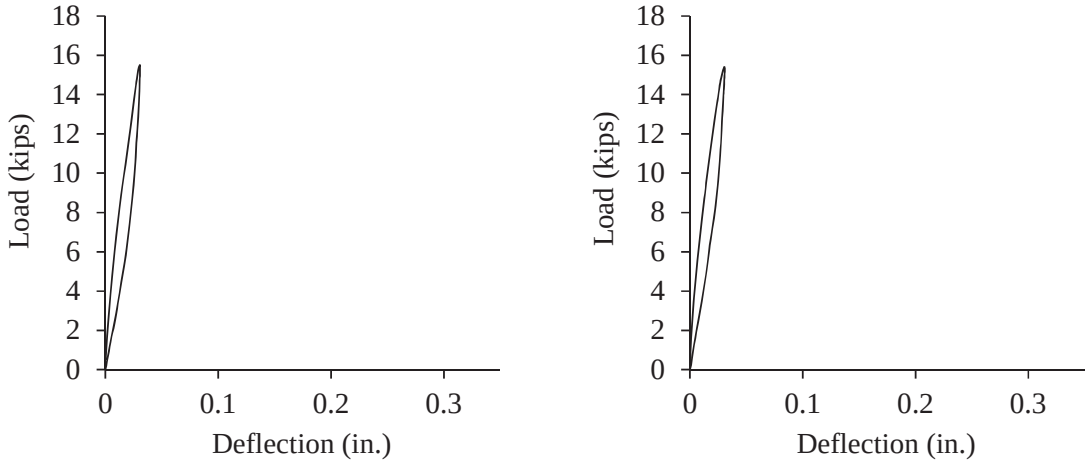

(c) Load-deflection response after 750,000 repeated load cycles

(d) Load-deflection response after 1,000,000 repeated load cycles

Figure 5-13 Load-deflection response of specimen exposed to 3,000 hours of saltwater

5.9 Ultimate Load Test Results

Ultimate load tests were carried out when the environmental exposure testing had been completed. The failure load, deflection values and the corresponding failure modes for each specimen are presented in Table 5-17. The ultimate failure mode for any specimen was either flexural mode as shown in Figure 5-14 (a) or combined flexural/shear mode as shown in Figure 5-14 (b). Graphical representations for all the load-deflection responses of the ultimate load test are presented in Figure 5-15. The ultimate load capacity for all the specimens (53.2 kips to 63.1 kips) are in close agreement with the theoretical capacity (52.6 kips) after 600 freeze-thaw cycles and 2,000,000 repeated load cycles or 10,000 hours of saltwater exposure and 3,000,000 repeated load cycles.

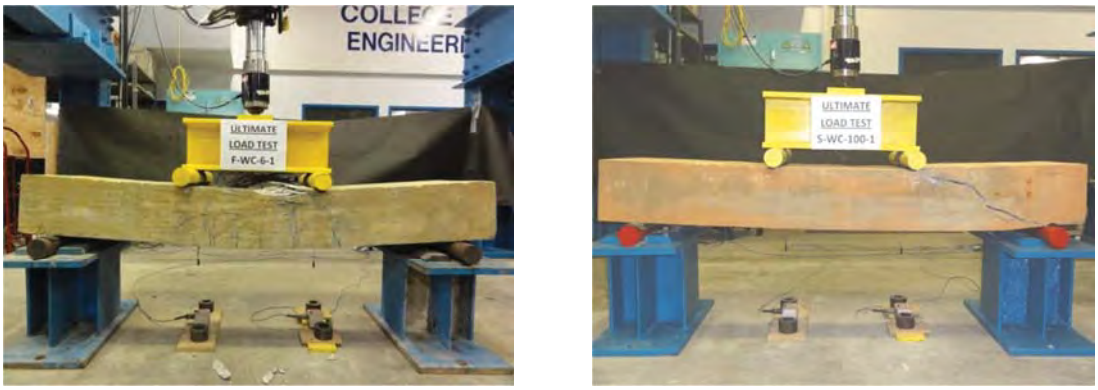

(a) Flexure mode (b) Flexure/shear mode

Figure 5-14 Failure modes from ultimate load tests

Table 5-17 Ultimate load test results

Specimen Designation	Failure Load (kips)	Deflection at Failure Load (in.)	Failure Mode
C-WO-1	53.9	0.47	Flexure/Shear
C-WO-2	56.8	0.52	Flexure/Shear
C-WC-1	56.7	0.47	Flexure/Shear
C-WC-2	56.7	0.54	Flexure/Shear
F-WO-3-1	59.3	0.65	Flexure
F-WO-3-2	58.9	0.67	Flexure
F-WC-3-1	58.3	0.65	Flexure/Shear
F-WC-3-2	58.7	0.69	Flexure
F-WC-3-3	56.3	0.62	Flexure
F-WC-6-1	63.1	0. 94	Flexure
F-WC-6-2	61.7	0. 85	Flexure
F-WC-6-3	59.4	0.67	Flexure/Shear
S-WC-30-1	58.2	0.49	Flexure/Shear
S-WC-30-2	58.7	0.48	Flexure/Shear
S-WC-60-1	59.4	0.64	Flexure
S-WC-60-2	61.3	0.74	Flexure
S-WC-80-1	53.2	0.39	Flexure/Shear
S-WC-80-2	62.2	0.62	Flexure
S-WC-100-1	62.8	0.74	Flexure/Shear
S-WC-100-2	61.0	0.52	Flexure/Shear

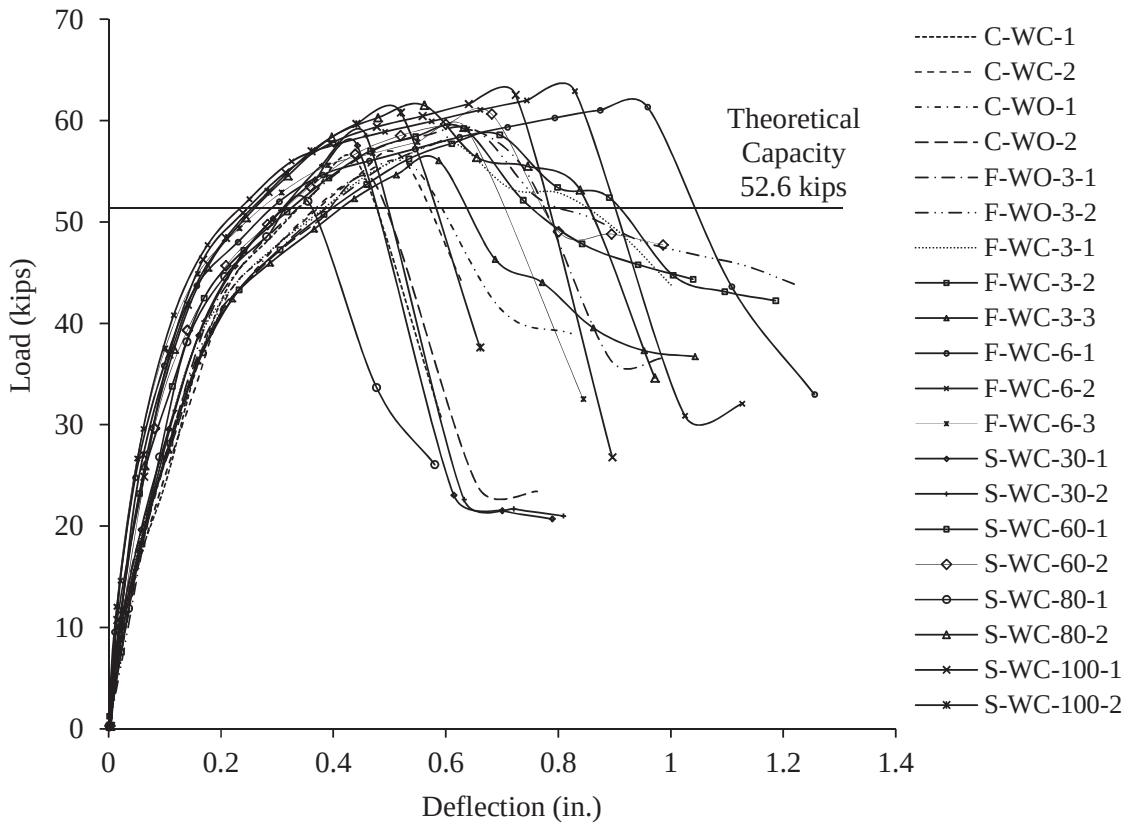

Figure 5-15 Load-deflection response of ultimate load test for all specimens

5.10 Rapid Chloride Test Results

Rapid chloride tests were carried out on several concrete dust samples to determine the chloride content in the specimens. The powdered concrete samples were obtained from the concrete cores after compressive strength had been obtained (Section 5.2). Fifteen chloride content tests were carried out and the results are presented in Table 5-18.

In addition, after the ultimate load test was conducted on the deck slab specimens, the chloride content was determined on a few selected specimens. The selected specimens were: F-WC-6-1, F-WC-6-2, S-WC-100-1 and S-WC-100-2. The powdered concrete samples were taken

at a depth of 2 inches and 4 inches from the surface of the specimens at four locations. The test results are presented in Table 5-19 and Table 5-20. The results show that there was no significant change in chloride content due to sustained environmental exposure.

Table 5-18 Chloride content in concrete dust sample
(before environmental exposure)

Concrete Dust Sample No.	**Cl^- by Concrete Weight (%)**	**Average Cl^- by Concrete Weight (%)**
1	0.235	0.282
2	0.225	
3	0.230	
4	0.235	
5	0.250	
6	0.370	
7	0.270	
8	0.280	
9	0.290	
10	0.310	
11	0.325	
12	0.325	
13	0.280	
14	0.300	
15	0.310	

From the data in Table 5-18, it can be observed that there is large variation among the chloride content measurements, which is likely attributed to inherent inhomogeneity of concrete (Section 3.5.4).

Table 5-19 Chloride content in concrete dust sample
of specimens exposed to 600 freeze-thaw cycles

Specimen Designation	Sample taken at depth of (in.)	Cl^- by Concrete Weight (%)	Average Cl^- by Concrete Weight (%)
F-WC-6-1	2	0.275	0.280
		0.280	
		0.285	
		0.280	
	4	0.275	0.279
		0.280	
		0.275	
		0.285	
F-WC-6-2	2	0.270	0.278
		0.275	
		0.280	
		0.285	
	4	0.280	0.279
		0.275	
		0.285	
		0.275	

Table 5-20 Chloride content in concrete dust sample
of specimens exposed to 10,000 hrs. of saltwater exposure

Specimen Designation	Sample taken at depth of (in.)	Cl^- by Concrete Weight (%)	Average Cl^- by Concrete Weight (%)
S-WC-100-1	2	0.270	0.281
		0.285	
		0.295	
		0.275	
	4	0.280	0.280
		0.285	
		0.280	
		0.275	
S-WC-100-2	2	0.265	0.279
		0.295	
		0.280	
		0.275	
	4	0.275	0.280
		0.290	
		0.285	
		0.270	

5.11 Correlation of Laboratory Freeze-Thaw Cycles and Age of Bridge Deck in Service

This study proposes, based on average daily temperatures from weather stations in Lansing and Muskegon, that the number of *laboratory freeze-thaw cycles* can be correlated to the number of *field freeze-thaw cycles* that a bridge deck would experience in its expected functional service life. The computation to arrive at the number of field freeze-thaw cycles per year is shown in Table 5-21. The number of freeze-thaw cycles that the bridge deck experiences in one year is considered as the number of intervals of temperature having at least a 40 °F range below and above the freezing temperature 32 °F. The temperature range of 40 °F is consistent with the

temperature range described in ASTM C 666/C 666M “Standard Test Method for Resistance of Concrete to Rapid Freezing and Thawing”.

Table 5-21 Average number of freeze-thaw cycles per year

Area of Station	Year*	Number of Field Freeze-Thaw Cycles per year	Average Number of Freeze-Thaw Cycles per year
Lansing	2007-08	11	12 (St. dev. = 1.95)
	2008-09	15	
	2009-10	11	
Muskegon	2007-08	11	
	2008-09	10	

*Data representing one calendar year.

Table 5-22 Number of freeze-thaw cycles in service age of bridge deck derived from ambient air temperature

Number of Lab. Freeze-Thaw Cycles per year	Number of Years*
300	25
400	33
500	41
600	50

* Number of years a bridge deck would experience the corresponding number of freeze-thaw cycles

Assuming that the annual number of average freeze-thaw cycles is 12, laboratory freeze-thaw cycles can be related to bridge age. the number of years of field freeze-thaw cycles. From Table 5-22, it can be observed that the laboratory freeze-thaw cycles can reasonably represent the actual field freeze-thaw cycles that a given bridge deck in southern Michigan would experience in its age of service.

CHAPTER 6: RESULTS AND DISCUSSIONS OF FIELD INVESTIGATION

6.1 Introduction

Results and discussions of the field investigation are presented in this chapter. In-situ concrete hardness, corrosion potential, chloride content and pH value results of 63174-S05-1 carrying I-75 NB over 14 Mile Road, 63022-S02-4 carrying I-96 WB over Milford Road, and 63022-S02-4 carrying I-96 WB over Kent Lake Road are presented first and ESEM (environmental scanning electron microscope) results that includes measurement of porous zone size and chemical element composition analysis are presented in detail later.

6.2 In-situ Concrete Hardness

The SilverSchmidt hammer was used to measure the in-situ hardness of the bridge deck concrete and it was accessed from below the bridge decks. Thirty data points were obtained from each test area on each bridge. The locations of areas of the bridges are previously defined in Chapter 4 (Figure 4-21, Figure 4-29 and Figure 4-32). The average results of the in-situ concrete hardness for the areas selected are presented in Table 6-1,

Table 6-2 and Table 6-3 for 63174-S05-1 carrying I-75 NB over 14 Mile Road, 63022-S02-4 carrying I-96 WB over Milford Road and 63022-S01 carrying I-96 WB over Kent Lake Road, respectively. The coefficient of variation (COV), defined as the standard deviation divided by the mean, is reported to demonstrate the consistency of the data.

Table 6-1 In-situ hardness of 63174-S05-1 carrying I-75 NB over 14 Mile Road.

Location	**A1**	**A2**	**A3**
Hardness (psi)	7,470	7,610	7,410
Coefficient of variation (%)	10.6	6.1	16.6

30 data points included in each data series

Table 6-2 In-situ hardness of 63022-S02-4 carrying I-96 WB over Milford Road

Location	A1	A2	A 3
Hardness (psi)	7,400	7,540	6,330
Coefficient of variation (%)	7.7	11.9	12.3

30 data points included in each data series

Table 6-3 In-situ hardness of 63022-S01 carrying I-96 WB over Kent Lake Road

Location	A 1	A 2	A3	B1	B2	B3
Hardness (psi)	7,250	7,130	6,840	7,250	6,700	7,720
Coefficient of variation (%)	7.4	10.5	12.1	16.9	16.9	1.8

30 data points included in each data series

From Table 6-1,

Table 6-2 and Table 6-3 it can be observed that the in-situ hardness of concrete decks of 63174-S05-1 carrying I-75 NB over 14 Mile Road, 63022-S02-4 carrying I-96 WB over Milford Road and I-96 WB over Kent Lake Road were fairly uniform in all the areas A1, A2, A3, B1, B2 and B3 ranging from 6,330 psi to 7,720 psi.

6.3 CANIN (Half-cell Potential Measurement)

The average half-cell potential differences (corrosion potential) of the reinforcement in the test areas selected for NDT were measured using CANIN based on the methodology presented in Section 4.3.4.3 of Chapter 4. Thirty-six data reading were taken from each area, and a total of 108 data were gathered from each bridge. The average measured potential differences are presented in Table 6-4, Table 6-5 and Table 6-6 for 63174-S05-1 carrying I-75 NB over 14

Mile Road, 3022-S02-4 carrying I-96 WB over Milford Road and 3022-S01 carrying I-96 WB over Kent Lake Road, respectively.

Interpretation of half-cell potential to chance of corrosion is given based on ASTM C 876 and the interpretation is presented in Table 4-2 of Chapter 4. Moreover, corrosion rate of the investigated bridges were determined based on the correlation made between average half-cell potential and corrosion rate measurements of laboratory specimens as described below.

6.3.1 Correlation between Corrosion Rate and Half-cell Potential

In the laboratory investigation the corrosion rate of the steel reinforcement was determined using the GalvaPulse method. Unfortunately, stable readings could not be obtained during the field investigations due to the inverted position of the measuring unit. On the other hand, half-cell potential measurements by the CANIN system were stable throughout the testing program. The results of the half-cell potential measurements were translated into a level of 'change of corrosion.' Therefore, to relate the field obtained potential measurements using the CANIN system to an apparent corrosion rate, such as determined by the GalvaPulse system, an empirical model was proposed based on the results of the laboratory investigation in this study.

The relationship between the corrosion rate data obtained from GalvaPulse and half-cell potential data CANIN on the laboratory specimens are shown in Figure 6-1. The relationship between the half-cell potential and the corrosion rate is described by a power relation with a correlation coefficient of 0.97. By using this correlation all the half-cell potential data (measured by CANIN) of the field investigated bridge decks were converted to corrosion rate which was later used to estimate the service life.

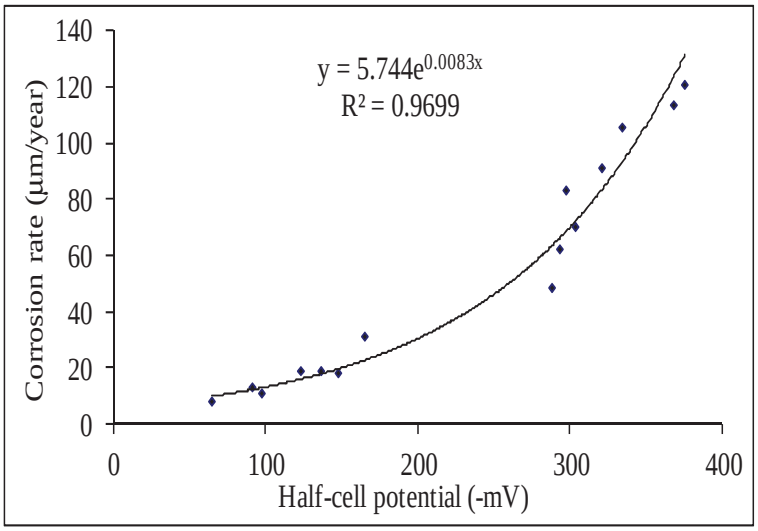

Figure 6-1 Relationship between half cell potential (CANIN) and corrosion rate (GalvaPulse) based on laboratory investigations. *(1 µm/year = 0.0395 mils/year)*

Table 6-4 Average half-cell potential difference of 63174-S05-1 carrying I-75 NB over 14 Mile Road

Location	**A1**	**A2**	**A3**
Average half-cell potential difference (mV)	-315	-220	-150
Coefficient of variation (%)	13.4	14.4	9.1
Chance of corrosion (ASTM C 879)	50%	50%	5%
Corrosion rate (µm/year)	78	36	20

36 data points included in each data series. (1 µm/year = 0.0395 mils/year)

Table 6-5 Average half-cell potential difference of 63022-S01 carrying I-96 WB over Milford Road

Location	A1	A2	A3
Average half-cell potential difference (mV)	-405	-400	-368
Coefficient of variation (%)	4.5	7.6	7.3
Chance of corrosion (ASTM C 879)	95%	95%	95%
Corrosion rate (µm/year)	>120	>120	114

36 data points included in each data series. (1 µm/year = 0.0395 mils/year)

Table 6-6 Average half-cell potential difference of 63022-S01 carrying I-96 WB over Kent Lake Road

Location	A1	A2	A 3	B1	B2	B3
Average half-cell potential difference (mV)	-411	-406	-344	-207	-397	-547
Coefficient of variation (%)	18.1	15.3	12.7	12	15.9	8.7
Chance of corrosion (ASTM C 879)	95%	95%	50%-95%	50%	95%	Visible evidence
Corrosion rate (µm/year)	>120	>120	97	42	110	>120

36 data points included in each data series. (1 µm/year = 0.0395 mils/year)

Table 6-4 demonstrates average chance of reinforcement corrosion on 63174-S05-1 carrying I-75 NB over 14 Mile Road, on areas A1 and A2 as 50% and 5% on area A3. Area A1, which was located in the right lane (decelerations lane), had higher magnitude of average half-cell potential than areas A2 and A3. Table 6-5 shows the chance of reinforcement corrosion in bridge deck of 63022-S02-4 carrying I-96 WB over Milford Road. All areas showed 95% chance

of reinforcement corrosion. Area A1 of 63022-S02-4 carrying I-96 WB over Milford Road revealed slightly higher magnitude of average half-cell potential than areas A2 and A3.

Chance of reinforcement corrosion of 63022-S01 carrying I-96 WB over Kent Lake Road is reported in Table 6-6. Areas A1, A2, A3 and B2 showed 95% chance of reinforcement corrosion, 50% of chance of corrosion was measured in area B1 while visible evidence of corrosion was observed in area B3 which was located on the right shoulder of the bridge. Areas A1 and B3, which are located in the right lane and on the right shoulder of the bridge respectively, experienced highest chance of reinforcement corrosion.

From this investigation, it is observed that higher chance of reinforcement bar corrosion was observed for the bridge decks on 63022-S01 carrying I-96 WB over Kent Lake Road and 63022-S02-4 carrying I-96 WB over Milford Road compared to that on the bridge deck of 63174-S05-1 carrying I-75 NB over 14 Mile Road.

6.4 Chloride Content (Rapid Chloride Test)

Chloride content test by RCT (rapid chloride test) was determined from concrete powder samples obtained from the test areas of each bridge deck. Concrete powder samples from a maximum depth of 4 in. from the bottom deck were collected using rotary drilling (detail methodology is explained in section 4.3.4.4 of Chapter 4). In addition, concrete powder samples were collected from full depth of cores from the bridge decks on 63174-S05-1 carrying I-75 NB over 14 Mile Road and 63022-S01 carrying I-96 WB over Kent Lake Road for chloride content evaluation of the full depth of the deck. The chloride content values are presented in Table 6-7 through Table 6-13, for the individual test areas and cores obtained from the bridges. Cores were not obtained from the bridge carrying 63022-S02-4 carrying I-96 WB over Milford Road.

Table 6-7 Chloride content of 63174-S05-1 carrying I-75 NB over 14 Mile Road (A1, A2 & A3)

Area	Depth from bottom of deck		Chloride content		
	(cm)	(in.)	(%) by weight	(lb/cyd)	(kg/m^3)
A1	2	0.8	0.018	0.713	0.423
A1	3.5	1.4	0.014	0.980	0.581
A1	4	1.6	0.025	1.025	0.608
A1	10	4.0	0.055	2.228	1.321
A1	10	4.0	0.050	2.005	1.189
A1	10	4.0	0.050	2.005	1.189
A2	2	0.8	0.018	0.713	0.423
A2	2	0.8	0.022	0.891	0.528
A2	10	4.0	0.062	2.495	1.479
A3	4	1.6	0.019	0.757	0.449
A3	4	1.6	0.014	0.579	0.343
A3	4	1.6	0.013	0.535	0.317
A3	4.5	1.8	0.018	0.713	0.423
A3	10	4.0	0.018	0.713	0.423
A3	10	4.0	0.017	0.668	0.396
A3	10	4.0	0.012	0.490	0.291

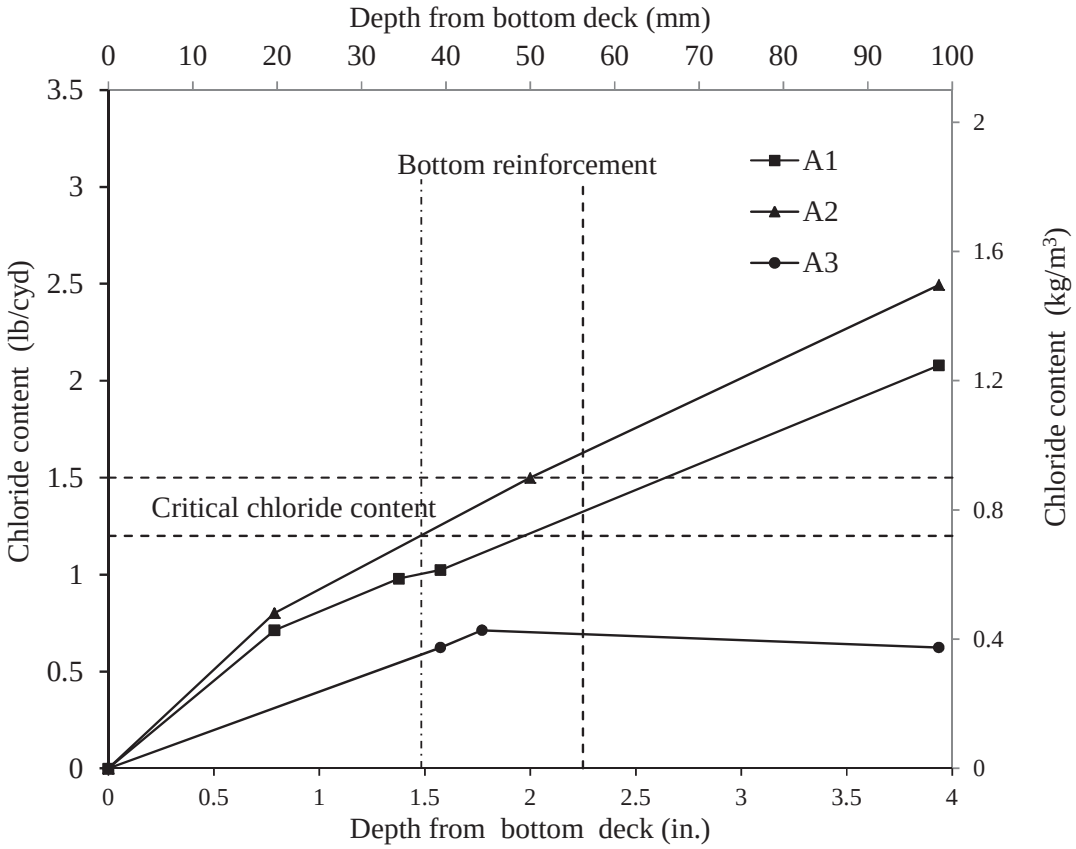

Figure 6-2 Chloride content versus depth graph of 63174-S05-1 carrying I-75 NB over 14 Mile Road

Table 6-8 Chloride content of 63174-S05-1 carrying I-75 NB over 14 Mile Road core (A3)

Depth from bottom deck		**Chloride content**		
(cm)	**(in.)**	**(%) by weight**	**(lb/cyd)**	**(kg/m^3)**
2	0.8	0.15	0.22	0.13
4	1.6	0.26	0.40	0.24
6	2.4	0.32	0.49	0.29
8	3.2	0.33	0.51	0.30
10	3.9	0.35	0.53	0.32
12	4.7	0.44	0.67	0.40
14	5.5	0.67	1.02	0.61
16	6.3	0.90	1.38	0.82
18	7.1	1.10	1.69	1.00
20	7.9	1.16	1.78	1.06
22	8.7	1.57	2.41	1.43

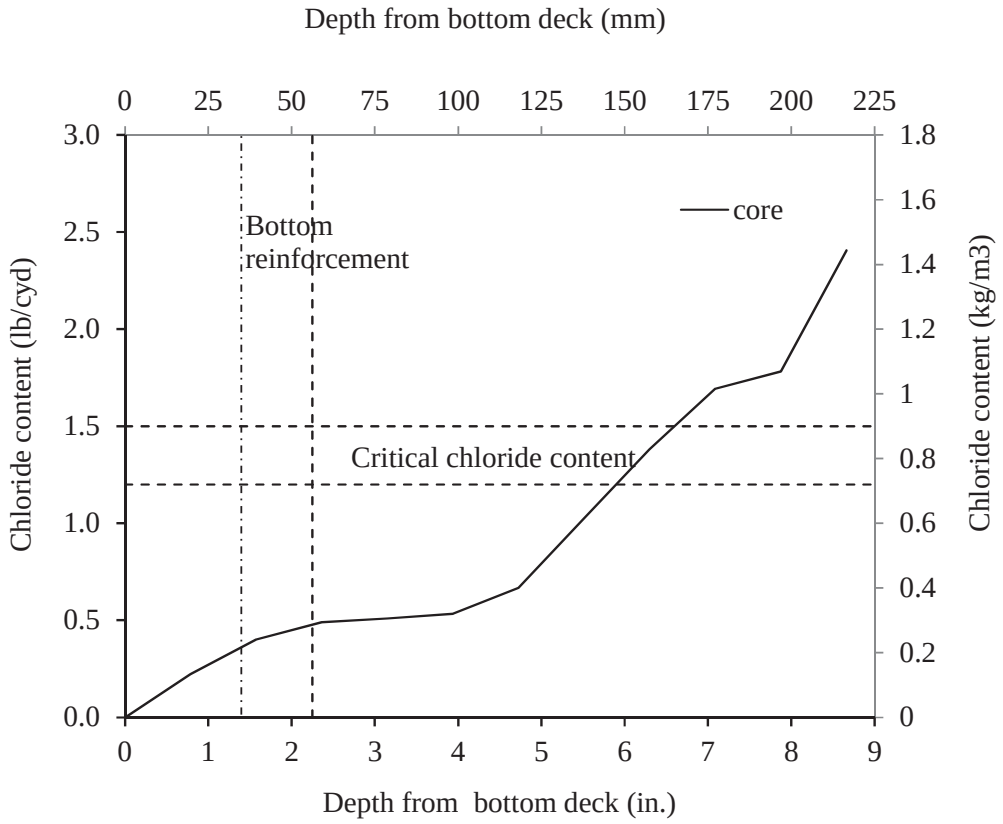

Figure 6-3 Chloride content versus depth graph of 1-75 NB over 14 Mile Road core

It can be observed from Table 6-7, Table 6-8, Figure 6-2 Chloride content versus depth graph of 63174-S05-1 carrying I-75 NB over 14 Mile Road that the chloride content of concrete powder collected from 63174-S05-1 carrying I-75 NB over 14 Mile Road core increases as depth from bottom deck increases. Furthermore, areas A1 and A2 showed higher chloride content value than area A3.

Corrosion initiation takes place when a chloride concentration at the reinforcement level reaches a critical level, which is 1.2-1.5 lb/cyd (Miki, 1990). Near the bottom reinforcement, at a depth of 2.25 in. from bottom deck, the chloride content on area A1 was above the critical value range and the chloride content on area A2 was in the critical value range. The chloride content

value on area A3 and on the core taken from area A3 showed lower value than the critical value range near the bottom reinforcement.

Table 6-9 Chloride content of 63022-S02-4 carrying I-96 WB over Milford Road (A1, A2 and A3)

Area	**Depth from bottom of deck**		**Chloride content**		
	(in.)	**(cm)**	**(%) by weight**	**(lb/cyd)**	**(kg/m^3)**
A1	0.8	2	0.02	0.89	0.53
A1	0.8	2	0.01	0.45	0.26
A1	1.6	4	0.05	1.87	1.11
A1	1.6	4	0.03	1.38	0.82
A1	2.4	6	0.06	2.23	1.32
A1	2.4	6	0.05	2.00	1.19
A2	0.8	2	0.01	0.31	0.18
A2	0.8	2	0.02	0.67	0.40
A2	0.8	2	0.01	0.31	0.18
A2	1.6	4	0.03	1.38	0.82
A2	1.6	4	0.04	1.56	0.92
A2	2.4	6	0.06	2.32	1.37
A3	0.8	2	0.01	0.40	0.24
A3	0.8	2	0.01	0.45	0.26
A3	1.6	4	0.03	1.11	0.66
A3	1.6	4	0.04	1.69	1.00
A3	1.6	4	0.03	1.25	0.74
A3	2.4	6	0.06	2.27	1.35

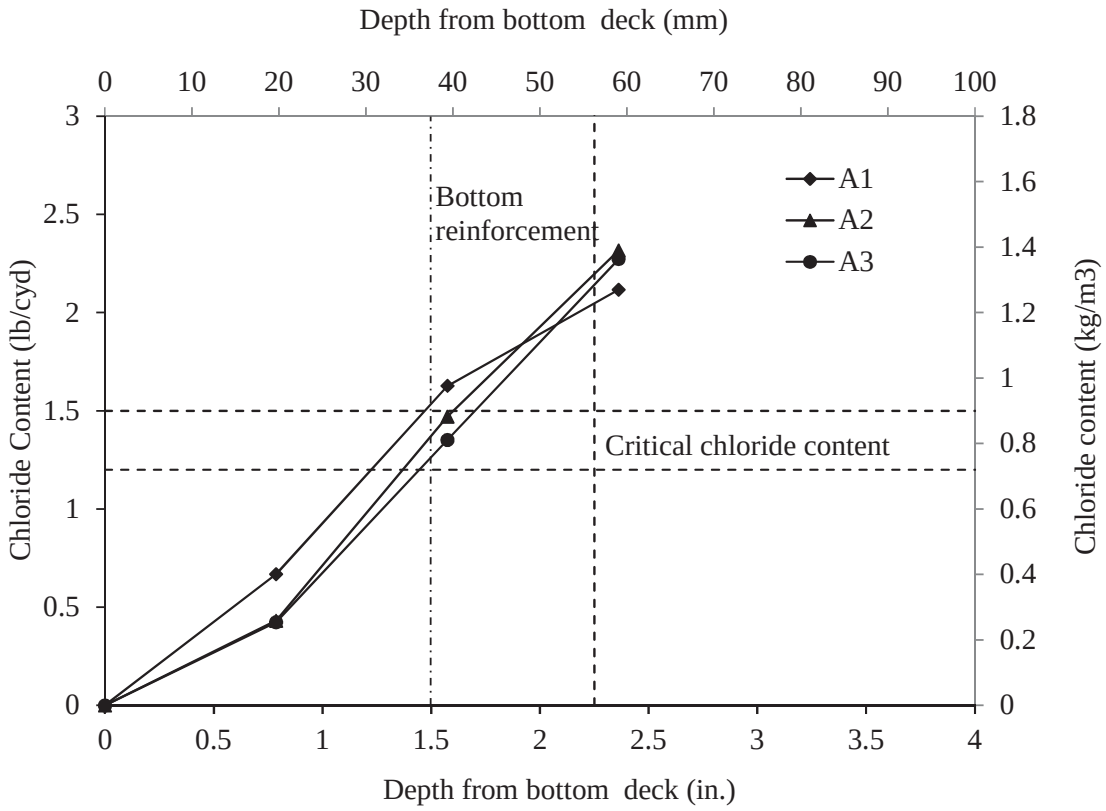

Figure 6-4 Chloride content versus depth graph of 63022-S02-4 carrying I-96 WB over Milford Road

It can be observed from Table 6-9 and Figure 6-4 that chloride content in the bridge deck of 63022-S02-4 carrying I-96 WB over Milford Road increases as the depth from bottom surface increases. Furthermore, on average areas A1 and A2 showed higher chloride content value than area A3. Near the location of the bottom reinforcement, at a depth of 2.25 in. from bottom deck, the chloride content values of areas A1, A2 and A3 were above the critical value range.

Table 6-10 Chloride content of 63022-S01 carrying I-96 WB over Kent Lake Road (A1, A2 and A3)

Area	Depth from bottom of deck		Chloride content		
	(cm)	(in.)	(%) by weight	(lb/cyd)	(kg/m^3)
A1	2	0.8	0.012	0.490	0.274
A1	2	0.8	0.022	0.891	0.498
A1	3	1.2	0.022	0.891	0.498
A1	4	1.6	0.039	1.559	0.872
A1	5	2.0	0.024	0.980	0.548
A1	6.5	2.6	0.050	2.005	1.121
A2	2	0.8	0.010	0.401	0.224
A2	2	0.8	0.020	0.802	0.449
A2	2	0.8	0.012	0.490	0.274
A2	4	1.6	0.014	0.579	0.324
A2	4	1.6	0.022	0.891	0.498
A2	6	2.4	0.051	2.049	1.146
A3	2	0.8	0.010	0.401	0.224
A3	2	0.8	0.009	0.356	0.199
A3	4	1.6	0.033	1.337	0.748
A3	4	1.6	0.028	1.114	0.623
A3	4	1.6	0.033	1.337	0.748
A3	6	2.4	0.046	1.871	1.047

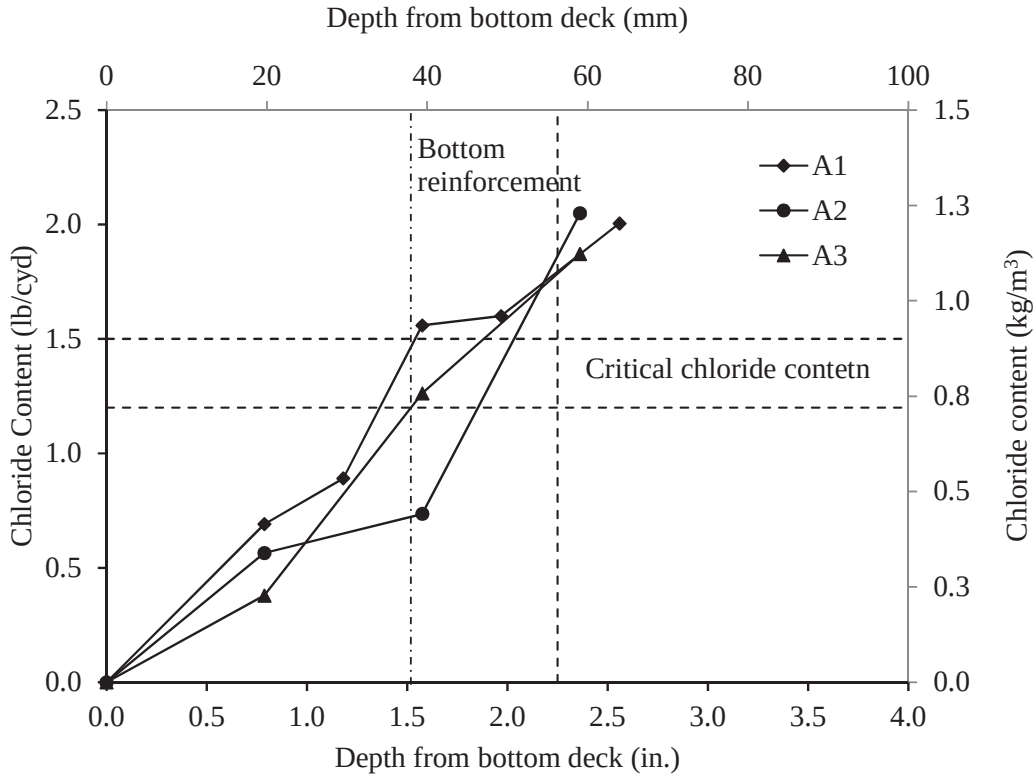

Figure 6-5 Chloride content versus depth of 63022-S01 carrying I-96 WB over Kent Lake Road

From Table 6-10 and Figure 6-5, it can be observed that, chloride content in the bridge deck of 63022-S01 carrying I-96 WB over Kent Lake Road increases as depth from bottom surface increases. Area A1 showed higher chloride content value than areas A2 and A3. Near the location of the bottom reinforcement, at a depth of 2.25 in. from bottom deck surface, the chloride content of Areas A1, A2 and A3 was above the critical value range.

Table 6-11 Chloride content of 63022-S01 carrying I-96 WB over Kent Lake Road (B1)

Depth from bottom of deck		Chloride content		
(cm)	(in.)	(%) by weight	(lb/cyd)	(kg/m^3)
20.5	8.4	0.099	4.410	2.615
18.5	7.4	0.086	3.831	2.272
16.5	6.6	0.071	3.163	1.876
14.5	5.8	0.056	2.495	1.479
12.5	5.0	0.024	1.069	0.634
10.5	4.2	0.017	0.757	0.449
8.5	3.4	0.017	0.757	0.449
6.5	2.6	0.011	0.490	0.291
4.5	1.8	0.01	0.446	0.264
2.5	1.0	0.009	0.401	0.238

Table 6-12 Chloride content of 63022-S01 carrying I-96 WB over Kent Lake Road (B2)

Depth from bottom of deck		Chloride content		
(cm)	(in.)	(%) by weight	(lb/cyd)	(kg/m^3)
19	7.5	0.13	5.792	3.434
17	6.7	0.12	5.346	3.170
15	5.9	0.1	4.455	2.642
13	5.1	0.095	4.232	2.510
11	4.3	0.07	3.119	1.849
9	3.5	0.048	2.138	1.268
7	2.6	0.042	1.871	1.110
5	2.0	0.04	1.782	1.057
3	1.2	0.03	1.337	0.793

Table 6-13 Chloride content of 63022-S01 carrying I-96 WB over Kent Lake Road (A3)

Depth from bottom of deck		Chloride content		
(cm)	(in.)	(%) by weight	(lb/cyd)	(kg/m^3)
19	7.5	0.097	4.321	2.562
17	6.7	0.095	4.232	2.510
15	5.9	0.09	4.010	2.378
13	5.1	0.07	3.119	1.849
11	4.3	0.04	1.782	1.057
9	3.5	0.037	1.648	0.977
7	2.6	0.036	1.604	0.951
5	2.0	0.035	1.559	0.925
3	1.2	0.021	0.936	0.555

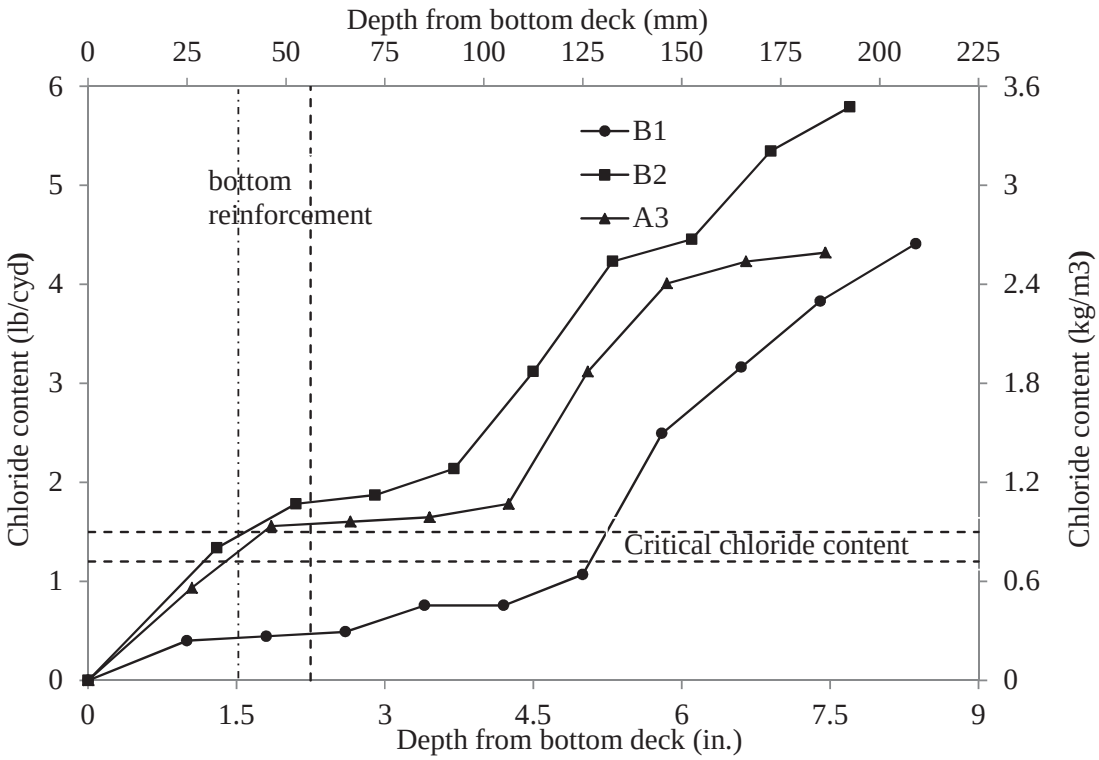

Figure 6-6 Chloride content versus depth of 63022-S01 carrying I-96 WB over Kent Lake Road cores

It can be observed from Table 6-11, Table 6-12, Table 6-13 and Figure 6-6 that the chloride content in the bridge deck of 63022-S01 carrying I-96 WB over Kent Lake Road cores increases as the depth from bottom surface increases, and areas A3 and B2 showed higher chloride value than area B1.

At a depth of 2.25 in. from bottom deck surface, which is near the location of the bottom reinforcement, the chloride content values of areas A3 and B2 were above the critical value range. However, the chloride content value of area B1 was below the critical value range. It was also noted that higher chloride content value along the depth was observed in the bridge decks of 63022-S01 carrying I-96 WB over Kent Lake Road and 63022-S02-4 carrying I-96 WB over Milford Road than 63174-S05-1 carrying I-75 NB over 14 Mile Road.

6.5 pH Level (Rainbow Indicator)

Concrete normally provides a high degree of protection to the reinforcing steel against corrosion, by virtue of the high alkalinity (pH> 13.5) of the pore solution (Ahmad, 2002). The natural alkalinity of cement paste in concrete results in a protective oxide coating on steel reinforcement that prevents the steel from rusting. However, presence of chloride ions, which may either have been present in the concrete ingredients right from the beginning or are introduced into the concrete through road salt ingress during the service life will eliminate/breakdown the passive layer. Corrosion rate increase with an increase in the chloride content (Hope BB, 1987). Consequently the knowledge of pH values in a sample is important parameter in determining corrosion condition.

The system denoted Rainbow Indicator was used to estimate the concrete pH value. Rainbow Indicator was sprayed and allowed to dry on the full depth of cores taken from 63174-S05-1 carrying I-75 NB over 14 Mile Road and 63022-S01 carrying I-96 WB over Kent Lake Road as presented in Figure 6-7 and Figure 6-9. The indicator changed from colorless into different colors and the approximate pH values were determined based on the change in color. Figure 6-8 and Figure 6-10 shows graphs of pH value versus depth of 63174-S05-1 carrying I-75 NB over 14 Mile Road and 63022-S01 carrying I-96 WB over Kent Lake Road respectively.

Figure 6-7 63174-S05-1 carrying I-75 NB over 14 Mile Road core exposed to Rainbow Indicator

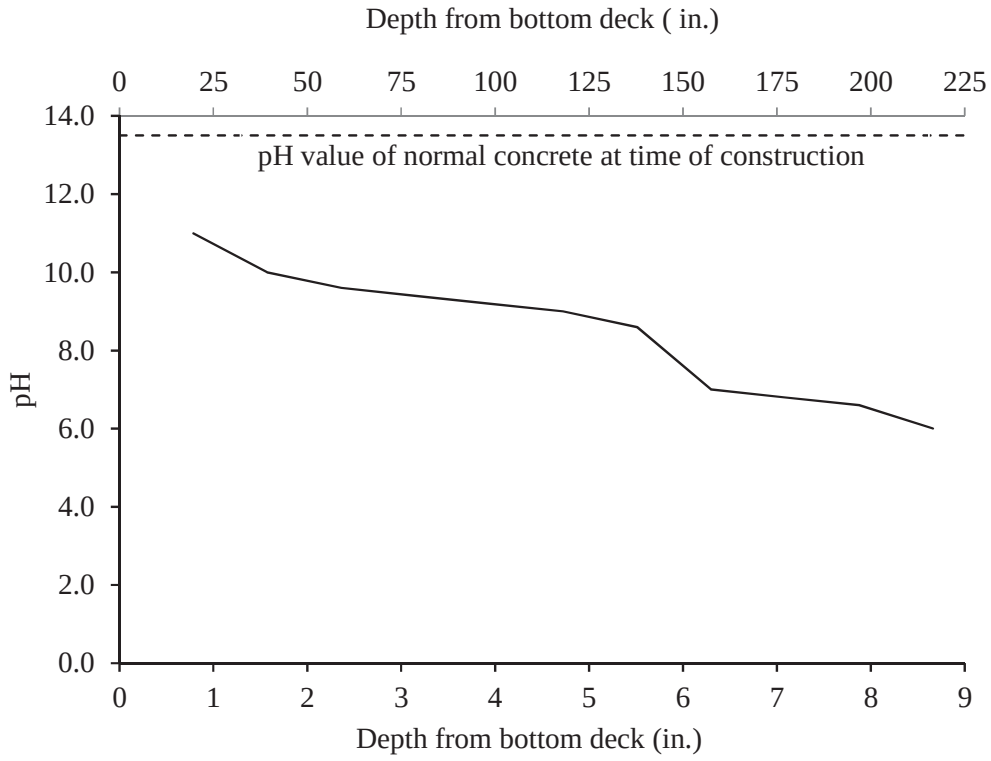

Figure 6-8 pH value versus depth graph of 63174-S05-1 carrying I-75 over 14 Mile Road core

Figure 6-9 63022-S01 carrying I-96 WB over Kent Lake Road core exposed to Rainbow Indicator

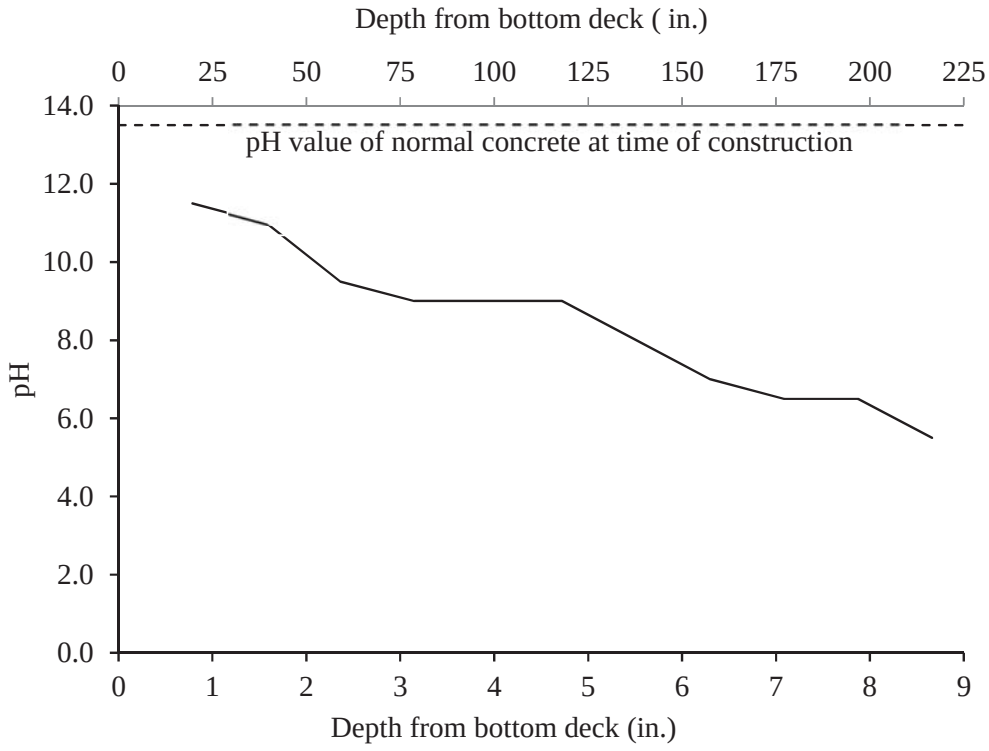

Figure 6-10 pH value versus depth graph of 63022-S01 carrying I-96 over Kent Lake Road core

The pH value decreases as depth from bottom surface increases for both 63174-S05-1 carrying I-75 NB over 14 Mile Road and 63022-S01 carrying I-96 over Kent Lake Road. Possible state of reinforcement corrosion at various pH levels is presented in Chapter 4 of Table 4-3. A pH value of 9.5 and less which is a critical value for commencement of steel corrosion (Berkely KGC et al., 1990) was observed near the bottom reinforcement of both bridges.

6.6 ESEM (Environmental Scanning Electron Microscope) Evaluation

ESEM (environmental scanning electron microscope) is used to determine porous zone size which is input for mathematical corrosion cracking model, element composition analysis and corrosion state of laboratory specimens and the field investigated bridge decks. Mathematical corrosion cracking model is discussed in detail in Chapter 7. The ESEM is set up for SI units and the applied mathematical model is also defined in SI units.

Samples were prepared from cores that were taken from the investigated bridge for ESEM (environmental scanning electron microscope) evaluation. In addition to the samples prepared from the cores, nine laboratory specimens representing control specimen with and without chloride introduce mixes, saltwater exposed specimen with chloride introduced mixes and freeze-thaw specimens with and without chloride introduced mixes were selected for ESEM evaluation. Three samples of size 3 in. x 3 in. x 1.5 in. were taken from each of the selected 9 laboratory specimens along with the samples taken from bridge cores.

6.6.1 Porous Zone Size

The samples were mounted in the ESEM chamber and the interface between the reinforcement and concrete was magnified by 1000x. Images were taken at this magnification around the periphery of the reinforcement bar and the porous zone sizes were measured as shown in Figure 6-11 and Figure 6-12. Summaries of the average value of the porous zone sizes of the laboratory specimens selected and samples taken from the bridge cores are presented in Table 6-14 and Table 6-15.

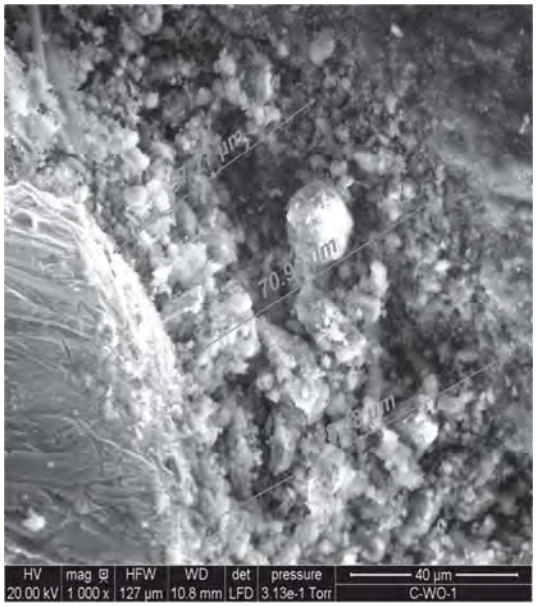

(a) Porous zone of C-WO

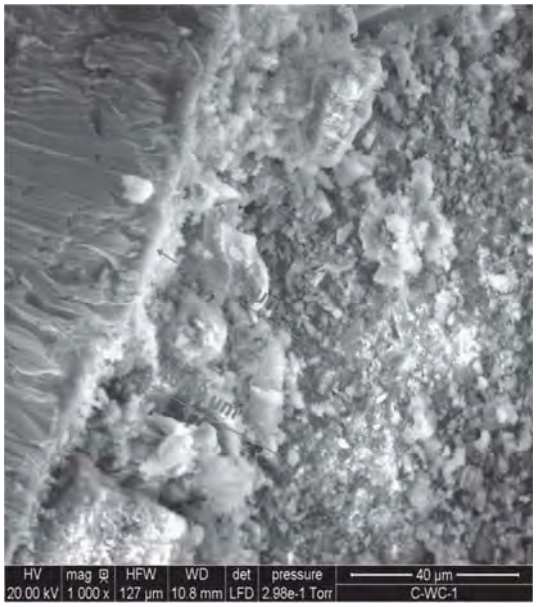

(b) Porous zone of C-WC

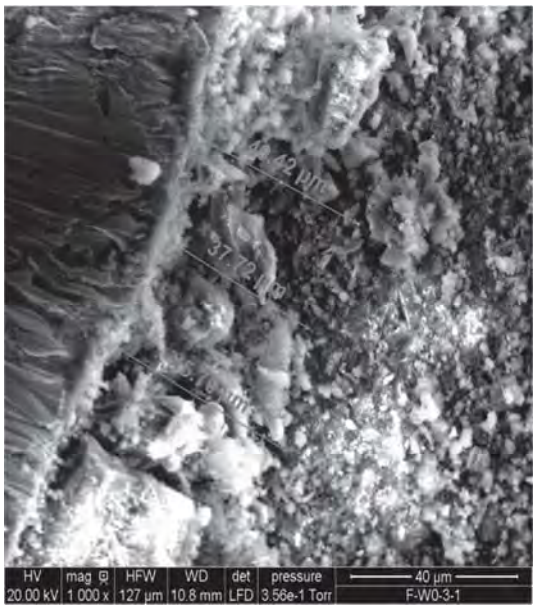

(c) Porous zone of F-WO-3

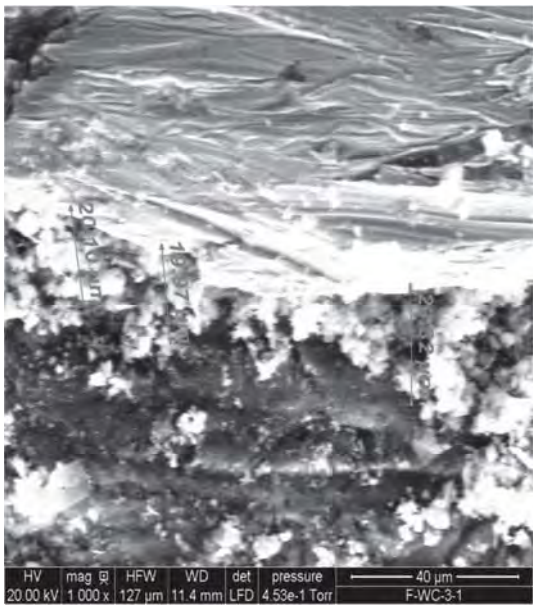

(d) Porous zone of F-WC-3

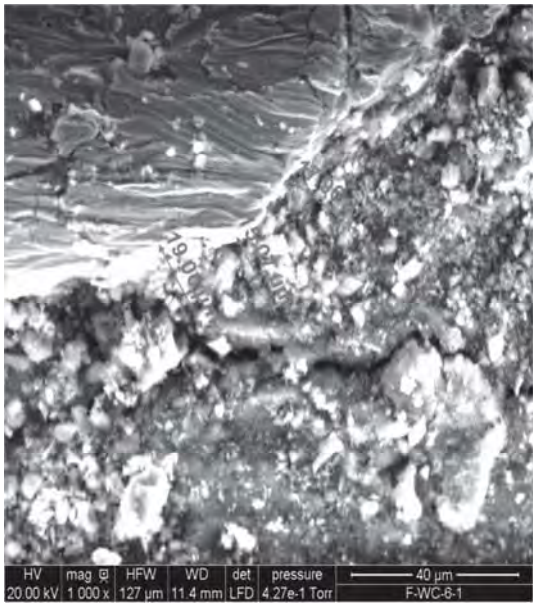

(e) Porous zone of F-WC-6

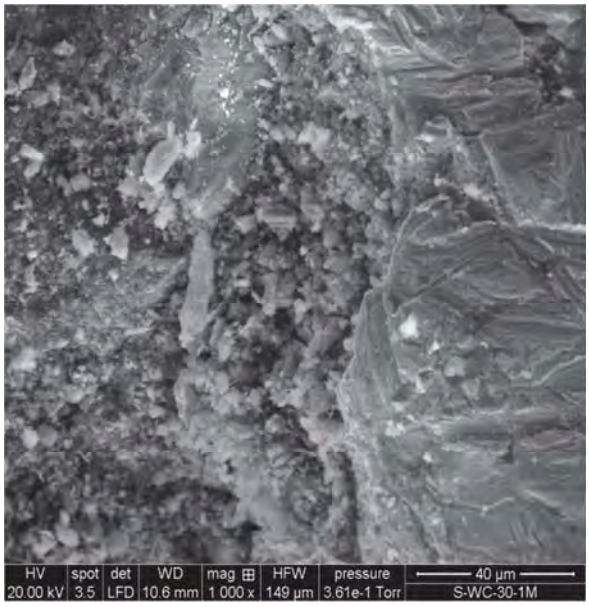

(f) Porous zone of S-WC-30

(g) Porous zone of S-WC-60

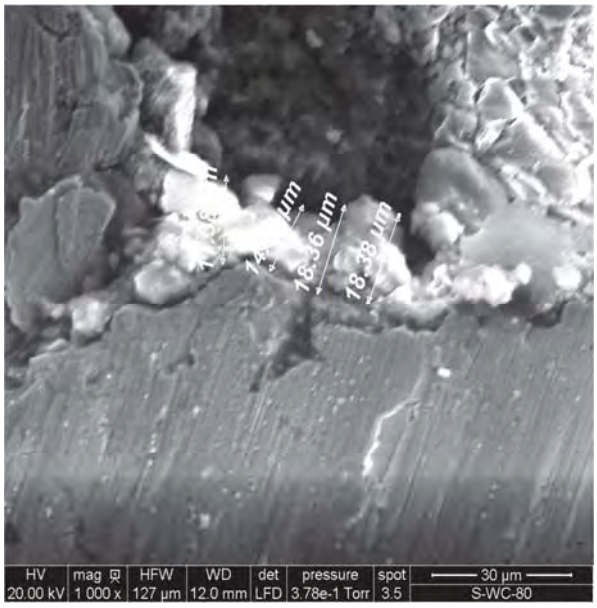

(h) Porous zone of S-WC-80

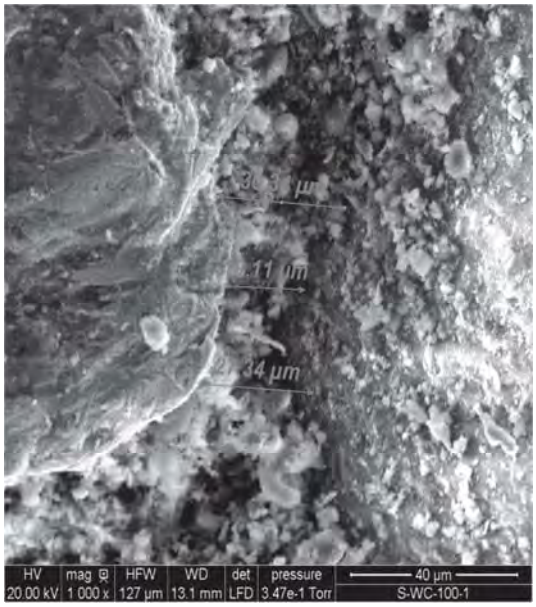

(i) Porous zone of S-WC-100

Figure 6-11 Porous zones of laboratory specimens (Magnification of 1000x)

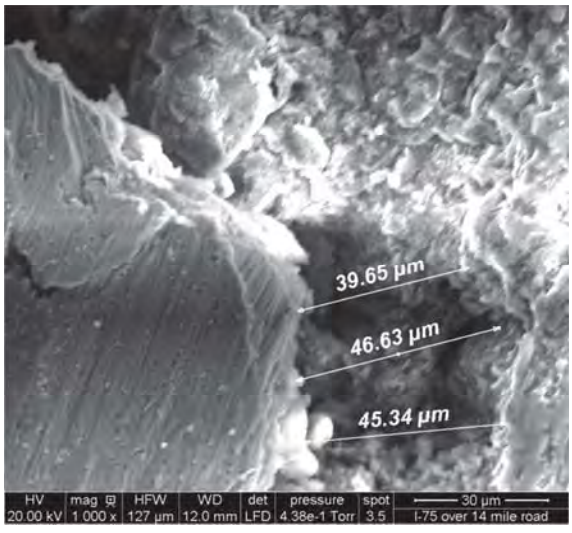

(a) 63174-S05-1 carrying I-75 NB over 14 Mile Road

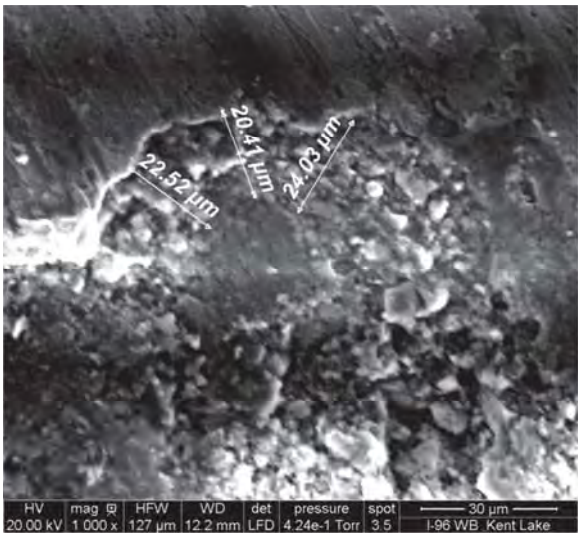

(b) 63022-S01 carrying I-96 WB over Kent Lake Road

Figure 6-12 Porous zones of field investigated bridges (Magnification of 1000x)

Table 6-14 Average porous zone size of laboratory specimens

Specimen	Average porous zone size (μm)	Standard deviation	Coefficient of variation (%)
C-WO	69	10.6	4.6
C-WC	44	2.0	9.8
F-WO-3	41	4.1	9.8
F-WC-3	21	1.9	8.9
F-WC-6	17	2.1	11.9
S-WC-30	39	1.1	2.8
S-WC-60	17	1.9	10.7
S-WC-80	18	1.6	8.7
S-WC-100	20	4.1	20.1

(1 μm/year = 0.03937 mils/year)

As presented in the literature review porous zone size ranges from 10 to 60 μm or 0.3937 to 2.362 mils, (Yuan and Ji 2009, and Thoft-Christensen 2000). The porous zone ranged from 17 to 69 μm or 0.669 to 2.716 mils for the laboratory tested specimens. Higher porous zone thickness was observed for control specimen without introduced chloride while lower porous zone thickness was observed for freeze-thaw and saltwater exposed specimens with introduced chloride.

Table 6-15 Average porous zone size of bridges investigated

Bridges	Average porous zone size (μm)	Standard deviation	Coefficient of variation (%)
63174-S05-1 carrying I-75 NB over 14 Mile Road	43	3.7	8.44
63022-S01 carrying I-96 WB over Kent Lake Road	22	1.8	8.15

(1 μm = 0.03937 mils)

Table 6-15 shows higher porous zone thickness samples taken from the original deck structure of 63174-S05-1 carrying I-75 NB over 14 Mile Road than samples of original deck structure of 63022-S01 carrying I-96 WB over Kent Lake Road.

6.6.2 Element Composition Analysis

Energy dispersive analysis by x-ray (EDAX) identifies and counts the impinging x-rays upon the characteristic energy level of elements. And by doing so, it can identify element composition on spots selected. Spots on concrete and steel were selected for EDAX analysis at excitation energy level of 20 kV. Element composition analyses of the samples are presented in Figure 6-14 through Figure 6-21.

The composition of elements determined were, elements of the cement used, corrosion product of steel, and chlorine on the chloride induced specimens. Portland cement consists of five major compounds, and a few minor compounds. The composition of a typical Portland cement is listed by weight percentage in Table 6-16. Major components of corrosion product of reinforcement are iron oxides and iron hydroxides in the form of FeO, Fe_3O_4, FeOOH $Fe(OH)_2$, $Fe(OH)_3$, and Fe_2O_3-$3H_20$ (Jaffer and Hansson 2008). Table 6-17 shows nomenclature of some of the elements observed in the samples.

Table 6-16 Composition of typical Portland cement

Cement Compound	Weight Percentage	Chemical Formula
Tricalcium silicate	50 %	Ca_3SiO_5 or $3CaO.SiO_2$
Dicalcium silicate	25 %	$Ca2SiO_4$ or $2CaO.SiO_2$
Tricalcium aluminate	10 %	$Ca_3Al_2O_6$ or $3CaO\ .Al_2O_3$
Tetracalcium aluminoferrite	10 %	$Ca_4Al_2Fe_2O_{10}$ or $4CaO.Al_2O3.Fe2O_3$
Gypsum	5 %	$CaSO_4.2H_2O$

Table 6-17 Nomenclature of elements observed in the samples

Symbol	Element	Symbol	Element
Na	Sodium	K	Potassium
Ca	Calcium	Pb	Lead
Fe	Iron	Mn	Manganese
Al	Aluminum	Cl	Chlorine
S	Sulfur	Si	Silicon

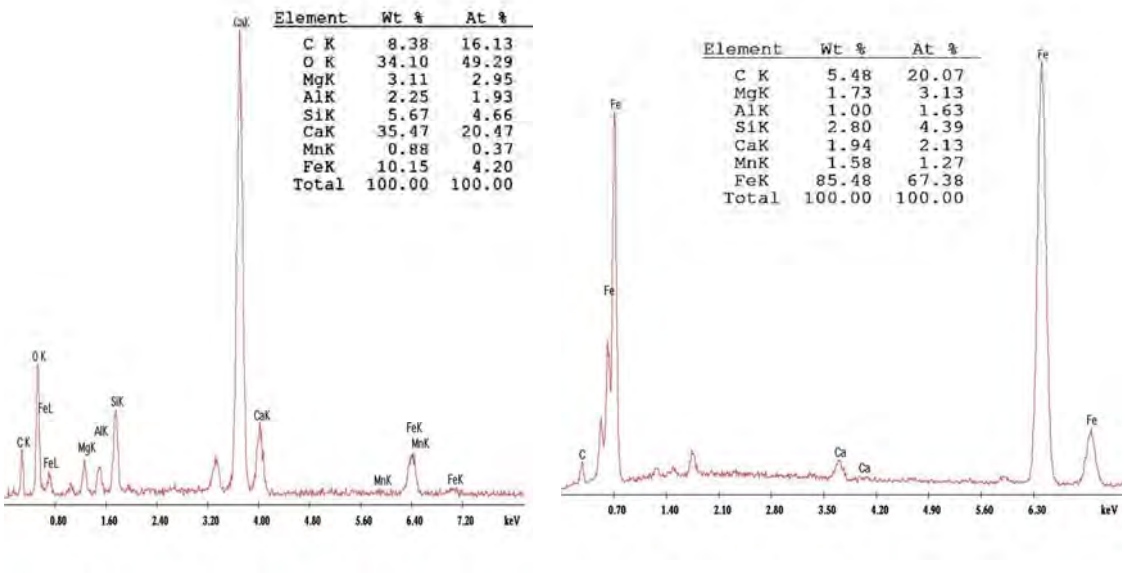

(a) Element composition of concrete (b) Element composition of reinforcement

Figure 6-13 Element composition of C-WO

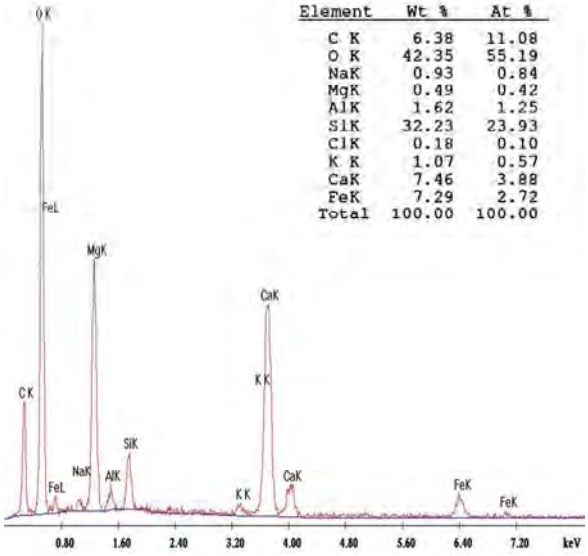

(c) Element composition of concrete

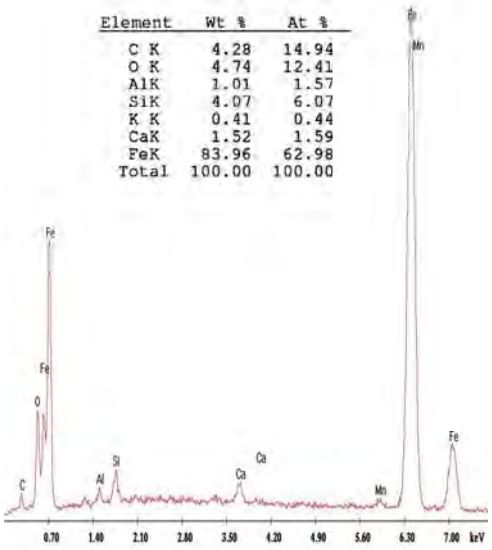

(d) Element composition of reinforcement

Figure 6-14 Element composition of C-WC

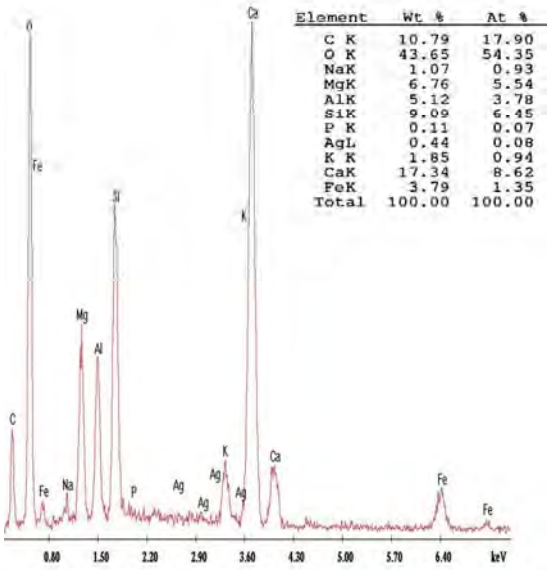

(a) Element composition of concrete

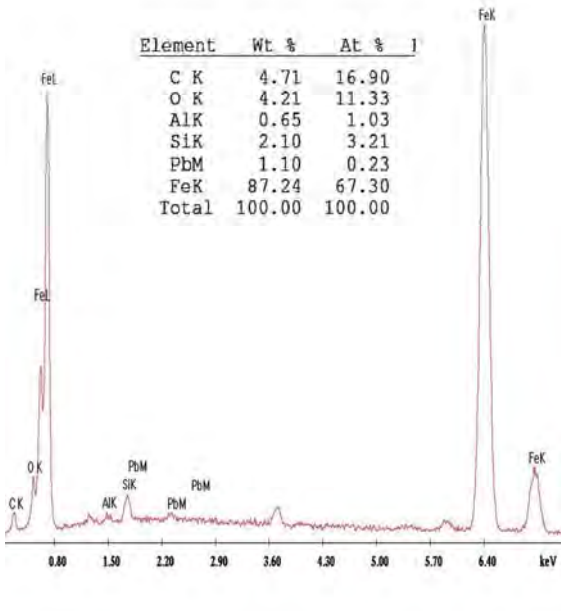

(b) Element composition of reinforcement

Figure 6-15 Element composition of F-WO-3

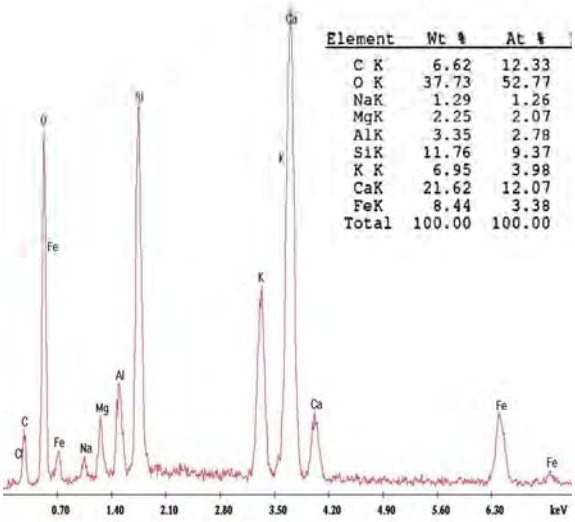

(a) Element composition of concrete

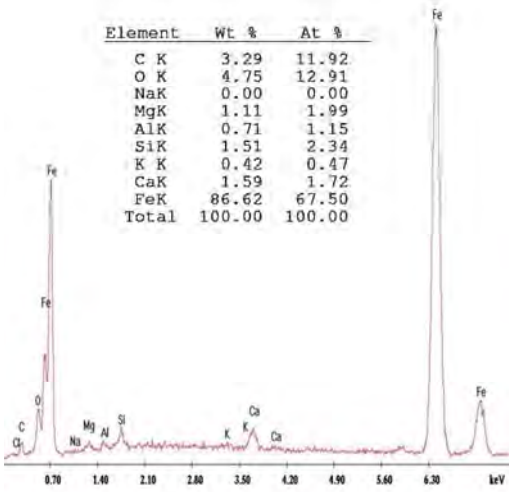

(b) Element composition of reinforcement

Figure 6-16 Element composition of F-WC-3

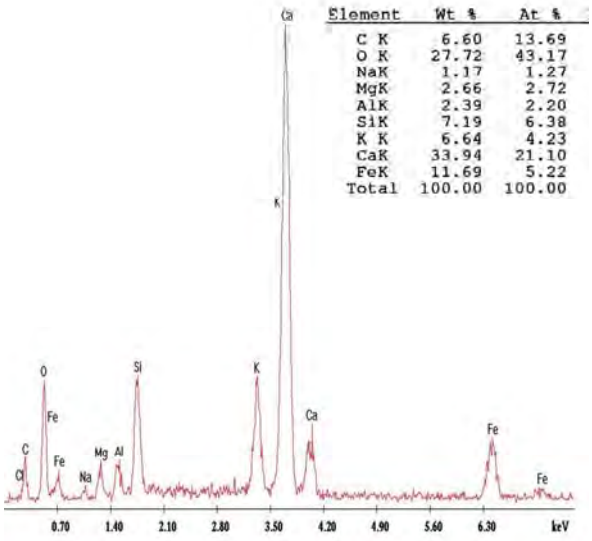

(a) Element composition of concrete

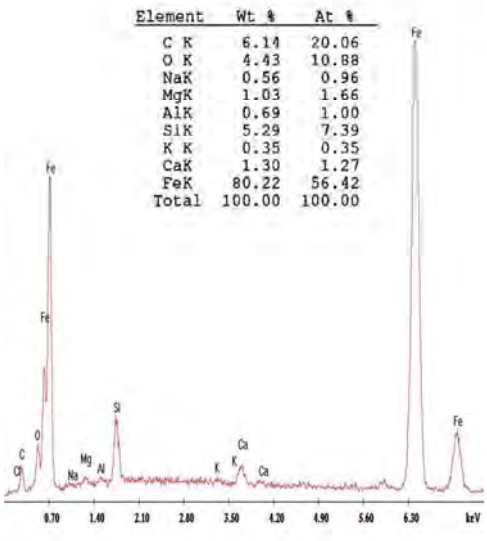

(b) Element composition of reinforcement

Figure 6-17 Element composition of F-WC-6

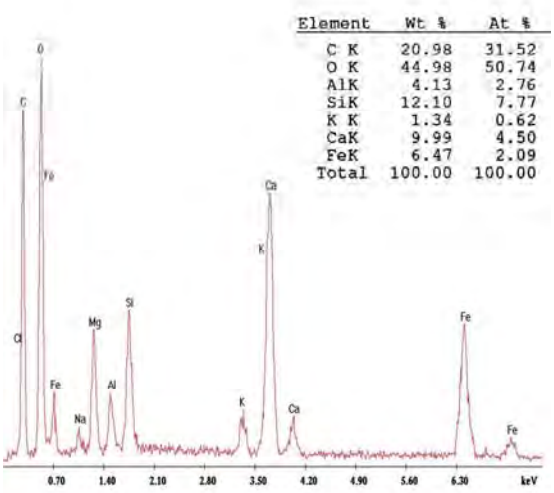

(a) Element composition of concrete

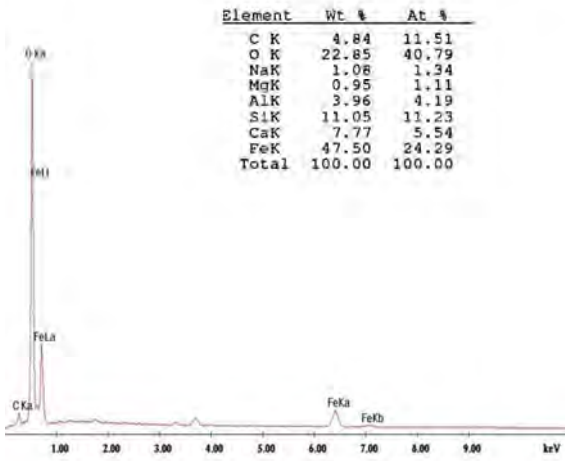

(b) Element composition of reinforcement

Figure 6-18 Element composition of S-WC-30

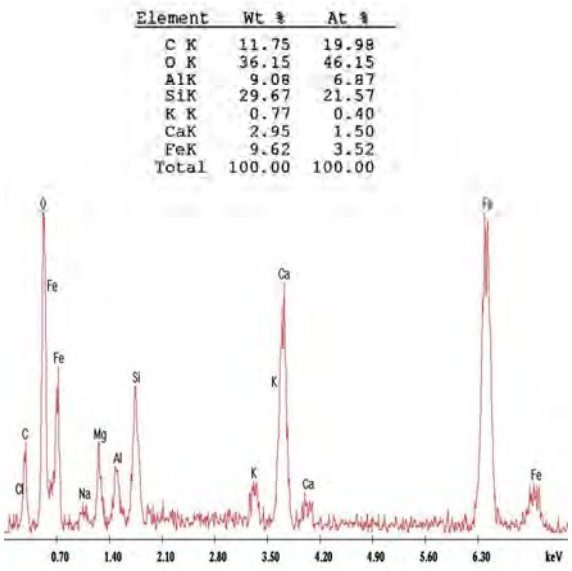

(a) Element composition of concrete

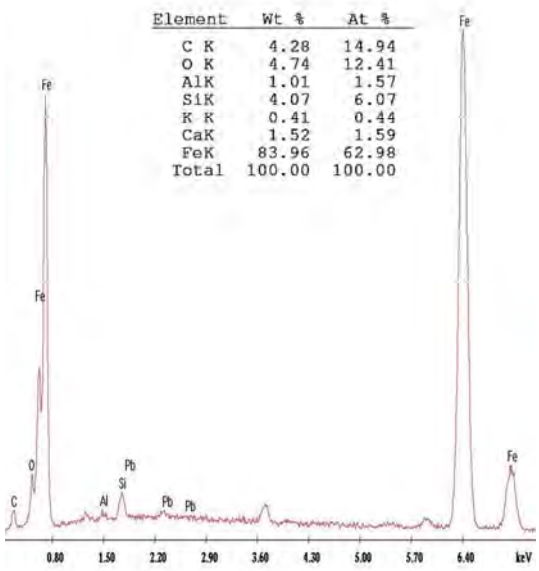

(b) Element composition of reinforcement

Figure 6-19 Element composition of S-WC-60

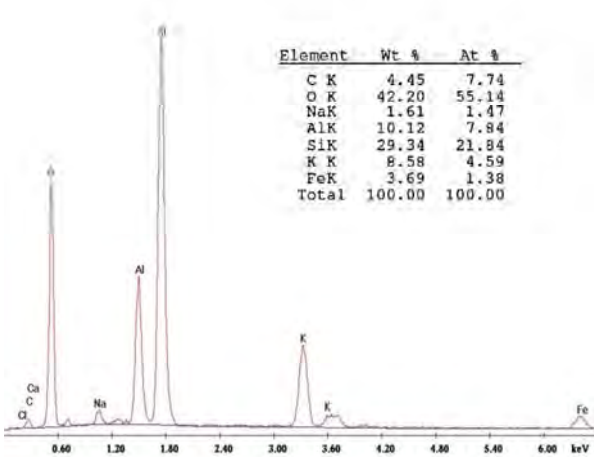

(a) Element composition of concrete

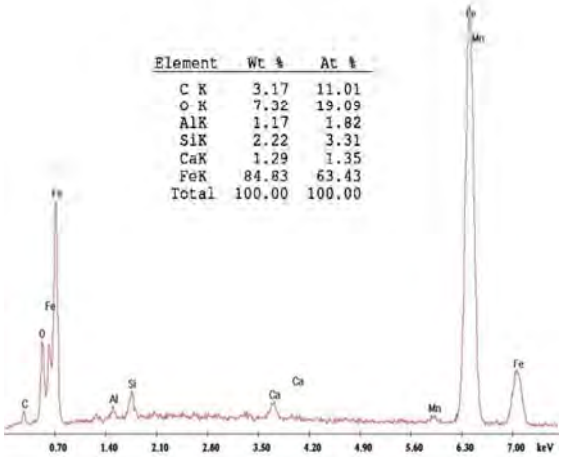

(b) Element composition of reinforcement

Figure 6-20 Element composition of S-WC-100

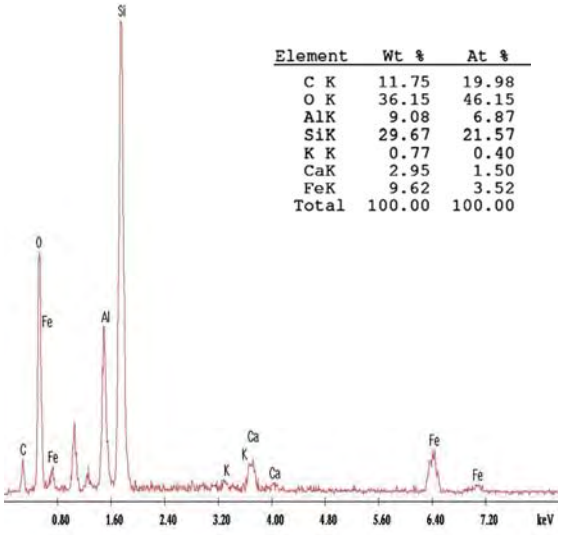

(a) Element composition of 63174-S05-1 carrying I-75NB over 14 Mile Road of concrete

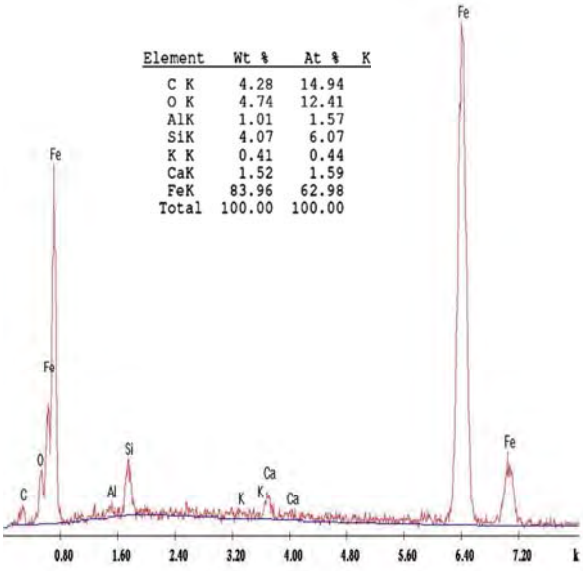

(b) Element composition of 63174-S05-1 carrying I-75NB over 14 Mile Road of reinforcement

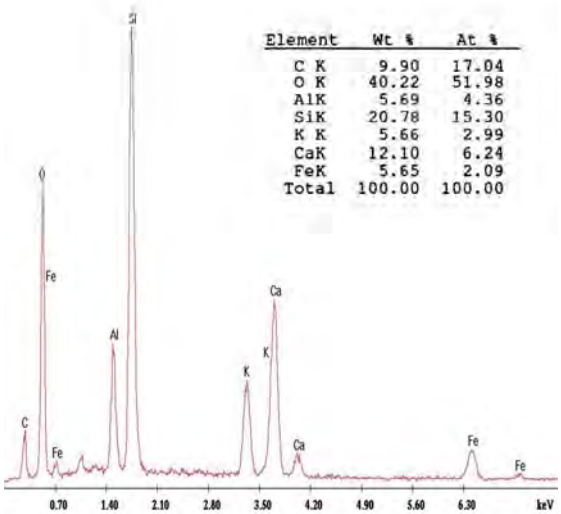

(c) Element composition of 63022-S01 carrying I-96 WB over Kent Lake Road of concrete

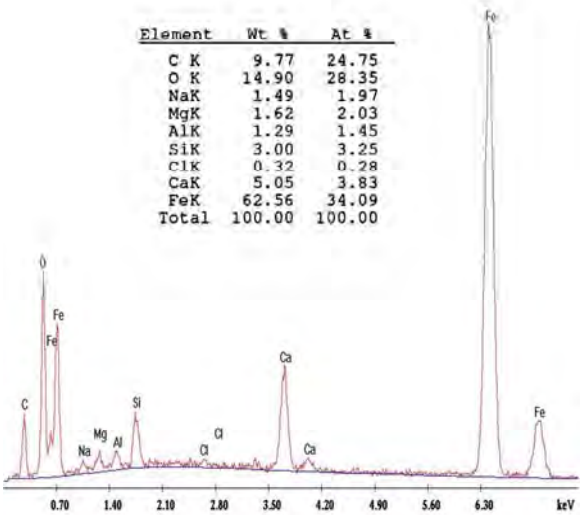

(d) Element composition of 63022-S01 carrying I-96 WB over Kent Lake Road of reinforcement

Figure 6-21 Element composition of field investigated bridges

It can be observed from Figure 6-13 to Figure 6-20 that apart from the different elements which are shown in the figures, oxygen and iron which are evidence of corrosion product were present on reinforcement of saltwater and freeze-thaw exposed specimens. However, oxygen was not present on the reinforcement of control specimen without chloride. This means insignificant corrosion product observed on the control specimen without chloride. Similarly, corrosion products were observed on samples of 63174-S05-1 carrying I-75 NB over 14 Mile Road and 63022-S01carrying I-96 WB over Kent Lake Road as shown in Figure 6-21.

CHAPTER 7: CONCRETE BRIDGE DECK SERVICE LIFE

7.1 General

The objective of this chapter is to propose a simple methodology to estimate the time to corrosion cracking of reinforced concrete bridge decks with known chloride diffusion coefficient and corrosion rate of the reinforcement. This information will support the state agencies in prioritizing maintenance and rehabilitation projects well ahead of any major risk of falling of concrete chunks from the bridge decks to the roadway below.

The chapter discusses service life modeling as defined by initiation time and time to corrosion cracking. The procedure for determining the initiation time is illustrated. The initiation time is the time required for the chloride content to reach critical threshold levels at the location of the reinforcement bar, based on the concrete diffusion coefficient and Fick's second law of diffusion. A description of the selected empirical model to determine the corrosion initiation to corrosion cracking time is presented in the next section. Finally, the service life prediction, based on the initiation time and corrosion cracking time is presented, the chapter concludes with a proposed methodology to implement the techniques within MDOT.

7.2 Service Life Model

7.2.1 Introduction

The service life of a structure can be defined as the expected life time where it remains fully functional without any major rehabilitation (Sohanghpurwala, 2006). Appearance of the first corrosion crack is usually used to define the end of functional service life where rehabilitation of the corroding structural element is required (Tutti 1980).

The service life as driven by chloride induced corrosion of bridge deck reinforcement can be divided into three time periods. First is the initiation time (T_i) which is associated with the time it takes for chloride ions to diffuse to the steel-concrete interface and activate corrosion reactions. Second is the expansion time (T_{free}), which is the duration expressed by the period where the corrosion products start expanding and filling the porous zone surrounding the reinforcement without resulting in pressure build up in the concrete. The third is the stress build-

up time (T_{stress}), which can be defined as the time starting from the beginning of stress development up to the first crack initiation. The expansion time and the stress build-up period is predicted from an empirical model and is presented later in this chapter. A schematic diagram of the service life model is presented below in Figure 7-1.

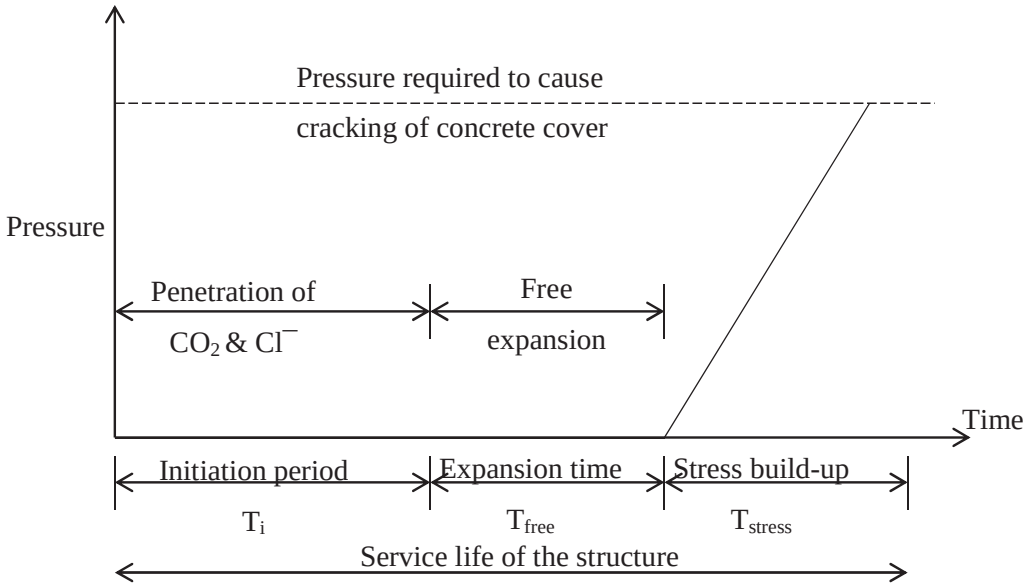

Figure 7-1 Service life model of reinforced concrete structure

7.2.2 Determination of Initiation Time (T_i)

The corrosion initiation time (Ti) is the time duration for chloride ions to diffuse to the steel-concrete interface and activate corrosion reactions. The corrosion initiation time (Ti) depends on the rate of ingress of chlorides into concrete, surface chloride concentration, depth of reinforcing bar, and the value of the critical chloride content. The corrosion is assumed to start when the chloride concentration at the reinforcement level reaches the critical value. The initiation time (T_i) was determined by applying Fick's second law of diffusion and a critical chloride concentration of 1.2-1.5 lb/cyd (Miki 1990).

7.2.2.1 Diffusion Coefficient of the Bridge Deck Concrete

Prediction models for the ingress of chlorides into concrete should consider the complex combination of several transport processes (Neville 1995; Kropp et al.1995) that include diffusion, capillary sorption (absorption of water containing chlorides into unsaturated concrete), and permeation (water flow in concrete due to a pressure gradient). However, diffusion of chlorides into a concrete bridge deck exposed to the periodic application of deicing salts can be assumed to be the governing transport mechanism (Cady & Weyers 1983). Once the chlorides have penetrated the concrete and reached the reinforcement and the concentration is above a critical chloride content value, the corrosion of the reinforcement can be initiated (Lounis et al. 2004). The time-dependent distribution of chloride concentration over the depth of the bridge deck can be obtained from the solution of Fick's second law of diffusion.

Fick's second law of diffusion is a convenient mathematical model to describe the diffusion processes of chloride ingress in a concrete structure. The value of chloride diffusion coefficient in the diffusion equation during the transient transport phase can be regarded as a variable dependent on chloride content varied with time and depth. Assuming that the concrete deck is a homogeneous isotropic semi-infinite medium, and assuming constant boundary condition; the initial chloride (C_i), exposed surface chloride content (C_s) and diffusion coefficient. The chloride content at depth x and time t is given by:

$$C(x, t) = C_i + (C_s - C_i)\ \mathrm{erfc}\left(\frac{x}{\sqrt{4tD}}\right) \qquad \text{(Equation 7-1)}$$

Where

C(x,t) =Chloride content at depth x and time t

C_i =Initial chloride content

C_s =Chloride content of the exposed concrete surface

D =Constant diffusion coefficient

Erfc =Error function

Despite its simplicity and extensive use, this model has some shortcomings, because: (i) the diffusion coefficient is not a constant but rather depends on time, temperature, and depth because of the heterogeneous nature and aging of concrete (Cady and Weyers 1982; Neville

1995; Kropp et al. 1995); and (ii) the top surface of the bridge deck is subjected to a continually changing chloride exposure. The chloride concentration at the deck surface varies with the season, however at some shallow depth near the deck surface (within the first ½ in), the chloride concentration, referred to as near-surface chloride concentration can be assumed at a quasi-constant maximum chloride content of exposed concrete surface (C_s) [Cady & Weyers 1982].

The diffusion coefficient values obtained from Equation 7-1 represents the diffusivity of the concrete during sampling. Using these values, as average diffusivity of the concrete deck during the period from the start of exposure to the time of sampling, undermines the time-dependent changes. Equation 5.1 does not consider the time dependent change. However, studies show that diffusion coefficient decreases with time, Thomas et al., 1998 proposed the time dependent diffusion coefficient as:

$$D_t = D_{28}\left(\frac{t_{28}}{t}\right)^m \qquad \text{(Equation 7-2)}$$

Where

D_t =diffusion coefficient at time t,

D_{28} =diffusion coefficient at time t_{28}, (28 days)

m =diffusion reduction coefficient., (m=0.1 for Portland cement, Thomas et al.,1998)

The relationship is consistent with similar mathematical descriptions proposed by Mangat et al., 1994 and M. Maages et al. Equation 7-2 can be used to determine the diffusivity at any time given the diffusivity at time of sampling.

Table 7-1 Time dependent diffusion coefficient of 63174-S05-1 carrying I-75 NB over 14 Mile Road

Time (years)	**D (mm^2/s)**	**D (in^2/s)**	**Time (years)**	**D (mm^2/s)**	**D (in^2/s)**
1	$2.18 \cdot 10^{-05}$	$3.38 \cdot 10^{-08}$	26	$1.57 \cdot 10^{-05}$	$2.43 \cdot 10^{-08}$
2	$2.03 \cdot 10^{-05}$	$3.15 \cdot 10^{-08}$	28	$1.56 \cdot 10^{-05}$	$2.42 \cdot 10^{-08}$
4	$1.9 \cdot 10^{-05}$	$2.99 \cdot 10^{-08}$	30	$1.55 \cdot 10^{-05}$	$2.40 \cdot 10^{-08}$
6	$1.82 \cdot 10^{-05}$	$2.82 \cdot 10^{-08}$	32	$1.54 \cdot 10^{-05}$	$2.39 \cdot 10^{-08}$
8	$1.77 \cdot 10^{-05}$	$2.74 \cdot 10^{-08}$	34	$1.53 \cdot 10^{-05}$	$2.37 \cdot 10^{-08}$
10	$1.73 \cdot 10^{-05}$	$2.68 \cdot 10^{-08}$	36	$1.52 \cdot 10^{-05}$	$2.36 \cdot 10^{-08}$
12	$1.70 \cdot 10^{-05}$	$2.64 \cdot 10^{-08}$	38	$1.51 \cdot 10^{-05}$	$2.34 \cdot 10^{-08}$
14	$1.67 \cdot 10^{-05}$	$2.59 \cdot 10^{-08}$	40	$1.51 \cdot 10^{-05}$	$2.34 \cdot 10^{-08}$
16	$1.65 \cdot 10^{-05}$	$2.56 \cdot 10^{-08}$	42	$1.50 \cdot 10^{-05}$	$2.33 \cdot 10^{-08}$
18	$1.63 \cdot 10^{-05}$	$2.53 \cdot 10^{-08}$	44	$1.49 \cdot 10^{-05}$	$2.31 \cdot 10^{-08}$
20	$1.62 \cdot 10^{-05}$	$2.51 \cdot 10^{-08}$	46	$1.49 \cdot 10^{-05}$	$2.31 \cdot 10^{-08}$
22	$1.60 \cdot 10^{-05}$	$2.48 \cdot 10^{-08}$	48	$1.48 \cdot 10^{-05}$	$2.29 \cdot 10^{-08}$
24	$1.59 \cdot 10^{-05}$	$2.46 \cdot 10^{-08}$	Average	$1.65 \cdot 10^{-05}$	$2.55 \cdot 10^{-08}$

($1.0\ in^2 = 645.16\ mm^2$)

Table 7-1 shows that the diffusion coefficient rapidly decreases with time at the early stage and the rate decreases gradually with time. This is also supported by Yeih et al. (1994), Thomas et al. (1998) and Cheng et al. (2009). The value at time of sampling is not the average diffusivity. Therefore, diffusivity with time was calculated using Equation 5.2 for each testing area. The average value over the time period from chloride exposure to sampling was used in calculating time for ingress of chloride to reach critical value on the surface of the reinforcement.

Concrete powder from the surface of cores of bridges 63174-S05-1 carrying I-75 NB over 14 Mile Road and 63022-S01 carrying I-96 WB over Kent Lake Road were tested with rapid chloride content test to determine C_s (chloride content of the exposed concrete surface), and the values are presented in Table 7-2. Initial chloride content (C_i) is estimated from regression analysis to be 0.2 lb/cyd, using the chloride content values with depth data and time based on the

construction year. Chloride content values were determined from powder samples taken from different testing areas of the bottom of the bridge deck and cores of the full-depth decks. Areas A2, A3, B1, and B2 are from the original concrete while Areas A1 and B3 are on the newly added lane.

The initial chloride content value estimated from regression analysis, exposed surface chloride content and chloride content data with depth were considered in the calculation of the diffusion coefficients (D) at time of sampling by using Equation 7.2 and are presented in Table 7-3 through Table 7-9 for testing areas of 63174-S05-1 carrying I-75 over 14 Mile Road, core of 63174-S05-1 carrying I-75 over 14 Mile Road, 63022-S02-3 I-96 over Milford Road and 63022-S01 carrying I-96 over Kent Lake Road, respectively.

Table 7-2 Chloride content of exposed concrete surface

Bridge	**Area**	**Chloride content (%) by weight**	**Chloride content (lb/cyd)**
63174-S05-1 carrying I-75 NB over 14 Mile Road (most left lane)	A3	0.613	2.5
63022-S01 I-96 WB over Kent Lake Road (most left lane)	B1	0.114	4.6
63022-S01 carrying I-96 WB over Kent Lake Road (inside shoulder)	B2	0.143	5.8
63022-S01 carrying I-96 WB over Kent Lake Road (most left lane)	A3	0.109	4.4

Table 7-3 Diffusion coefficient of 63174-S05-1 carrying I-75 NB over 14 Mile Road

Area	Depth from top surface, x (mm)	Depth from top surface, x (in.)	Chloride content, C(x,t) (lb/cyd)	Surface chloride content, C_s (lb/cyd)	Initial chloride content, C_i (lb/cyd)	Time, t (year)	D (mm^2/s)	D (in^2/s)
	208	8.2	0.713				$1.43 \cdot 10^{-05}$	
	193	7.6	0.98				$2.03 \cdot 10^{-05}$	
	188	7.4	1.025	2.5	0.2*	40	$2.10 \cdot 10^{-05}$	
A1	127	5.0	2.228				$4.08 \cdot 10^{-04}$	
	127	5.0	2.005				$1.21 \cdot 10^{-04}$	
	127	5.0	2.005				$1.21 \cdot 10^{-04}$	
						Mean	$1.18 \cdot 10^{-04}$	$1.83 \cdot 10^{-07}$
A2	208	8.2	0.713	2.5	0.2	48	$1.19 \cdot 10^{-05}$	
	208	8.2	0.891				$1.65 \cdot 10^{-05}$	
						Mean	$1.42 \cdot 10^{-05}$	$2.20 \cdot 10^{-08}$
	188	7.4	0.757				$2.15 \cdot 10^{-05}$	
	188	7.4	0.579				$1.53 \cdot 10^{-05}$	
A3	188	7.4	0.535				$1.39 \cdot 10^{-05}$	
	183	7.2	0.713	2.5	0.2	48	$1.89 \cdot 10^{-05}$	
	127	5.0	0.713				$1.01 \cdot 10^{-05}$	
	127	5.0	0.668				$9.29 \cdot 10^{-06}$	
						Mean	$1.48 \cdot 10^{-05}$	$2.29 \cdot 10^{-08}$

*The initial chloride content of A1 and A2 is assumed based on the result of initial chloride content calculated from the core of A3.

(1.0 in^2 = 645.16 mm^2)

Table 7-4 Diffusion coefficient of 63174-S05-1 carrying I-75 NB over 14 mile Road core

Area	Depth from top surface, x (mm)	Depth from top surface, x (in.)	Chloride content, C(x,t) (lb/cyd)	Surface chloride content, C_s (lb/cyd)	Initial chloride content, C_i (lb/cyd)	Time, t (year)	D (mm^2/s)	D (in^2/s)
A3	190	7.5	0.401	2.5	0.2	48	$9.17 \cdot 10^{-06}$	
	170	6.7	0.490				$8.96 \cdot 10^{-06}$	
	150	5.9	0.490				$6.98 \cdot 10^{-06}$	
	130	5.1	0.535				$5.75 \cdot 10^{-06}$	
	110	4.3	0.668				$5.32 \cdot 10^{-06}$	
	90	3.5	1.025				$6.71 \cdot 10^{-05}$	
	70	2.8	1.381				$7.96 \cdot 10^{-05}$	
	50	2.0	1.693				$8.34 \cdot 10^{-05}$	
	30	1.2	1.782				$3.85 \cdot 10^{-05}$	
	10	0.4	2.406				$2.61 \cdot 10^{-05}$	
						Mean	$1.41 \cdot 10^{-05}$	$2.19 \cdot 10^{-08}$

($1.0\ in^2 = 645.16\ mm^2$)

The average diffusion coefficient, during sampling, for areas A1, A2 and A3 of 63174-S05-1 carrying I-75 NB over 14 Mile Road is $1.83 \cdot 10^{-07}$ in^2/sec, $2.20 \cdot 10^{-08}$ in^2/sec and $2.29 \cdot 10^{-08}$ in^2/sec, respectively. Area A1 has a higher magnitude of diffusion coefficient. The difference can be attributed to the newer concrete lane added to the bridge and signifies a different quality of concrete as compared to areas A2 and A3. The average diffusion coefficient, during sampling, of the core taken from area A3 is $2.19 \cdot 10^{-08}$ in^2/sec, which is also in close agreement with the results obtained from concrete powder samples taken from the bottom of the deck slab in area A3.

Table 7-5 Diffusion coefficient of 63022-S02-4 carrying I-96 WB over Milford Road

Area	Depth from top surface, x (mm)	Depth from top surface, x (in.)	Chloride content, C(x,t) (lb/cyd)	Surface chloride content, C_s (lb/cyd)	Initial chloride content, C_i (lb/cyd)	Time, t (year)	D (mm^2/s)	D (in^2/s)
	231	9.1	0.891				$8.78 \cdot 10^{-06}$	
	231	9.1	0.446				$4.91 \cdot 10^{-06}$	
A1	211	8.3	1.871				$1.80 \cdot 10^{-05}$	
	211	8.3	1.381	4.9**	0.2*	46	$1.17 \cdot 10^{-05}$	
	191	7.5	2.228				$2.04 \cdot 10^{-05}$	
	191	7.5	2.005				$1.66 \cdot 10^{-05}$	
						Mean	$1.34 \cdot 10^{-05}$	$2.08 \cdot 10^{-08}$
	231	9.1	0.312				$3.08 \cdot 10^{-06}$	
	231	9.1	0.668				$5.80 \cdot 10^{-06}$	
A2	231	9.1	0.312				$3.08 \cdot 10^{-06}$	
	211	8.3	1.381	4.9	0.2	54	$9.97 \cdot 10^{-06}$	
	211	8.3	1.559				$1.17 \cdot 10^{-05}$	
	191	7.5	2.317				$1.89 \cdot 10^{-05}$	
						Mean	$8.75 \cdot 10^{-06}$	$4.26 \cdot 10^{-09}$
	231	9.1	0.401				$3.83 \cdot 10^{-06}$	
	231	9.1	0.446				$4.18 \cdot 10^{-06}$	
	211	8.3	1.114				$7.79 \cdot 10^{-06}$	
A3	211	8.3	1.693	4.9	0.2	54	$1.31 \cdot 10^{-05}$	
	211	8.3	1.247				$8.82 \cdot 10^{-06}$	
	191	7.5	2.272				$1.81 \cdot 10^{-05}$	
						Mean	$9.30 \cdot 10^{-06}$	$1.44 \cdot 10^{-08}$

*The initial chloride content is based on the result from 63174-S05-1 carrying I-75 NB over 14 Mile Road core.

**Surface chloride content used is the average value of 63022-S01 carrying I-96 WB over Kent Lake Road, *(1.0 in^2 = 645.16 mm^2)*

It can be observed from the Table 7-5 that the average diffusion coefficient, during sampling, of areas A1, A2 and A3 of 3022-S02-4 I-96 WB over Milford Road is $2.08 \cdot 10^{-08}$ in^2/sec, $4.26 \cdot 10^{-09}$ in^2/sec and $1.44 \cdot 10^{-08}$ in^2/sec, respectively.

Table 7-6 Diffusion coefficient of 63022-S01 carrying I-96 over Kent Lake Road

Area	Depth from top surface, x (mm)	Depth from top surface, x (in)	Chloride content, C(x,t) (lb/cyd)	Surface chloride content, Cs (lb/cyd)	Initial chloride content, Ci (lb/cyd)	Time, t (year)	D (mm^2/s)	D (in^2/s)
	183	7.2	0.49				$7.09 \cdot 10^{-06}$	
	183	7.2	0.891				$1.07 \cdot 10^{-05}$	
	173	6.8	0.891	4.4	0.2*	44	$1.07 \cdot 10^{-05}$	
A1	163	6.4	1.559				$1.59 \cdot 10^{-05}$	
	153	6.0	0.98				$8.79 \cdot 10^{-06}$	
	137	5.4	2.005				$1.80 \cdot 10^{-05}$	
						Mean	$1.19 \cdot 10^{-05}$	$1.84 \cdot 10^{-08}$
	183	7.2	0.401				$4.43 \cdot 10^{-06}$	
	183	7.2	0.802				$6.89 \cdot 10^{-06}$	
A2	183	7.2	0.49				$4.95 \cdot 10^{-06}$	
	163	6.4	0.579	4.4	0.2	63	$4.57 \cdot 10^{-06}$	
	163	6.4	0.891				$6.24 \cdot 10^{-06}$	
	142	5.6	2.049				$1.37 \cdot 10^{-05}$	
						Mean	$6.80 \cdot 10^{-06}$	$1.05 \cdot 10^{-08}$
	183	7.2	0.401				$4.43 \cdot 10^{-06}$	
	183	7.2	0.356				$4.16 \cdot 10^{-06}$	
	163	6.4	1.337	4.4	0.2	63	$9.22 \cdot 10^{-06}$	
A3	163	6.4	1.114				$7.62 \cdot 10^{-06}$	
	163	6.4	1.337				$9.22 \cdot 10^{-06}$	
	142	5.6	1.871				$1.18 \cdot 10^{-05}$	
						Mean	$7.74 \cdot 10^{-06}$	$1.20 \cdot 10^{-08}$

*The initial chloride content is based on the result from 63174-S05-1 carrying I-75 NB over 14 Mile Road core. *($1.0\ in^2 = 645.16\ mm^2$)*

The average diffusion coefficient, during sampling, of areas A1, A2 and A3 of 63022-S01 carrying I-96 over Kent Lake Road is $1.84 \cdot 10^{-08}$ in^2/sec, $1.05 \cdot 10^{-08}$ in^2/sec and $1.20 \cdot 10^{-08}$ in^2/sec, respectively. From Table 7-6, it can be also observed that the diffusion coefficient is highest in area A1. Area A1 is located in the lane added after the original construction and signifies a different quality of concrete as compared to A2 and A3.

Table 7-7 Diffusion coefficient of 63022-S01 carrying I-96 over Kent Lake Road Core (B1)

Area	Depth from top surface, x (mm)	Depth from top surface, x (in)	Chloride content, C(x,t) (lb/cyd)	Surface chloride content, Cs (lb/cyd)	Initial chloride content, Ci (lb/cyd)	Time, t (year)	D (mm^2/s)	D (in^2/s)
	20	0.8	4.410				$3.78 \cdot 10^{-05}$	
	40	1.6	3.831				$9.03 \cdot 10^{-06}$	
	60	2.4	3.163				$5.60 \cdot 10^{-06}$	
	80	3.1	2.495				$4.34 \cdot 10^{-06}$	
	100	3.9	1.069	4.6	0.2*	63	$1.76 \cdot 10^{-06}$	
B1	120	4.7	0.757				$1.88 \cdot 10^{-06}$	
	140	5.5	0.757				$2.55 \cdot 10^{-06}$	
	160	6.3	0.490				$2.47 \cdot 10^{-06}$	
	180	7.1	0.446				$2.96 \cdot 10^{-06}$	
	200	7.9	0.401				$3.44 \cdot 10^{-06}$	
						Mean	$7.18 \cdot 10^{-06}$	$1.11 \cdot 10^{-08}$

(1.0 in^2 = 645.16 mm^2)

Table 7-8 Diffusion coefficient of 63022-S01 carrying I-96 over Kent Lake Road Core (B2)

Area	Depth from top surface, x (mm)	Depth from top surface, x (in)	Chloride content, C(x,t) (lb/cyd)	Surface chloride content, Cs (lb/cyd)	Initial chloride content, Ci (lb/cyd)	Time, t (year)	D (mm^2/s)	D (in^2/s)
	20	0.8	5.792				$1.89 \cdot 10^{-04}$	
	40	1.6	5.346				$2.89 \cdot 10^{-05}$	
	60	2.4	4.455				$9.30 \cdot 10^{-06}$	
	80	3.1	4.232				$1.23 \cdot 10^{-05}$	
	100	3.9	3.119	5.8	0.2	63	$6.33 \cdot 10^{-06}$	
B2	120	4.7	2.138				$4.37 \cdot 10^{-06}$	
	140	5.5	1.871				$4.93 \cdot 10^{-06}$	
	160	6.3	1.782				$6.05 \cdot 10^{-06}$	
	180	7.1	1.337				$5.58 \cdot 10^{-06}$	
						Mean	$2.97 \cdot 10^{-05}$	$4.60 \cdot 10^{-08}$

(1.0 in^2 = 645.16 mm^2)

Table 7-9 Diffusion coefficient of 63022-S01 carrying I-96 over Kent Lake Road Core (A3)

Area	Depth from top surface, x (mm)	Depth from top surface, x (in)	Chloride content, C(x,t) (lb/cyd)	Surface chloride content, Cs (lb/cyd)	Initial chloride content, Ci (lb/cyd)	Time, t (year)	D (mm^2/s)	D (in^2/s)
	20	0.8	4.232				$4.39 \cdot 10^{-05}$	
	40	1.6	4.232				$1.76 \cdot 10^{-04}$	
	60	2.4	4.010				$7.27 \cdot 10^{-05}$	
	80	3.1	3.119	4.4	0.2	63	$1.15 \cdot 10^{-05}$	
	100	3.9	1.782				$3.63 \cdot 10^{-05}$	
A3	120	4.7	1.648				$4.60 \cdot 10^{-05}$	
	140	5.5	1.604				$6.00 \cdot 10^{-06}$	
	160	6.3	1.559				$7.51 \cdot 10^{-06}$	
	180	7.1	0.936				$5.25 \cdot 10^{-06}$	
						Mean	$3.58 \cdot 10^{-05}$	$5.55 \cdot 10^{-08}$

(1.0 in^2 = 645.16 mm^2)

From Table 7-7 through Table 7-9, the average diffusion coefficient of the cores taken from bridge 63022-S01 I-96 over Kent Lake Road of areas B1, B2 and A3 is $1.11 \cdot 10^{-08}$ in^2/sec, $4.60 \cdot 10^{-08}$ in^2/sec and is $5.55 \cdot 10^{-08}$ in^2/sec, respectively.

The results of this study are in general agreement with results reported in the literature for chloride content and diffusion coefficients obtained on concrete bridges decks in Virginia and North Carolina, respectively (Weyer et al, 2003 and Janos et al. 2006).

7.2.2.2 Determination of Initiation Time (T_i) of the Investigated Bridges

The initiation time (T_i) which is the period required for the chloride concentration to reach critical value, 1.2 to 1.5 lb/cyd (Miki 1990), around the bottom reinforcement level of the deck is determined by using Fick's second law of diffusion. The results are shown in Table 7-10.

Table 7-10 Time to reach critical chloride content (1.2 lb/cyd) at bottom reinforcement

Bridge	Area	Diffusion coefficient (from time of exposure to sampling), in^2/s	T_i (years) for 1.2 lb/cyd	T_i (years) for 1.5 lb/cyd
63174-S05-1 carrying I-75 over 14 Mile Road	A1	$2.05 \cdot 10^{-07}$	3.0	6.0
	A2	$2.46 \cdot 10^{-08}$	25.5	49.0
	A3	$2.56 \cdot 10^{-08}$	24.5	47.5
	A3 (core)	$2.43 \cdot 10^{-08}$	26.0	50.0
63022-S02-4 carrying I-96 over Milford Road	A1	$2.34 \cdot 10^{-08}$	27.0	52.0
	A2	$1.52 \cdot 10^{-08}$	42.0	80.0
	A3	$1.61 \cdot 10^{-08}$	39.0	75.0
63022-S01 carrying I-96 over Kent Lake Road	A1	$2.06 \cdot 10^{-08}$	31.0	59.0
	A2	$1.18 \cdot 10^{-08}$	44.0	103.0
	A3	$1.34 \cdot 10^{-08}$	38.5	91.0
	B1 (core)	$1.24 \cdot 10^{-08}$	41.5	98.0
	B2 (core)	$5.12 \cdot 10^{-08}$	12.5	24.0
	A3 (core)	$6.06 \cdot 10^{-08}$	11.5	20.0

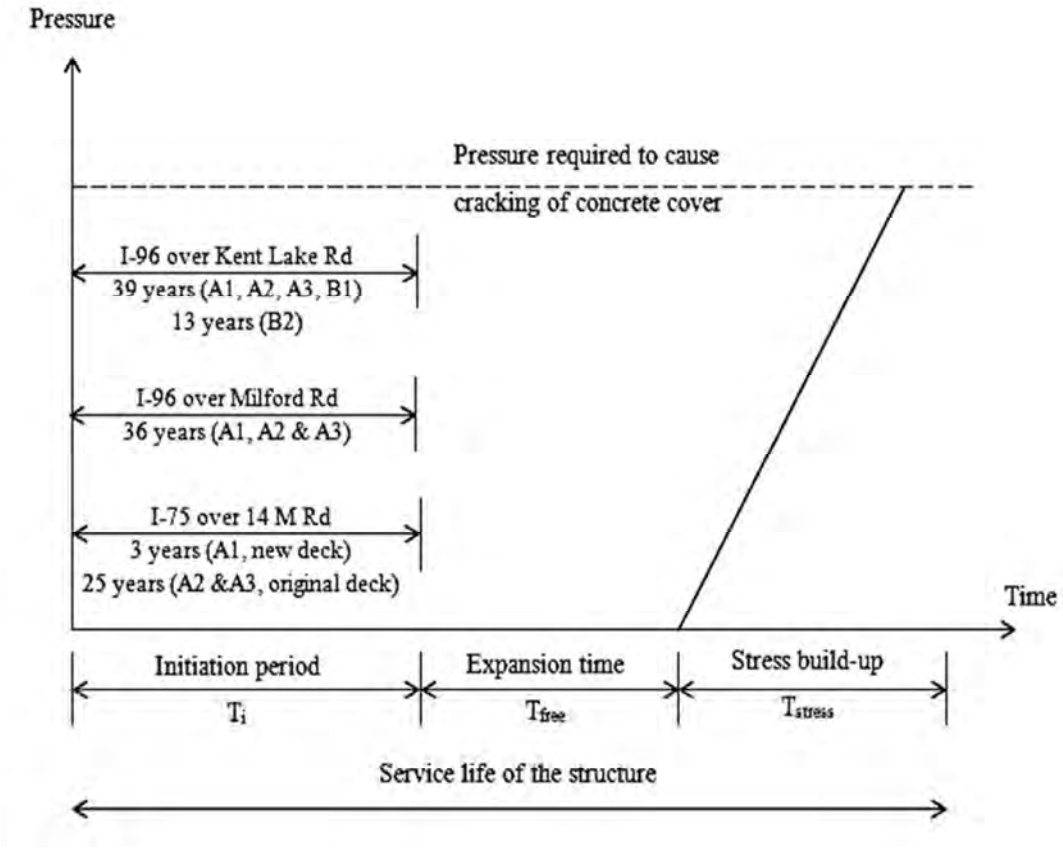

Figure 7-2 Summary of corrosion initiation time of the investigated bridges

It can be observed from Table 7-10 that area A1 of 63174-S05-1 carrying I-75 NB over 14 Mile Road is quite poor as the threshold chloride (1.2 lb/cyd) is estimated to be reached at the reinforcement level in 3.0 years only. The time to reach the critical chloride (1.2 lb/cyd) is estimated to be 25 years, 36 years and 30 years for the remaining areas of bridge 63174-S05-1 carrying I-75 NB over 14 Mile Road, bridge 3022-S02-4 carrying I-96 WB over Milford Road and 63022-S01 carrying I-96 WB over Kent Lake Road, respectively.

7.2.3 Determination of Time from Corrosion Initiation to Corrosion Cracking (T_{cor})

T_{cor} is the time required from corrosion initiation to corrosion cracking. Corrosion initiates when the chloride concentration reaches the critical value. The corrosion product starts to freely expand and fill the porous zone. Once the porous zone is filled, the expansive corrosion

products create tensile stresses on the concrete surrounding the corroding steel reinforcing bar until cracked is formed, which lead to cracking and spalling of concrete cover. The model proposed by Maaddawy and Soudki has been chosen for predicting the time to corrosion cracking of the concrete because of the simple mathematical approach. This model relates the steel mass loss and the internal radial pressure caused by the expansion of corrosion products developed. The concrete around a corroding steel reinforcing bar is modeled as a thick-walled cylinder with a wall thickness equal to thinnest concrete cover. The concrete ring is assumed to crack when the tensile stresses in the circumferential direction at every part of the ring have reached the tensile strength of concrete. The internal radial pressure at cracking is then determined and related to steel mass. With the help of Faraday's law the time from corrosion initiation to corrosion cracking is then predicted. P_{cor}, internal radial pressure caused by corrosion and T_{cr}, time from corrosion initiation to corrosion cracking is presented in Equation 7-3 and Equation 7-4, respectively.

$$P_{cor} = \frac{2M_{loss}E_{ef}\left[\left(1/o.622\rho_r\right)-\left(1/\rho_s\right)\right]}{\pi D\left(1+\nu+\varphi\right)\left(D+2\delta_0\right)} - \frac{2\delta_0 E_{ef}}{\left(1+\nu+\varphi\right)\left(D+2\delta_0\right)} \qquad \text{(Equation 7-3)}$$

$$T_{cr} = \left[\frac{7117.5\left(D+2\delta_0\right)\left(1+\nu+\varphi\right)}{iE_{ef}}\right]\left[\frac{2Cf_{ct}}{D} + \frac{2\delta_0 E_{ef}}{\left(1+\nu+\varphi\right)\left(D+2\delta_0\right)}\right] \qquad \text{(Equation 7-4)}$$

Where

C = clear concrete cover (mm)

D = diameter of steel reinforcing bar (mm)

E_{ef} = effective elastic modulus of concrete

f_{ct} = tensile strength of concrete

I = current density

P_{cor} = internal radial pressure caused by corrosion

T_{cr} = time from corrosion initiation to corrosion cracking

M_{loss} = mass of steel per unit length consumed to produce M_r

M_r = mass of rust per unit length

δ_0 = thickness of porous zone

ν = Poisson's ratio (0.18 for concrete)

ρ_s = mass density of steel

ρ_r = mass density of rust

ψ = factor depends on D, C and δ_0

Porous zone size is an important parameter for determining the time from corrosion initiation to corrosion cracking, and as discussed earlier the typical range of the porous zone size is 10 to 60 μm or 0.3937 to 2.362 mils. The corrosion cracking model proposed by Sudoky and Maadawy takes corrosion current density as the driving input. A typical plot showing the corrosion current density and the corrosion cracking time based on the data from this study is presented in Figure 7-3. It can be observed from the figure that the time to corrosion cracking is inversely proportional to the corrosion current density. Further the unit conversion from corrosion current density to corrosion rate is presented in Table 7-11. Corrosion rate versus the corrosion cracking time plot is presented in Figure 7-4. The time to corrosion cracking is inversely proportional to the corrosion rate. It is to be noted that by determining the corrosion rate of reinforcing steel in any concrete deck, the range of the time from corrosion initiation to corrosion cracking can be determined from Figure 7-4.

7.2.3.1 Corrosion Cracking Time (T_{cor}) of the Investigated Bridges

For bridges 63174-S05-1 carrying I-75 over 14 Mile Road and 63022-S01 I-96 WB over Kent lake Road, corrosion cracking time was determined based on actual porous zone size of 43 and 22 μm (1.694 and 0.867 mils), respectively, measured by the scanning electron microscope (ESEM). The corrosion cracking time for these bridges is presented in Table 7-12. Core samples for bridge 3022-S02-4 I-96 WB over Milford Road were not obtained and hence the porous zone size was not measured. As an alternative and based on the literature review, a conservative porous zone thickness of 20 μm (0.788 mils) was used.

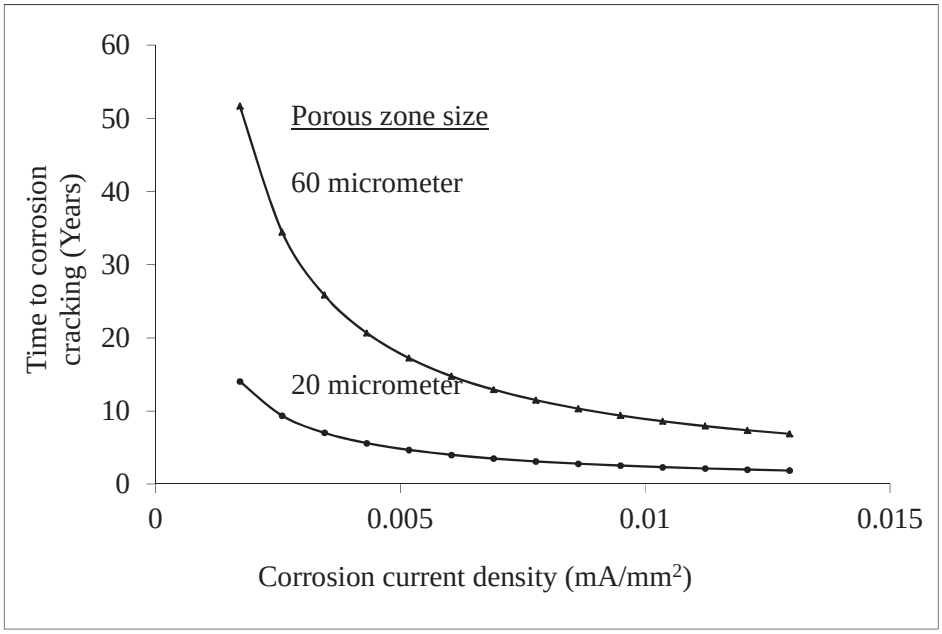

Figure 7-3 Relationship between corrosion current density and time to corrosion cracking

Table 7-11 Unit conversation from corrosion rate to corrosion current density

	mA cm^{-2}	**mm year^{-1}**	**mpy**	**g m^{-2} day^{-1}**
mA cm^{-2}	1	11.6	456	249
mm year^{-1}	0.0863	1	39.4	21.6
mpy*	0.00219	0.0254	1	0.547
g m^{-2} day^{-1}	0.00401	0.0463	1.83	1

* mpy = milli-inch per year

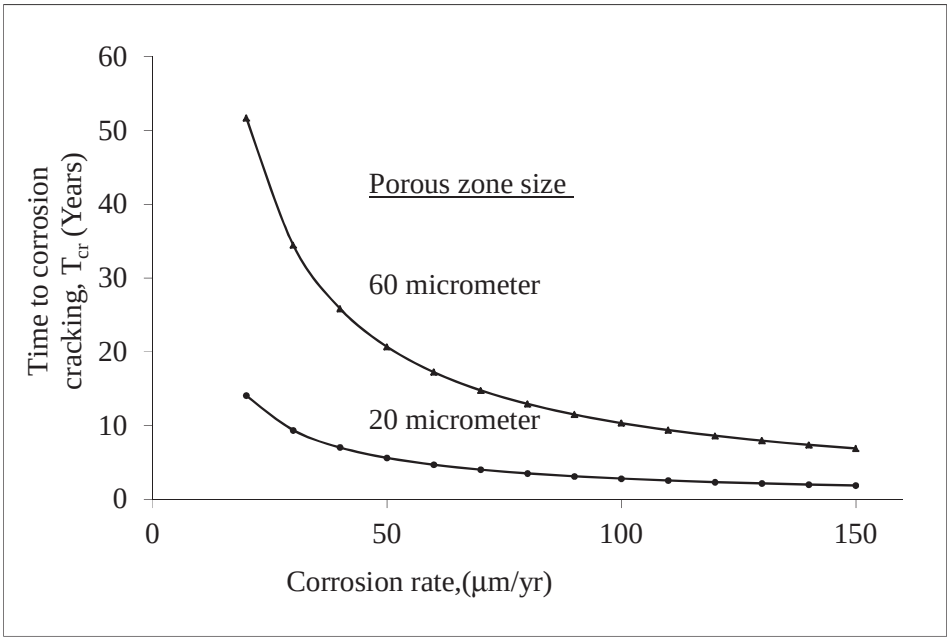

Figure 7-4 Relationship between corrosion rate and time to corrosion cracking (T_{cr})

Table 7-12 Service life of the investigated bridges

Bridge	Area (age, years)	Corrosion Rate (μm/year)	Corrosion Current Density (mA/cm^2)	T_{cor} (years)	Critical chloride content (1.2 lb/cyd).		Critical chloride content (1.5 lb/cyd).	
					T_i (years) for 1.2lb/cyd	Functional Service Life ($T_i + T_{cor}$)	T_i (years) for 1.5lb/cyd	Service Life ($T_i + T_{cor}$
63174-S05-1 carrying I-75 NB over 14 Mile Road	A1* (40)	78	0.0067	9.2	3.0	12.7	6.0	15.2
	A2 (48)	36	0.0031	19.8	25.5	45.3	49.0	68.8
	A3 (48)	20	0.0017	35.7	24.5	60.2	47.5	83.2
3022-S02-4 I-96 WB over Milford Road	A1 (46)	120	0.0100	2.0	27.0	33.0	52.0	54.0
	A2 (54)	120	0.0100	2.0	42.0	44.0	80.0	82.0
	A3 (54)	114	0.0098	2.0	39.0	41.0	75.0	77.0
63022-S01 I-96 WB over Kent Lake Road	A1 (54)	120	0.0100	2.6	31.0	33.6	59.0	61.6
	A2 (44)	120	0.0100	2.6	44.0	46.6	103.0	105.6
	A3 (63)	97	0.0084	3.3	38.5	41.8	91.0	94.3
	B1 (63)	42	0.00632	7.0	41.5	48.5	98.0	105
	B2 (63)	110	0.0095	2.8	12.5	15.3	24.0	26.8

*Newer lane and poorer concrete quality. *(1μm = 0.0394 mils/year)*

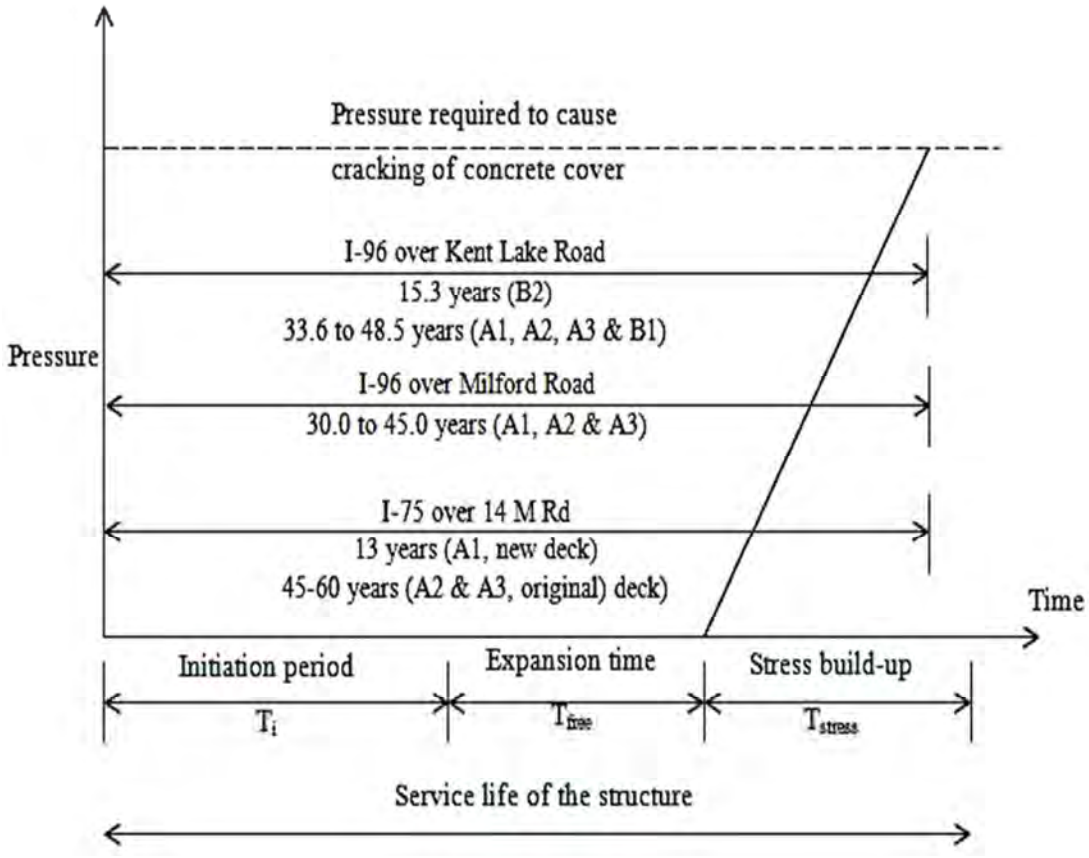

Figure 7-5 Summary of service life of the investigated bridges

It is to be noted from Table 7-12 and Figure 7-6 that for critical chloride content value of 1.2 lb/cyd, the range of service life before corrosion cracking of bridge 63174-S05-1 carrying I-75 NB over 14 Mile Road is 13 years for area A1 and 45 to 60 years for areas A2 and A3. This could be attributed to the newer concrete lane added to the bridge and signifies a lesser quality of concrete with regard to diffusivity as compared to A2 and A3. Area A1 has a higher magnitude of diffusion coefficient, one order difference than areas A2 and A3.

The service life before corrosion cracking for bridge 3022-S02-4 carrying I-96 WB over Milford Road is 30 to 45 years and for bridge 63022-S01 I-96 WB over Kent Lake Road is 15 years for area B2 and 34 to 49 years for the rest of the areas. In all the bridges, the ramps or outside lane (area A1) have reduced predicted service life compared to the remaining. This could

be attributed to the amount of deicing salt added and possibly facilitation of ingestion of chloride by trucks braking.

Corrosion rate of the reinforcing steel changes with time and it is recommended to have a periodic maintenance plan, including measurement of corrosion rate and estimating the service life, this would assist in prioritizing maintenance and rehabilitation projects well ahead of any major risk of falling of concrete from the bridge decks to the roadway below.

7.2.3.2 Corrosion Cracking Time of Laboratory Tested Specimens

Table 7-13 presents the data of the corrosion rate and the time to corrosion cracking of the laboratory tested specimens. It can be observed that the control specimens without any introduced chloride and aggressive exposure has the maximum resistance and time to corrosion cracking. However, the specimens with introduced chloride and exposed to saltwater and freeze-thaw are severely affected by corrosion at an early age of around five to eight years.

Table 7-13 Time required to corrosion cracking for the laboratory tested specimens

Specimen	Corrosion rate (μm/year)	Corrosion Current Density (mA/cm^2)	Porous zone size (μm)	Time to corrosion cracking (years)
C-WO	8	0.0007	69	48.0
C-WC	11	0.0009	44	35.0
F-WO-3	18	0.0016	41	21.0
F-WC-3	83	0.0072	21	4.7
F-WC-6	120	0.0100	17	3.5
S-WC-3	50	0.0043	39	8.0
S-WC-6	60	0.0052	17	6.5
S-WC-8	70	0.0060	18	5.5
S-WC-10	90	0.0078	20	4.5

(1μm = 0.0394 mils/year)

Specimens with introduced chloride are severely affected by the saltwater, freeze/thaw exposures and repeated load cycles. Therefore, the corrosion rate is higher and the specimens

have less than 10 years of time to corrosion cracking. However, for the specimens F-WO-3 (specimen without introduced chloride and exposed to 300 cycles of freeze/thaw), time to corrosion cracking is 21 years. This may be considered as a guide line on the time to corrosion cracking, based on the exposure type to take the necessary precautions to prevent any happening of incident such as falling of concrete chunks from the bridge deck. On the other hand, for specimens C-WO (control specimen without any introduced chloride) the time to corrosion cracking takes place at the end of 48 years.

As indicated in Table 7-13, the maximum corrosion rate corresponds to specimen F-WC-6 after it was subjected to 600 freeze-thaw cycles. The 600 freeze-thaw cycles is equivalent to the number of field freeze-thaw cycles that a bridge deck in southern Michigan would experience in approximately 50 years of functional service life as described in section 5.11. It can be inferred from the data obtained that, in general, the laboratory concrete with chlorides and exposed to 600 freeze-thaw cycles experienced similar environmental conditions to that of 46 to 54 year old bridge decks (see Table 7-12). However, it should be recognized that that while freeze-thaw exposure is a contributing factor to the onset of steel corrosion, other factors are also required such as the presence of cracks, moisture and ingress of chloride ions.

7.2.3.3 Corrosion Cracking Time Spreadsheet

A sample copy of the spreadsheet chart for calculation of time to corrosion cracking is presented in Table 7-14. It can be observed from the table that the time from corrosion initiation to corrosion cracking (T_{cr}) is mainly dependent on corrosion rate, thickness of porous zone, cover depth, spacing between steel reinforcing bars, diameter of the steel reinforcing bar, and properties of concrete such as tensile strength, modulus of elasticity, and Poisson's ratio.

Table 7-14 A sample copy spreadsheet showing the time required to corrosion crack. Method defined in metric system units.

PARAMETERS	**VALUE**
Internal Radius of the Cylinder (a), mm	8.02
Effective Elastic modulus of a thick walled cylinder (E_{ef}), Mpa	29000
Exterior Radius of the cylinder (b), mm	46.02
Poisson's Ratio(ν)	0.20
Diameter of the Steel Reinforcing Bar(D), mm	16
Thickness of the porous Zone (δ_0), mm	0.02
Total Diameter of the Steel reinforcing (D'), mm	16.04
Wall Thickness of the Cylinder C, mm	38
Reconsidered (a), mm	8.02
Reconsidered (b), mm	46.02
Considering ψ	0.06
Mass of Rust per unit length of bar (M_r), kg/mm	0.0013
Ratio of Molecular Mass of Steel to molecular mass of rust (γ)	0.622
Mass density of Rust (ρ_r), kg/m^3	5240
Mass Density of steel (ρ_s), kg/m3	7850
Percentage Steel Mass Loss (m_1)	53.42
Concrete Tensile Strength (f_{ct}), Mpa	5.17
Current Density (i), mA/cm^2	0.01
Time from corrosion initiation to corrosion cracking(T_{cr}), Years	2.6
Time from corrosion initiation to corrosion cracking(T_{cr}), Days	947

7.3 Implementation Strategy

7.3.1 General

Based on the results presented in this study, an implementation strategy is proposed for evaluating and determining future maintenance and repair activities based on combined field inspection, sampling and predictions. The method can be deployed by MDOT engineers. The strategy includes visual inspection, non-destructive testing, and a service life prediction of the bridge deck. It is emphasized that service life in this strategy represents the time to corrosion initiation as well as time to corrosion cracking. It does not represent MDOT's design definition of service life. A flow chart showing the steps of the procedural implementation strategy is presented in Figure 7-6.

Step1:

Step one of the strategy is a visual inspection of the bridge deck. The visual inspection will quantify for longitudinal and transverse cracks on the top and bottom surfaces of the deck, spalling of concrete from the bottom of the deck, and stains on the sides and bottom of the deck. If such corrosion indicators are observed, step 2 follows. Otherwise, the next inspection should follow the master plan.

Step 2:

If presence of corrosion indicators exists, then the visual inspection should be followed by non-destructive testing. Inspectors should conduct measurements of the half-cell potential, pH values and chloride content on the bottom surface of the deck and on core samples from locations of high risk of corrosion. Examine the half-cell potential measurements, the chloride content and pH values against their respective critical values. If:

- The half-cell potential is less than -350mV
- The chloride content at a level of the bottom reinforcement is greater than 1.2-1.5 lb/cyd
- The pH is less than 9.5

If all three critical values are exceeded, proceed to step 3. If not met, the follow up evaluation should be performed according to the State's inspection plan.

It is recommended also recommended to perform Step 2 if the bridge is scheduled for a deck overlay activity. This data can serve as a baseline for future activities.

Step 3:

A detailed evaluation representative of the entire bottom surface of the bridge deck should determine the chloride content profile and estimate the corrosion rate at different location. The coefficient of diffusivity, from the chloride content profile, can be calculated as outline in section 7.2.2.1.

Step 4:

The service life is estimated, as presented in section 7.2, and compared against actual age of bridge. This information will be used in prioritizing repair before further damage occurs due to spalling and falling of concrete from the bridge decks. Finally, the repair and/or rehabilitation can be implemented accordingly.

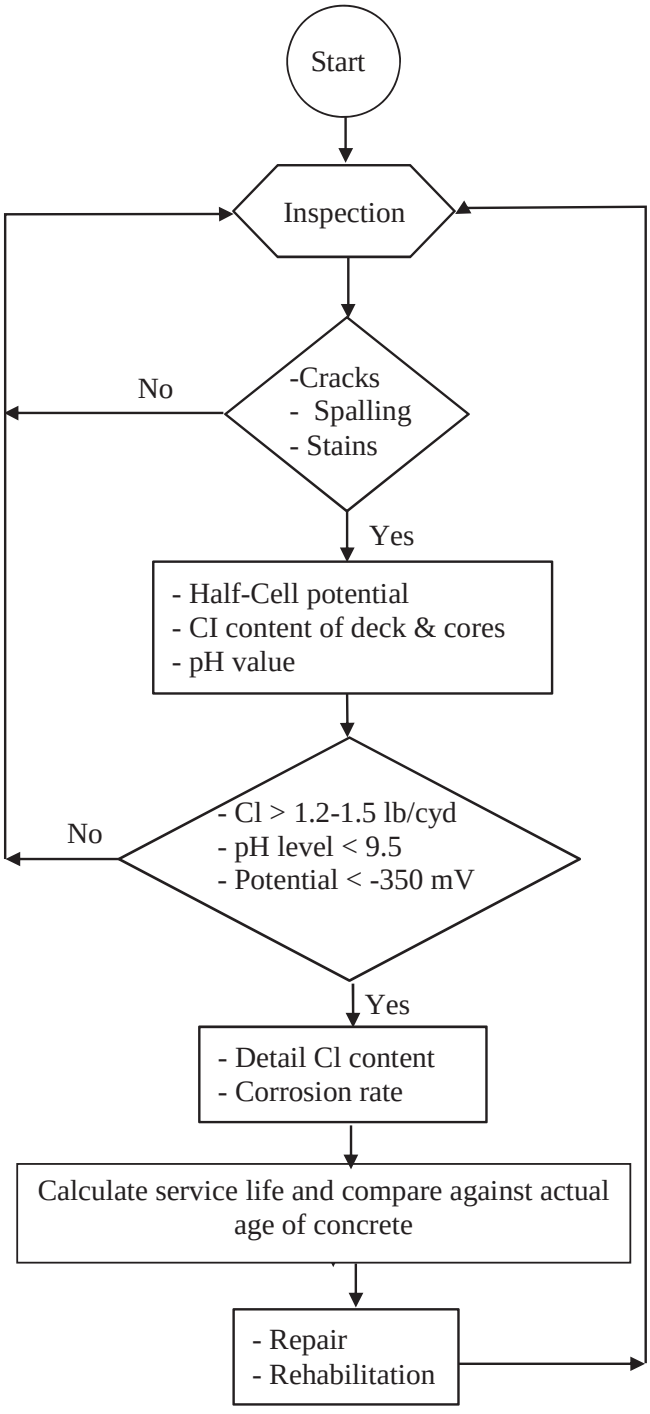

Figure 7-6 Flow chart of the recommended procedure

The implementation strategy which is based on the relationships and correlations made between the laboratory investigations and field investigations carried out in the southern Michigan. It is recommended that the further field investigations are carried out to establish the relationships for other regions of Michigan (e.g. Upper Peninsula).

The following graph (Figure 7-7) is developed as a guide to schedule timing of future repair/rehabilitation activity for a critical chloride content value of 1.2 lb/cyd and a porous zone size of 30 μm or 1.182 mils. The time to corrosion cracking of concrete bridge decks can be determined from the graph with known value of corrosion rates and diffusion coefficients. The graph is developed for the observed minimum and maximum value of diffusivity for the field bridges. The remaining time before rehabilitation should be initiated can be calculated by subtracting the actual age of the bridge deck from the time to corrosion cracking. The remaining time before rehabilitation are compared with each other to prioritize repair/rehab timing.

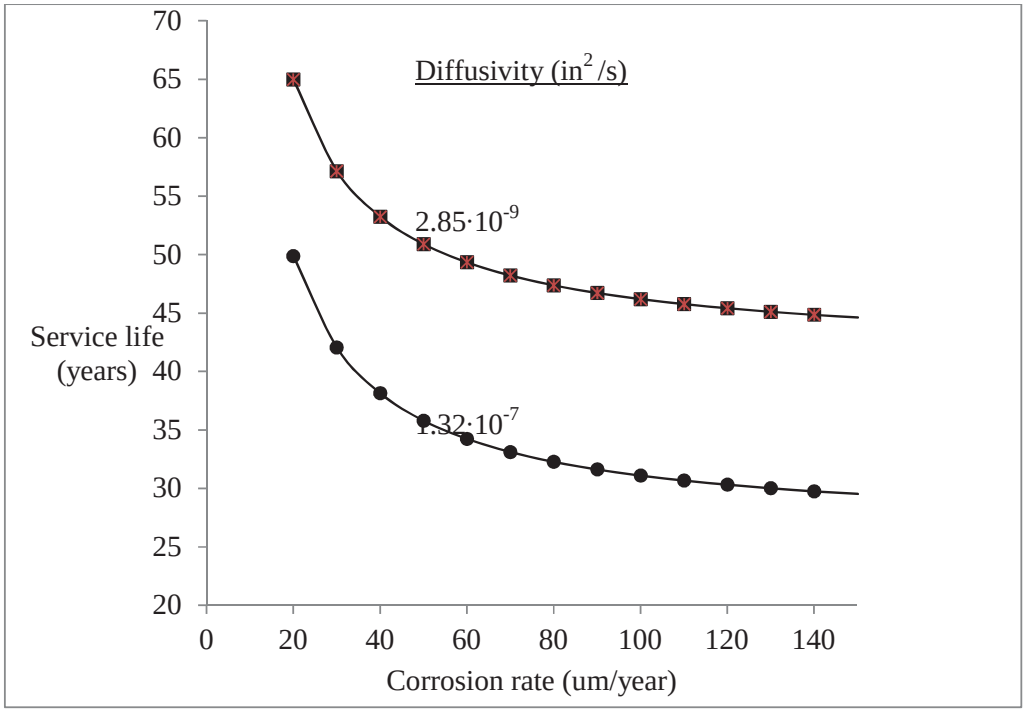

Figure 7-7 Relationship between service life, corrosion rate and diffusion coefficient for a critical chloride content of 1.2 lb/cyd and porous zone size of 1.182 mils.

CHAPTER 8: SUMMARY, FINDINGS AND RECOMMENDATIONS

8.1 Summary

A comprehensive research investigation was conducted to determine the concrete properties, conditions and steel conditions that are highly associated with falling concrete, to develop performance thresholds and procedures to identify decks with spalling potential, to evaluate and select non-destructive field test methods to identify spalling potential, to determine the service life of the bridge decks, and to propose a strategy for engineers to assess the timing of future maintenance and repair activities. The terminology, service life, is used in this study as the age at which surface cracking are visible on the bottom of the bridge deck due to corrosion of the bottom reinforcement. Applications of saltwater exposure, freeze/thaw cycling, and repeated load cycles were used on laboratory specimens constructed from concrete mix designs with and without introduced chloride. Non-destructive tests including measurements of half-cell potential, rate of corrosion, and hardness of concrete were conducted.

The research investigation program included field and laboratory investigations on three poor performing bridge decks located in Southern Michigan. The investigation included visual inspection, non-destructive testing and analysis of cores obtained from bridge decks. The service life was determined for field investigated bridges, and an implementation strategy is proposed for evaluating the current deck condition to aid in the selection of timing of future maintenance and repair activities. Half-cell potential measurement was used to evaluate the chance of reinforcement corrosion on representative areas of the bridge deck. Powder samples of concrete were collected from both the bridge decks and the full-depth cores for chloride content evaluation, and pH variation along the depth of the deck was examined on full-depth cores. Concrete core samples were evaluated under the ESEM (environmental scanning electron microscope) to determine the porous zone (interface between the steel reinforcement and the concrete) thickness and to evaluate the state of corrosion. The in-situ concrete hardness of the deck was assessed from the bottom.

A laboratory durability investigation was conducted on 20 large-scale bridge deck specimens. Four specimens were used as control specimens, and the remaining 16 specimens were subjected to either both saltwater exposure and repeated load cycles or both freeze/thaw

cycling and repeated load cycles. At various stages during and after the environmental exposures; half-cell potential measurements were conducted to determine the chance of corrosion in the reinforcements, galvanostatic measurements were conducted to determine the associated rate of corrosion in the reinforcements, rebound hammer tests were conducted to determine the surface hardness the specimens. Static load tests at every 250,000 cycles of repeated load were performed to determine changes in the load response of the deck specimens. Furthermore, chloride content measurements were performed on sample concrete powder before the environmental exposures and on selected specimens after they were tested for ultimate load failure.

8.2 Findings

The knowledge of expected remaining service life of bridge decks, at the time when early visual corrosion cracking at the bottom of the deck is observed, is urgently needed for the state agency to determine when a deck will need major repairs or rehabilitation. The aim is to schedule repair and rehabilitation activities before the unset of falling concrete due to corrosion related spalling. The predicted service life for the investigated bridge decks as well as the laboratory bridge decks are summarized below.

1. The range of service life of bridge 63174-S05-1 carrying I-75 NB over14 Mile Road is 12.7 years in A1 and 45.3 to 60.2 years in areas A2 and A3, the range for bridge 63022-S02-4 carrying I-96 WB over Milford Road is 30.0 to 41.0 years and for bridge 63022-S01 carrying I-96 WB over Kent Lake Road is 15.3 years in B2 and 33.6 to 48.5 years in the remainder of the bridge (assuming a critical chloride content value of 1.2 lb/cyd.) For the three bridges, the outside lanes and ramps (typically denoted test areas A1) have lower service life than the rest of the deck areas; this could be attributed to the amount of deicing salt applied.

2. The laboratory specimens, constructed from the concrete mix with chloride are severely affected by the saltwater or freeze/thaw exposures. Therefore, the corrosion rate is higher and the specimens have less than 10 years of time to corrosion cracking. However, for the specimens F-WO-3 (specimen without introduced chloride and exposed to 300 cycles of

freeze/thaw), time to corrosion cracking is 21 years. On the other hand, for specimens C-WO (control specimen without any introduced chloride) the time to corrosion cracking takes place at the end of 48 years. Under the presence of cracks, moisture and ingress of chloride ions, the time to corrosion cracking indicated in Table 7-13 can give a useful basis for planning of rehabilitation of bridge decks in southern Michigan after assessing the age and corrosion rate of the area of interest based on the number of freeze-thaw cycles that the bridge deck would experience.

The corrosion initiation time is determined by the concrete coefficient of diffusivity. It is extremely important to use a low diffusivity concrete in bridge decks. Bridge decks constructed with different concretes indicate that, high diffusivity values correlated with higher chance of corrosion.

3. Chloride diffusivity with time was calculated for the test area in each of the investigated bridges. The average value over the time period from chloride exposure to sampling was used in calculating time for ingress of chloride, initiation time, to reach critical value on the surface of the bottom reinforcement. Test area A1 of 63174-S05-1 carrying I-75 NB over 14 Mile Road demonstrated a high value for the chloride diffusivity resulting in the time required to reach a threshold chloride content (1.2 lb/cyd) at the reinforcement (initiation time) is only 3.0 years. This could be attributed to the widening project (lane added to the bridge) using a different quality concrete as compared to the original concrete deck. For the remaining structures, it is estimated that time to reach critical chloride concentrations at the bottom reinforcement was 25 years, 36 and 30 years for 63174-S05-1 carrying I-75 NB over 14 Mile Road, bridge 63022-S02-4 carrying I-96 WB over Milford Road and 63022-S01 carrying I-96 WB over Kent Lake Road, respectively.

4. The average diffusion coefficient, during the time of sampling, for areas A1, A2 and A3 of 63174-S05-1 carrying I-75 NB over 14 Mile Road is $1.83 \cdot 10^{-07}$ in^2/sec, $2.20 \cdot 10^{-08}$ in^2/sec and $2.29 \cdot 10^{-08}$ in^2/sec, respectively. Note that A1 is located in the lane added after the original structure completed, hence the difference in the concrete properties.

5. The average diffusion coefficients, during the time of sampling, of the remaining two investigated bridges ranged from $5.55 \cdot 10^{-08}$ in^2/sec to $1.05 \cdot 10^{-08}$ in^2/sec. Based on the literature, these values are within the expected range for concrete bridge decks.

Half-cell potential, chloride content values, and pH measurements were conducted and evaluated against the critical values both on field investigated and laboratory specimen bridge decks to assess the chance of corrosion and associated cracking, and to infer the associated risk of falling of concrete. The laboratory specimens were exposed to saltwater, freeze-thaw and loading condition representing the prevailing environmental and loading condition of bridges in Michigan.

6. The chances of corrosion were higher on test areas A1 and A2 than test area A3 for bridges 63174-S05-1 carrying I-75 NB over 14 Mile Road and 63022-S02-4 carrying I-96 WB over Milford Road. The chance of corrosion was higher in areas A1, A2 and B3 than A3, B1 and B2 of bridge 63022-S01 I-96 WB over Kent Lake Road. In the investigation carried out, areas in the most right lane (A1, A2 and B3) showed higher chance corrosion of reinforcement bar (bottom mat) and degradation of concrete that is associated with corrosion of reinforcement bar.

7. The chloride content in the bridge deck of 63174-S05-1 carrying I-75 NB over 14 Mile Road in test areas A1 and A2, near the bottom reinforcement exceeded the critical value, and the chloride content in test area A3 had not yet reached the critical range. The chloride content at the location of the lower reinforcement mat exceeded the critical range for both 3022-S02-4 I-96 WB over Milford Road and 63022-S01 carrying I-96 WB Kent Lake Road. As expected due to age of the bridges the chloride contents tended to be higher on the older two bridges in this investigation (63022-S01 I-96 WB over Kent Lake Road and 3022-S02-4 carrying I-96 WB over Milford Road).

The pH values were 9.5 or less at the location of the bottom reinforcement for the cores obtained from 63174-S05-1 carrying I-75 NB over 14 Mile Road and 63022-S01 carrying I-96

over Kent Lake Road. Based on additional laboratory investigations the following conclusions are drawn:

8. The combined effect of environmental exposures such as deicing of salt, freeze/thaw cycling and the presence of cracks accelerates the formation of chloride ions induced corrosion of bridge deck reinforcement. Measurements of half-cell potential at locations where cracks, stains and/or spalling are observed should indicate a higher (95%) chance of corrosion.

9. At the early stages of chloride ion induced corrosion, the ultimate strength and the concrete surface hardness of the bridge decks subjected environmental exposures may not be affected by the corrosion development.

10. Increased deflections of the bridge deck due to the repeated loads may not occur throughout the early stages of corrosion. Consequently, deflections should not be the only indicator of the potential for falling concrete from bridge decks.

Supporting conclusions based on field and laboratory investigation:

a. The half-cell potential difference (chance of corrosion) increased with increasing environmental exposure considering both the number of freeze-thaw cycles and duration of saltwater exposure. Specimens subjected to 10,000 hours of saltwater exposure showed 50% chance of corrosion while specimens subjected to 600 cycles freeze-thaw exhibited 95% chance of corrosion. The control specimens indicated only 5% chance of corrosion at eighteen months of age.

b. Corrosion rate of the specimens subjected to saltwater exposure and freeze-thaw cycling was increased with increasing duration of saltwater and cycles of freeze-thaw exposures, respectively. As expected, control specimens not subjected to any environmental exposure exhibited a low (dormant) corrosion rates.

c. The ultimate strength of all specimens (53.2 kips to 63.1 kips) were in close agreement with the theoretical capacity (52.6 kips) after 600 freeze-thaw cycles and 2,000,000

repeated load cycles or 10,000 hours of saltwater exposure and 3,000,000 repeated load cycles. Moreover, it can be noted that the ultimate strength of any of the specimens were not less than the predicted value of 52.6 kips.

d. Static load tests conducted on each specimen at the end of every 250,000 cycles of repeated load and environmental exposure sequence indicated that the load-deflection responses remained within the elastic range.

e. The porous zone size ranged from 21 to 39 μm or 0.83 to 1.54 mils for the freeze-thaw and saltwater exposed laboratory tested specimens, with introduced chloride. Higher porous zone size was observed for control specimen without introduced chloride while lower porous zone thickness was observed for freeze-thaw and saltwater exposed specimens with introduced chloride. A higher porous zone size of 43 μm or 1.69 mils was observed for cores taken from 63174-S05-1 carrying I-75 NB and 14 Mile Road and 22 μm 63022-S01 carrying I-96 WB over Kent Lake Road. Hence, an average porous zone size of 30 μm or 1.18 mils is recommended for calculation purposes for Michigan bridge deck concrete.

f. ESEM (environmental scanning electron microscope) showed that Oxygen and Iron elements, which are evidence of corrosion products, were present on the perimeter of the reinforcement of saltwater as well as freeze-thaw exposed specimens. Similarly, corrosion products were observed on the reinforcement of samples of I-75 NB over 14 Mile Road and I-96 WB over Kent Lake Road.

8.3 Recommendations

The findings of this study outlines when supplemental testing and service life predictions (relative to corrosion cracking) are recommended as part of the scheduled biennial inspection. In general, the onset of corrosion cracking near the bottom layer reinforcement in concrete bridge decks is expected after 50+ years, based on the three bridges included in this study. A general recommendation is to conduct supplemental testing and associated service life predictions when any of the following three events occur:

- time of an overlay
- appearance of surface cracking and rust stains on the bottom deck
- concrete deck age of 35 years.

The supplemental testing and service life predictions should follow the implementation strategy presented in Section 7.3 of this report and should include conducting measurements of the

- half-cell potential (critical values less than -350mV)
- chloride content at a level of the bottom reinforcement (critical values greater than 1.2-1.5 lb/cyd)
- pH (critical values less than 9.5).

If any of the three critical values are exceeded it is recommended to conduct detailed mapping of the chloride content profile to determine the coefficient of diffusivity as well as estimating the corrosion rate. This information is applied to predict the service life to corrosion cracking.

REFERENCES

ACI subcommittee 222R-01 (2001). "Protection of Metals in Concrete against Corrosion," American Concrete Institute, Farmington Hills, MI, pp. 1-41.

Alampalli, S., Owens, F., Sandhu, D., and Haddock, J. (2002). "A Qualitative Study of Correlation between Bridge Vibration and Bridge Deck Cracking," Transportation Research Board Annual Meeting CD-ROM.

Al-Harthy. A. S, and Stewart, M. G. (2006). "A Review of Predictive Models for Cracking in Concrete due to Reinforcement Corrosion". Research report no. 258.06.06, Centre for Infrastructure Performance and Reliability, The University of Newcastle.

Almusallam, A. A., Al-Gahtani, A. S., Aziz, A. R., Dakhil, F. H., and Rasheeduzzafar (1996). "Effect of Reinforcement Corrosion on Flexural Behavior of Concrete Slabs." Journal of Materials in Civil Engineering, ASCE, Vol. 8(3), pp. 123-127.

Alonso, C., Andrade, C., Castellote, M., and Castro, P. (2000). "Chloride Threshold Values to Depassivate Reinforcing Bars Embedded in a Standardized OPC Mortar." Cement and Concrete Research, Vol. 30, pp. 1047–1055.

Amasaki, S. (1991). "Estimation of Strength of Concrete Structures by the Rebound Hammer". CAJ Proc Cem Conc 45, pp. 345–351.

ASTM Standard (2000). C805-85: "Standard Test Method for Rebound Number of Hardened Concrete", Annual Book of ASTM Standards, Vol. 04.02, ASTM International, West Conshohocken, PA.

ASTM Standard (2000) C876: "Standard Test Method for Half-Cell Potentials of Uncoated Reinforcing Steel in Concrete", Annual Book of ASTM Standards, Vol. 04.02, ASTM International, West Conshohocken, PA.

ASTM Standard (2000) C666-97: “Standard Test Method for Resistance of concrete to Rapid Freezing and Thawing”, Annual Book of ASTM Standards, Vol. 04.02, ASTM International, West Conshohocken, PA.

ASTM Standard (2000) C617-98: “Practice for Capping Cylindrical Concrete Specimens”, Annual Book of ASTM Standards, Vol. 04.02, ASTM International, West Conshohocken, PA.

ASTM C231 / C231M, “Standard Test Method for Air Content of Freshly Mixed Concrete by the Pressure Method”, Annual Book of ASTM Standards, Vol. 04.02, ASTM International, West Conshohocken, PA.

ASTM C143 / C143M, “Standard Test Method for Slump of Hydraulic-Cement Concrete”, Annual Book of ASTM Standards, Vol. 04.02, ASTM International, West Conshohocken, PA.

ASTM C39 / C39M-09, “Standard Test Method for Compressive Strength of Cylindrical Concrete Specimens”, Annual Book of ASTM Standards, Vol. 04.02, ASTM International, West Conshohocken, PA.

ASTM C78 / C78M, “Standard Test Method for Flexural Strength of Concrete (Using Simple Beam with Third-Point Loading)”, Annual Book of ASTM Standards, Vol. 04.02, ASTM International, West Conshohocken, PA.

BS 1881: Part 202, (1986). “Recommendations for Surface Hardness Tests by the Rebound Hammer”, BSI, UK.

Cady, P. D., and Renton, J. B. (1977). “Durability of Steel-Formed, Sealed Bridge Decks”, Final Report, The Pennsylvania State University, University Park, Pennsylvania.

Cairns, J., and Melville, C.(2003). “The Effect of Concrete Surface Treatments on Electrical Measurements of Corrosion Activity”, Construction and Building Materials, Vol. 17 (5), Pages 301-309.

Callister, W. D., Jr. (1997). “Materials Science and Engineering”, John Wiley and Sons, Inc., New York.

Chamberlin, W. P., Amsler, D. E., and Jaqueway, J. K. (1972). “A Condition Survey of Monolithic Bridge Decks in New York State”, Special Report 11, Engineering Research and Development Bureau.

Choi, O. C., Hossain, H. G., Darwin, D., and McCabe, S. L. (1990). “Bond of Epoxy Coated Reinforcement to Concrete: Bar Parameters”, Report No. 90-1, University of Kansas Transportation Centre, Lawrence, Kansas.

Christensen, T. P. (2000), “Stochastic Modelling of the Crack Initiation Time for Reinforced Concrete Structures”. ASCE Structures Congress, Philadelphia, pp. 8.

Clear, K. C. (1980). “Cost-Effective Rigid Concrete Construction and Rehabilitation in Adverse Environments”, FCP Annual Progress Report, Project No. 4K

Cleary, D. B., and Ramirez, J. A. (1992). “Bond of Epoxy-Coated Reinforcement under Repeated Loading”, Structural Engineering Report No. CE-STR-92-1, Purdue University.

Cleary, D. B., and Ramirez, J. A. (1991). “Bond Strength of Epoxy-Coated Reinforcement”, ACI Materials Journal, Vol. 88 (2), pp. 146-149.

Cordon, W.A. (1979). “Properties, Evaluation, and Control of Engineering Materials”, McGraw-Hill, New York, New York.

Elsener B. and Bohni, H. (1992). “Electrochemical Methods for the Inspection of Reinforcement Corrosion”. In: Concrete structures-field experience, Material Science

Forum, pp. 635–646.

Elsener, B., (2001). “Half-Cell Potential Mapping to Assess Repair Work on RC Structures”, Construction and Building Materials, Vol. 15 (2-3), pp. 133-139.

Enright, M. P., and Frangopol, D. M. (2000). “Survey and Evaluation of Damaged Concrete Bridges.” Journal of Bridge Engineering, ASCE, Vol. 5(1), pp. 31-38.

Faber, M. H., and Rostam, S. (2001), “Durability and Service Life of Concrete Structures, the Owners’ Perspective”, International Conference on Safety, Risk and Reliability Rends In Engineering. IABSE, Malta, pp. 369–74.

Fanous, F. S. and Wu, H-C. (200). “Service Live of Iowa Bridge Decks Reinforced with Epoxy Coated Bars,” Mid-Continent Transportation Symposium Proceedings, pp. 259 – 262.

Francois, R., and Arligui, G. (1998). “Influence on Service Cracking on Reinforcement Steel Corrosion.” Journal of Materials in Civil Engineering, ASCE, Vol. 10(1), pp. 14-20.

Garces, P., Andrade, M. C., Saez, A., and Alonso, M. C. (2005). “Corrosion of Reinforcing Steel In Neutral and Acid Solutions Simulating the Electrolytic Environments in the Micropores of Concrete in the Propagation Period.” Corrosion Science, Vol. 47, pp. 289–306.

Gergely, J., Bledsoe, J. E., Tempest, B. Q., and Szabo, I. F. (2006). “Concrete Diffusion Coefficients and Existing Chloride Exposure in North Carolina” North Carolina Detartment of Transportation Research Project No: HWY-2004-12.

Glass, G. K., and Buenfeld, N. R. (1997). “The Presentation of the Chloride Threshold Level for Corrosion of Steel in Concrete”, Corrosion Science, Vol. 39, pp. 1001–1013.

Glass, G. K., Page, C. L., Short, N. R., and Yu, S.W. (1993). “An Investigation of Galvanostatic

Transient Methods used to Monitor the Corrosion of Rate of Steel in Concrete", Corrosion Science, Vol.35, (5–8), pp. 1585.

Grieb, W., (1958). "Use of the Swiss Hammer for Estimating the Compressive Strength of Hardened Concrete", FHWA Public Roads 30, Washington, DC, pp. 45–50.

Hamad, B. S., and Jirsa, J. O. (1993). "Strength of Epoxy Coated Reinforcing Bar Splices Confined with Transverse Reinforcement", ACI Structural Journal, pp. 77-88.

Hester, C. J., Salamizavaregh, S., Darwin, D., and McCabe, S. L. (1991). "Bond of Epoxy-Coated Reinforcement to Concrete: Splices", SL Report 91-1, University of Kansas.

Hongseob, O., Jongsung, S., and Christian, M. (2005). "Fatigue Life of Damaged Bridge Deck Panels Strengthened with Carbon Fiber Sheets", ACI Structural Journal, Vol. 102, pp. 85-92.

Ibrahim, M., Al-Gahtani, A. S., Maslehuddin, M., and Dakhil, F. H. (1999). "Use of Surface Treatment Materials to Improve Concrete Durability." Journal of Materials in Civil Engineering, ASCE, Vol. 11(1), pp. 36-40.

Kirkpatrick, T. J., Weyers, R. E., Sprinkel, M. M., and Anderson-Cook, C. M. (2001). "Impact of Specification Changes on Chloride Induced Corrosion Service Life of Bridge Decks," Transportation Research Board 2002 Annual Meeting CD-ROM.

Kosmatka, S. H. and Panarese, W. C. (1988). "Design and Control of Concrete Mixtures", Portland Cement Association, Skokie, Illinois.

Koubaa, A., and Snyder, M. B. (1990). "Assessing Frost Resistance of Concrete Aggregates in Minnesota", Journal of Cold Regions Engineering, ASCE, Vol. 15(4), 2001, pp. 187-210. Labounty, Roy E. (HC2, Box 105E, Two Harbors, MN, 55616).

Krauss, P. D., Lawler, J.S. and Steiner, K.L. (2009). "Guideliens for Selection of Bridge Deck Overlays, Sealers and Treatments", NCHRP Project 20-07 National Cooperative Highway Research Program, Transportation Research Board of the National Research Council.

Lee, S-K., Krauss, P. D. (2004). "Long-Term Performance of Epoxy-Coated Reinforcing Steel in Heavy Salt-Contaminated Concrete", Report No. FHWA-HRT-04-090, Federal Highway Administration, McLean, VA.

Lee, S-K., Krauss, P.D., and Virmani, Y.P. (2005). "Resisting Corrosion", Public Roads. Vol. 68, No. 6.

Leshchinsky, A. (1991). "Non-Destructive Methods Instead of Specimens and Cores, Quality Control of Concrete Structures". In: L. Taerwe and H. Lambotte, Editors, Proceedings of the International Symposium held by RILEM, Belgium, E&FN SPON, UK, pp. 377–386.

Leung, C. K. Y. (2001). "Modeling of Concrete Cracking Induced by Steel Expansion," Journal of Materials in Civil Engineering, ASCE, Vol. 13(3), pp. 169-175.

Li, Y., Vrouwenvelder, T., Wijnants, G. H., and Walraven, J. (2004). "Spatial Variability of Concrete Deterioration and Repair Strategies", Structural Concrete, 5 (3), pp. 121–129.

Lloyd, J.P. and Heidersbach, R.H. (1985), "Use of the Scanning Electron Microscope to Study Cracking and Corrosion in Concrete", Concrete International, USA, pp. 45-50.

Maaddawy, T. E. and Soudki, K. A. (2007). "Model for Prediction of Time from Corrosion Initiation to Corrosion Cracking, Cement & Concrete Composites, 29 (3), pp. 168–175.

Maheswaran, T., and Sanjayan, J. G. (2004). "A Semi-Closed-Form Solution for Chloride Diffusion in Concrete with Time-Varying Parameters", Magazine of Concrete Research, Vol. 56(6), pp. 359–366.

Marusin, S.L. (1993). “SEM Studies of Concrete Failures Caused by Delayed Ettringite Formation”, Proceedings of the 4th Euro-seminar on Microscopy Applied to Building Materials, USA.

Mays, G., (1992). “Durability of Concrete Structures: Investigation, Repair, Protection” Chapman Hall, London.

Mehta, P. K. (1993). “Concrete Structure, Properties and Materials”, Prentice-Hall, Inc.

Miki, F., (1990). “Predicting Corrosion-free Service Life of a Concrete Structure in a Chloride Environment”, ACl Materials Journal, Vol. 87 (6), pp. 581-587.

Miller, R., Krouskop, B., Minkarah, I., Bodocsi, A. (1993). “Chloride Penetration and the Effect on Porosity in a Pavement”, Paper No. 930327, Transportation Research Board, 72nd Annual Meeting.

Misra, S. and Uomoto, T. (1990). “Corrosion of Rebars under Different Conditions”. Proceedings of JCI, 12(2), 825-830.

Mohamed, O. A., Rens, K. L., and Stalnaker, J. J. (2000). “Factors Affecting Resistance of Concrete to Freezing and Thawing Damage,” Journal of Materials in Civil Engineering, ASCE, Vol. 12(1), pp. 26-32.

Newton, C. J., and Sykes, J. M. (1998). “A Galvanostatic Pulse Technique for Investigation of Steel Corrosion in Concrete”, Corrosion Science, Vol. 28, pp. 1051.

Novak, A., Szerszen, M.M., and Juntunen, A. A. (2000). “Michigan Deck Evaluation Guide.” Michigan Department of Transportation. RC-1389B.

Oh, B. H., Jang, S. Y., and Shin, Y. S. (2003). “Experimental Investigation of the Threshold

Chloride Concentration for Corrosion Initiation in Reinforced Concrete Structures." Magazine of Concrete Research, Vol. 55 (2), pp. 117–124.

Ollivier, J.P. (1985). "A Non-Destructive Procedure to Observe the Micro Cracks of Concrete by Scanning Electron Microscopy", Cement and Concrete Research, Vol. 15 No. 6, USA, pp. 1055-60.

Page, C. L., and Treadaway K.W.J. (1982). "Aspects of Electrochemistry of Steel in Concrete," Nature, vol. 297, pp.109-115.

Prabakar, J., Bharathkumar, B. H., and Chellappan, A. (2007). "Prediction of Rebar Profile in a Earth Retaining RCC Structure Using Cover Meter Survey", Construction and Building Materials, Vol. 21, pp. 873–878.

Pradhan, B., and Bhattacherjee, B. (2009). "Half-Cell Potential as an Indicator of Chloride-Induced Rebar Corrosion Initiation in RC", Journal of Materials in Civil Engineering, Vol. 21, Issue 10, pp. 543-552.

Pyc, W. A. (1998). "Field Performance of Epoxy-Coated Reinforcing Steel in Virginia Bridge DECKS", Dissertation in Civil and Environmental Engineering, Virginia Polytechnic Institute and State University.

Qian, S., and Cusson, D. (2004). "Electrochemical Evaluation of the Performance of Corrosion-inhibiting Systems in Concrete Bridges", Cement and Concrete Composites, Vol. 26, pp. 217-233.

Ramey, G. E., and Wright, R. L. (1997). "Structural Design Actions to Mitigate Bridge Deck Cracking." Practice Periodical on Structural Design and Construction, ASCE, 2(3), pp. 118-124.

Ramey, G. E., Wolff, A. R., and Wright, R. L. (1997). "DOT Management Actions to Enhance

Bridge Durability/Longevity." Practice Periodical on Structural Design and Construction, ASCE, 2(3), 125-130.

Ramirez, J., and Hasan, H. (1995). "Behavior of Concrete Bridge Decks and Slabs Reinforced with Epoxy Coated Steel", Joint Highway Research Project No: C-36-56CC, Federal Highway Administration.

Rangaraju, P. R. (2001). "Investigation into Premature Deterioration of Concrete on USTH 169 Near Hibbing, Minnesota," Transportation Research Board 2001 Annual Meeting CD-ROM.

RILEM TC 154-EMC (2003). "Electrochemical Techniques for Measuring Metallic Corrosion Half-Cell Potential Measurements - Potential Mapping on Reinforced Concrete Structures", Materials and Structures, Vol.36 (261), pp. 461-471.

Russell, H. J., (2004). "Concrete Bridge Deck Performance", National Cooperative Highway Research Program, NCHRP synthesis 333.

Sarja, A. and Vesikari, E., Eds. (1996). "Durability Design of Concrete Structures". Chapman and Hall, London.

Sarkar, S.L. (1992). "Micro structural investigation of renaissance mortar from Montreal, Quebec and Canada", Cement and Concrete Research, Vol.22 No.6, USA, pp. 1011-18.

Sarkar, S.L., Chandra, S. and Rodhe, M. (1992). "Micro Structural Investigation of Natural Deterioration of Building Materials in Gothenburg, Sweden", Materials and Structures, Vol. 25, France, pp. 429-35.

Sathiyanarayanan, S., Natarajan, P., Saravanan, K., Srinivasan, S., and Venkatachari, G. (2006). "Corrosion Monitoring of Steel in Concrete by Galvanostatic Pulse Technique", Cement and Concrete Composites, Vol. 28, Issue 7, pp. 630-637.

Shayan, A. (1985). “Warping of precast, white concrete panels”, Cement and Concrete Research, Vol. 15 No. 2, USA, pp. 245-52.

Shayan, A. and Quick, G.W. (1992). “Microscopic features of cracked and uncracked concrete railway sleepers”, American Concrete Institute Materials Journal, Vol. 89 No. 2, USA, pp. 348-61.

Stewart, M. G., and Mullard, J. A. (2007). “Spatial Time-Dependent Reliability Analysis of Corrosion Damage and the Timing of First Repair for RC Structures, Engineering Structures, 29 (7), pp. 1457–1464.

Taly, N. (1998). “Design of Modern Highway Bridges”, McGraw Hill, New York.

Teodoru, G. (1988). “The Use of Simultaneous Nondestructive Tests to Predict the Compressive Strength of Concrete”. In: H.S. Lew, Editor, Nondestructive Testing, Vol. 1, ACI, Detroit pp. 137–148 ACI SP-112.

Townsend, H. E., Cleary H. J., Allegra L. (1981). “Breakdown of Oxide films in Steel Exposure to Chloride Solutions,” Corrosion - NACE, vol. 37, pp. 384-391.

Trejo, D., and Monteiro, P. J. (2005). “Corrosion Performance of Conventional (ASTM A615) and Low-alloy (ASTM A706) Reinforcing Bars Embedded in Concrete and Exposed to Chloride Environments.” Cement and Concrete Research, Vol. 35, 2005, pp. 562–571.

Trejo, D., and Pillai, R.G. (2003). “Accelerated Chloride Threshold Testing: Part 1-ASTM A615 and A706 reinforcement”, ACI Materials Journal, Vol. 100, pp. 519–527.

Tsiatas, G. and Robinson, J. (2002). “Durability Evaluation of Concrete Crack Repair Systems,” Transportation Research Board 2002 Annual Meeting.

Verbeck, G. J. (1975). “Mechanism of Corrosion in Concrete”, Corrosion of Metals in Concrete, ACI SP-49.

Vu, K. A. T., and Stewart, M. G. (2005). “Predicting the Likelihood and Extent of Reinforcement Concrete Corrosion-Induced Cracking”, Journal of Structural Engineering, 131 (11), pp. 1681–1689.

Waddell, J. J. and Dobrowolski, J. A. (1993). “Concrete Construction Handbook”, McGraw Hill, New York.

Weed, R. M. (1974). “Recommended Depth of Cover Depth for Bridge Deck Steel”. Transp. Res. Rec. 500, 1974, pp. 32–35.

Weyers, R. E., Sprinkel, M. M., and Brown, M. C. (2006). “Summary Report of the Performance of Epoxy-Coated Reinforcing Steel in Virginia,” VTRC 06-R29.

Weyers, R. E. (2006a). “Discussion of “Performance of Coated Reinforccing Bars in Cracked Bridge Decks” by F. Fanousand H. Wu. Journal of Bridge Engineering. Vol. 11. Issue 5. September/October 2006. Pp. 661-662.

Willetts, C. (1958). “Investigation of Schmidt Concrete Test Hammer”, Miscellaneous Paper No. 6-267, U.S. Army Engineer Waterways Experiment Station, Vicksburg, MS.

Wong, H. S., Zhao, Y. X., Karimi A. R., Buenfeld, N. R., Jin, W. L. (2010). “On the penetration of corrosion products from reinforcing steel into concrete due to chloride-induced corrosion”, Corrosion Science, Vol. 52, pp. 2469–2480.

Young, J. F., Mindess, S., Gray, R. J., and Bentur, A. (1998). “The Science and Technology of Civil Engineering Materials”, Prentice Hall, Upper River Saddle, New Jersey.

Yuan, Y., and Ji, Y. (2009). "Modeling Corroded Section Configuration of Steel Bar in Concrete Structure", Construction and Building Materials, Vol. 23, pp. 2461–2466.

CONVERSION TABLE FOR THE U.S. CUSTOMARY AND METRIC UNITS

Length

1 centimeter (cm)	= 10 millimeters (mm)
1 inch	= 2.54 centimeters (cm)
1 foot	= 0.3048 meters (m)
1 foot	= 12 inches
1 yard	= 3 feet
1 meter (m)	= 100 centimeters (cm)
1 meter (m)	≅3.280839895 feet
1 furlong	= 660 feet
1 kilometer (km)	= 1000 meters (m)
1 kilometer (km)	≅0.62137119 miles
1 mile	= 5280 ft
1 mile	= 1.609344 kilometers (km)
1 nautical mile	= 1.852 kilometers (km)

Weight

1 milligram (mg)	= 0.001 grams (g)
1 gram (g)	= 0.001 kilograms (kg)
1 gram (g)	≅0.035273962 ounces
1 ounce	= 28.34952312 grams (g)
1 ounce	= 0.0625 pounds
1 pound (lb)	= 16 ounces
1 pound (lb)	= 0.45359237 kilograms (kg)
1 kilogram (kg)	= 1000 grams
1 kilogram (kg)	≅35.273962 ounces
1 kilogram (kg)	≅2.20462262 pounds (lb)
1 stone	= 14 pounds
1 short ton	= 2000 pounds
1 metric ton	= 1000 kilograms (kg)

Area

1 square foot	= 144 square inches
1 square foot	= 929.0304 square centimeters
1 square yard	= 9 square feet
1 square meter	≅10.7639104 square feet
1 acre	= 43,560 square feet
1 hectare	= 10,000 square meters
1 hectare	≅2.4710538 acres
1 square kilometer	= 100 hectares
1 square mile	≅2.58998811 square kilometers
1 square mile	= 640 acres

Speed

1 mile per hour (mph) ≅ 1.46666667 feet per second (fps)

1 mile per hour (mph) = 1.609344 kilometers per hour

1 knot ≅ 1.150779448 miles per hour

1 foot per second ≅ 0.68181818 miles per hour (mph)

1 kilometer per hour ≅ 0.62137119 miles per hour (mph)

Volume

1 US tablespoon = 3 US teaspoons

1 US fluid ounce ≅ 29.57353 milliliters (ml)

1 US cup = 16 US tablespoons

1 US cup = 8 US fluid ounces

1 US pint = 2 US cups

1 US pint = 16 US fluid ounces

1 liter (l) ≅ 33.8140227 US fluid ounces

1 liter (l) = 1000 milliliters (ml)

1 US quart = 2 US pints

1 US gallon = 4 US quarts

1 US gallon = 3.78541178 liters

Temperature

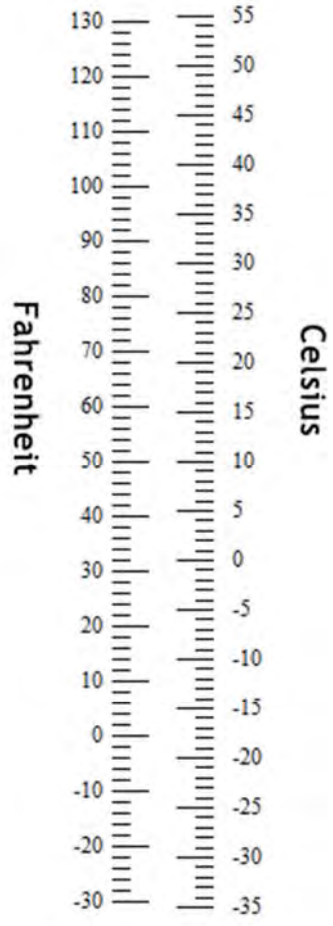

Source: http://metricconversioncharts.org/